NTNU
Norwegian University of
Science and Technology

Factors Affecting the Rheological Properties and Stability of Water-in-Oil Emulsions

Ingunn Lervik

ABSTRACT

The focus of this master thesis has been water-in-oil emulsions. Rheological behavior and factors affecting the formation and stability of such emulsions have been investigated. A set of emulsions have been made using engine oil and synthetic brine, with water content ranging from 10-70%. Factors investigated includes temperature, maturation, shear stress and mixing time. The emulsions showed properties that coincides with the Herschel-Bulkley fluid model.

The size and distribution of the dispersed droplets have been investigated. This was done by visually inspecting the emulsion using an optical microscope.

A flow facility was constructed based on the emulsion parameters obtained from the rheological experiments. Theoretical flow rates were calculated based on power law and Herschel-Bulkley fluid models, and these rates were compared to the actual flow rates. The Herschel-Bulkley model gave the best prediction, with theoretical flow rates deviating 1.55-25.64% from the actual flow rates.

SAMMENDRAG

Hovedfokuset i denne masteroppgaven har vært vann-i-olje emulsjoner. Reologiske egenskaper og faktorer som påvirker dannelsen og stabiliteten av slike emulsjoner er blitt undersøkt. Motorolje og syntetisk saltvann ble brukt til å lage emulsjoner med vanninnhold fra 10-70%. Faktorer som er undersøkt inkluderer temperatur, modning, skjærspenning og blandingstid. Emulsjonene viste egenskaper som sammenfaller med Herschel-Bulkley-væskemodellen.

Størrelsen og fordelingen til emulsjonens dispergerte dråper har blitt undersøkt. Dette ble gjort ved å visuelt inspisere emulsjonen ved hjelp av et optisk mikroskop.

Et strømningsanlegg ble konstruert basert på emulsjonsparametrene funnet fra de reologiske eksperimentene. Teoretiske strømningshastigheter ble beregnet ut fra potenslov- og Herschel-Bulkley-væskemodeller, og disse hastighetene ble sammenlignet med de faktiske strømningshastighetene. Herschel-Bulkley-modellen var best til å beregne strømningshastigheten, med teoretiske strømningshastigheter som avvek 1,55-25,64% fra de faktiske strømningshastighetene.

ACKNOWLEDGEMENTS

1 TABLE OF CONTENTS

LIST OF FIGURES

LIST OF TABLES

LIST OF ABBREVIATIONS AND SYMBOLS

API	American Petroleum Institute
DSA	Drop Shape Analyzer
EOR	Enhanced Oil Recovery
IFT	Interfacial tension
HLB	Hydrophile-Lipophile Balance
O/O	Oil-in-Oil emulsion
O/W	Oil-in-Water emulsion
O/W/O	Oil-in-Water-in-Oil emulsion
O/W/O/W	Oil-in-Water-in-Oil-in-Water emulsion
PIT	Phase Inversion Temperature
rpm	Rounds per minute
W/O	Water-in-Oil emulsion
W/O/W	Water-in-Oil-in-Water emulsion
A	contact area between plate and fluid (Couette flow model), m^2
cP	centi Poise, *1 cP= 0.001 kg/m·s*
ε	energy dissipation, *W/kg*
F	force acting on upper plate (Couette flow model), *N*
f_d	frictional force acting between droplet and continuous phase, *N*
g	gravitational constant, kg/s^2
K	consistency index, $Pa \cdot s^n$
L	pipe length, *m*
L_h	hydrodynamic entrance length, *m*
n	power law index, *dimensionless*
Δ*P*	hydraulic potential, *Pa*
P_i	pressure inside droplet, *Pa*
P_o	pressure outside droplet, *Pa*
p_f	surface correction factor
ρ	density of incompressible Newtonian fluid, kg/m^3

ρ_2	density of the dispersed phase, kg/m^3
ρ_1	density of the continuous phase, kg/m^3
Q	volumetric flow rate, m^3/s
Re	Reynolds number, *dimensionless*
r_0	radius for firm plug flow, *m*
r_d	radius of droplet, *m*
$r_{Feret,max}$	maximum Feret diameter, μm
$r_{Feret,min}$	minimum Feret diameter, μm
r_w	pipe wall radius, *m*
σ_s	Suface tension, *N/m*
S_f	droplet surface area, μm^2
τ	shear stress, Pa, N/m^2
τ_0	yield stress, *Pa, N/m^2*
u	velocity (Couette flow model), *m/s*
μ	dynamic viscosity, *Pa·s, cP*
μ_p	plastic viscosity, *Pa·s, cP*
Υ	shear rate, s^{-1}
v_0	plug velocity, *m/s*
V	droplet volume, m^3
v	droplet velocity, *m/s*
x	distance between plates (Couette flow model), *m*

2   INTRODUCTION

An emulsion is a mixture of two normally immiscible fluids. In the oil industry, emulsions consisting of oil and water is not uncommon. These emulsions can have viscosities and flow properties that differ greatly from the oil and water the emulsion originates from, and can cause problems in several parts of the oil recovery.

The emulsions can be very stable and hard to break. During production, separation problems is a great inconvenience that increases the cost both in producing, refining and transportation. If the emulsion is spilled into the ocean, it can cause severe environmental damage.

Emulsions are not only a disadvantage. Their rheological properties make them a very effective tool for enhanced oil recovery. For heavy crude oils, the formation of an emulsion could result in a viscosity reduction, making production easier. Emulsions are also often used as drilling fluids, as its rheological properties makes it ideal for safe and efficient drilling.

All these factors considered, it is of great interest to get a better understanding of the mechanisms and factors involved in emulsion formation and stabilization.

The objective of this thesis has been to explore emulsions in general, and to better understand what factors affect the stability of water-in-oil emulsions. Emulsions have been created using engine oil and a synthetic brine. A set of rheological experiments have been conducted, and different stability factors have been explored. These factors include temperature, water content, droplet size and distribution, aging and mixing time. The rheological properties were found using a modular compact rheometer, and the droplet size and distribution investigated using a microscope.

Another objective has been to determine how well laminar emulsion flow in pipes can be predicted using different emulsion parameters and flow models. Based on the rheological experiments, one is able to conclude with a fluid model that is best suited to approximate the emulsion flow behavior. For this thesis, the power law and Herschel-Bulkley models are used.

A flow facility was constructed based on the emulsion parameters obtained from the rheological experiments. Different emulsions were run through the flow facility, and the volumetric flow rate recorded. The results were compared to the flow rates calculated using different flow models. Based on this, a prediction about the accuracy of non-Newtonian fluid flow approximations can be made.

3 THEORY

Some of the following theory is taken and further developed from the specialization project fall 2017.
(Lervik, 2017)

3.1 EMULSIONS

3.1.1 Colloidal disperisons

A colloidal dispersion, or a colloidal system, is a heterogeneous system which consist of a dispersed phase and a continuous phase. (Acherson, 1990) When one liquid is dispersed in another liquid of different composition, the colloidal dispersion is called an emulsion.

The dispersed liquid is often referred to as the internal phase, while the continuous phased liquid is referred to as the external phase. During oil production, it is common for the hydrocarbons to form emulsions with the formation water. The hydrocarbon is from now on referred to as crude oil, or just oil. Figure 1 is an illustration of emulsions consisting of oil and water. If water is the dispersed phase, it is called a water-in-oil emulsion (W/O). This is the most encountered emulsion during oil production. If water is the continuous phase, and the oil is dispersed, it is called an oil-in-water emulsion (O/W). These are the simplest kinds of emulsions, where one phase is dispersed in the other. Multiple emulsions can also be formed, where you can have a water-in-oil-in-water emulsion (W/O/W), or an oil-in-water-in-oil emulsion (O/W/O). These are called double emulsions, and even larger multiple emulsions, like (O/W/O/W) are possible. One can even have an oil-in-oil emulsion (O/O), if one of the oils is polar and one is non-polar, but this is rare.
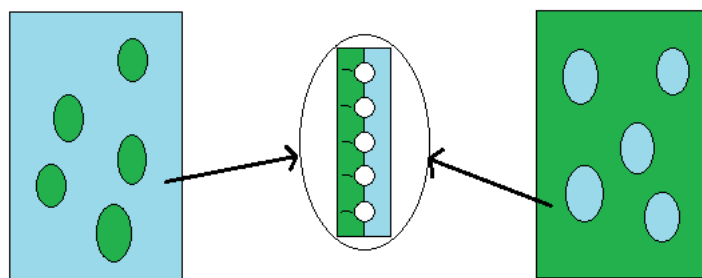
Figure 1: Oil and water emulsions. Left: Oil-in-Water emulsion. Right: Water-in-Oil emulsion. Middle: Surfactant layer between the two fluids.

In order for a stable W/O or O/W emulsion to form, an emulsifier and some sort of energy input need to be present. During oil production, the emulsifier can be found naturally in the crude in form of asphaltenes, and the energy may be present in all parts of the oil production chain.

While oil and water are what we call Newtonian fluids, most emulsions show a non-Newtonian fluid behavior. These non-Newtonian qualities can be very useful, especially in oil recovery. The

characteristics and applications of Newtonian and non-Newtonian fluids will be discussed later in the thesis.

3.1.2 Interfacial tension

Consider a scenario where you have a cup of oil. If you were to pour some water into the oil, the water would just form separated drops suspended in the oil. The two liquids would not mix and form an emulsion. This is because of interfacial tension.

The water droplets behave like water-filled balloons, where the water surface acts like an elastic membrane under tension. The force that causes this tension comes from the attractive forces between the molecules of the liquid. The cohesive forces between the water molecules are larger than the adhesive forces between the water and the oil. This imbalance in forces pulls the water into a spherical shape, and causes a tension in the surface of the droplet. This tension is called interfacial tension, σ_s, and its unit is *N/m*. For systems where the interface is between a liquid and a gas, the tension is referred to as surface tension. (Kantzas, Bryan, & Taheri, 2016)

The curvature caused by the imbalance of forces acting on the droplet and its surroundings can be seen as a pressure difference across the interface. The pressure is highest on the concave side, that is inside the droplet. The pressure difference can be determined by considering the forces acting on the droplet. From Figure 2 one can see that the pressure acts on the area, while the surface tension acts on the circumference of the droplet. A horizontal force balance of the droplet gives

$$(2\pi R)\sigma_s = (\pi R^2)\Delta P_{droplet}$$

Rearranging gives

$$\Delta P_{droplet} = P_i - P_o = \frac{2\sigma_s}{R} \tag{1}$$

where P_i and P_o are the pressure inside and outside the droplet, respectively. This is known as the Young-Laplace equation.
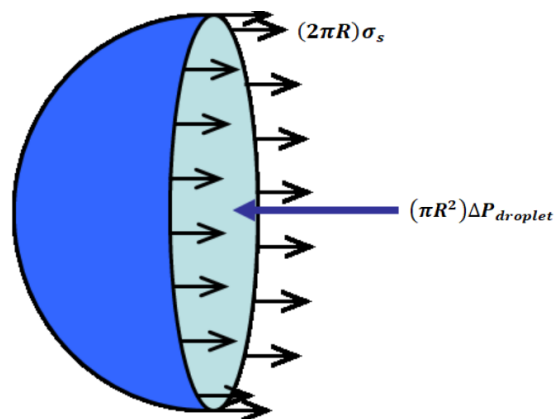
Figure 2: Forces acting on a droplet. Photo adapted from Wikiversity (2018).

Interfacial tension is highly dependent on temperature. The general trend is that an increase in temperature results in a decrease of the IFT. (Eötvös, 1886) This will be investigated later in the thesis.

3.1.3 Surfactants - Emulsifiers

A surfactant is a substance that lowers the interfacial tension between either a liquid and a solid, or between two liquids. An emulsifier is a surfactant with the specific purpose to either form or keep an emulsion stable. When added to reservoirs it can lead to increased recovery and production. A surfactant mainly consists of two parts, a polar hydrophilic head and a non-polar hydrophobic, or lypophilic tail. Hydrophilic means water-loving, and lypophilic means oil-loving. As the names imply, the hydrophilic head will attach itself to the polar water molecules, while the lypophilic tail will attach to the non-polar oil molecules. In an O/W emulsion, where water is the continuous phase, the surfactants lypophilic tails will interact with the oil droplets, forming a small particle called a micelle. This is shown in Figure 3. The hydrophilic heads will interact with the surrounding water, forming a barrier around the micelle. This barrier prevents the micelles from merging together to form larger oil droplets, which could have led to the emulsion breaking. Surfactants help increase emulsion stability by increasing surface viscosity and surface elasticity. (Schramm, 2014) (Kosswig, 1994)
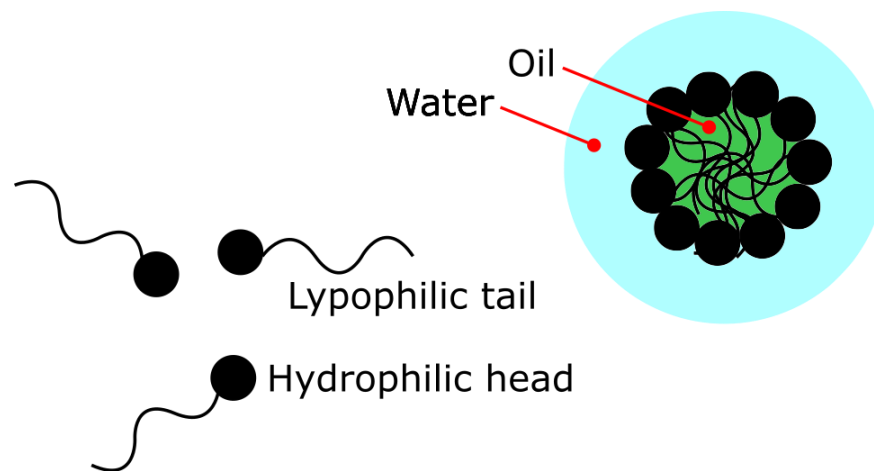
Figure 3: Surfactants consisting of a lypophilic tail and a hydrophilic head. The surfactants form a micelle.

An emulsifier that is more soluble in oil will tend to form W/O emulsions, while an emulsifier that is more water soluble will tend to form O/W emulsions.

Asphaltenes are natural emulsifiers found in the oil. There are several definitions of what asphaltenes are, but the "oil field" definition is that they are the dissolved solids components of crude oils. (Buenrostro-Gonzalez, Groenzin, Lira-Galeana, & Mullins, 2001) An increased amount of asphaltenes in the crude oil results in a tighter emulsion, with smaller dispersed droplet size. (Kokal & Al-Juraid, 1999)

3.1.4   Droplet size and distribution

The droplet size and distribution of the dispersed droplets affect the stability of emulsions. According to Pal (1996), a decrease in droplet size will result in a viscosity increase. He also found that smaller droplets of the dispersed phase resulted in a stronger shear-thinning effect.

According to Schramm (1992) a higher volume fraction of the dispersed phase will result in a larger difference in droplet size distribution.

Knowing the size of the dispersed droplets can be critical if the emulsion is used to increase oil production. In EOR, a frequently used recovery method is the injection of water into the reservoir, waterflooding. Sometimes, in the more permeable and heterogenous parts of the reservoir, bypassing of the oil can occur, and this results in low oil recovery. McAuliffe (1973) wanted to find out if emulsions, in his case O/W emulsions, injected in a reservoir could help increase the reservoir homogeneity and therefore increase the oil recovery. He found that if the oil droplet diameter is sufficiently large, emulsion injection is an effective way of reducing reservoir permeability.
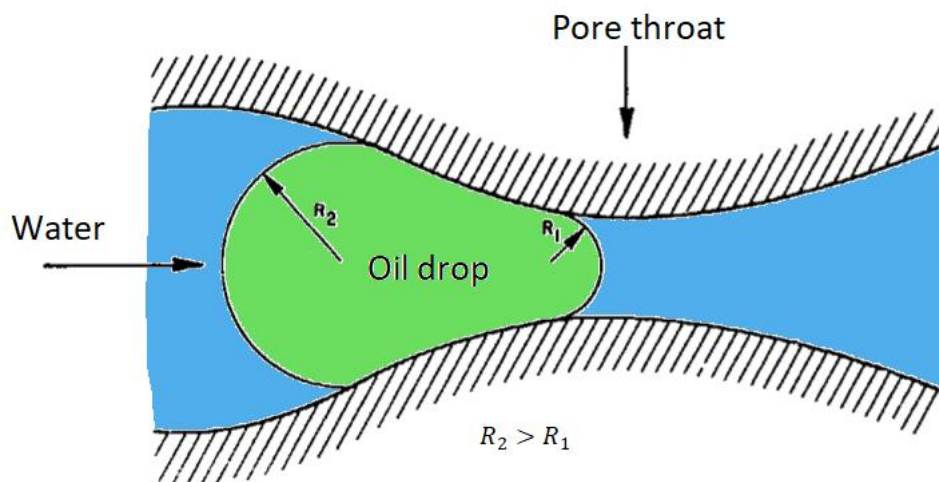
Figure 4: Oil drop flowing through a pore. Picture adapted from McAuliffe (1973)

If the dispersed oil droplet is slightly larger than the pore throat it is trying to flow through, the drop will block the pore and restrict further fluid flow through the pore. If an O/W emulsion is injected into a heterogenous reservoir, the emulsion will mainly flow through the more permeable zones. As it does so, the oil drops will block the pores, forcing the flooded water to flow through the more impermeable zones, displacing more oil in the process.

McAuliffe (1973) found that emulsions most efficiently reduced water flow when there was a low pressure difference across the core sample, compared to a high pressure difference. Since the largest pressure difference in an oil reservoir occurs around the wellbore, the emulsion will most effectively restrict the water flow at some distance away from the wellbore.

3.1.5   Mono- and polydispersity

Dispersity is a measure of the size heterogeneity of the particles in a system. If the particles are of the same size or mass, the system is called monodispersed, or uniform. If the particles are not consistent in size or mass, the system is polydisperse. (Brown, Foote, Iverson, & Anslyn, 2011)

The polydispersity of an emulsion decreases as the dispersed phase droplet size decreases (Pal, 1996). Finer emulsions, that is emulsions with smaller dispersed droplets, tend to be more monodisperse. A higher level of monodispersity results in a higher viscosity. Finer emulsions are therefore expected to have higher viscosities than coarse ones. This will be investigated later in the thesis.

3.2   FORMATION FACTORS AND DEMULSIFICATION MECHANISMS

Most emulsions are thermodynamically unstable, and do not form spontaneously. It cannot remain emulsified naturally, and it will in time break. There are a lot of different factors and mechanism that promotes either the formation or the breaking of emulsions. Knowledge about these mechanisms is important. If an emulsion form undesirably, you need to know what measures to take to break it, and which methods are the safest, easiest and cheapest.

3.2.1   Temperature

Kokal et al. published an article in 1999 that investigates the effect temperature has on emulsion stability. The results showed a clear link between temperature and emulsion stability. They found that higher temperatures will increase the thermal energy, making the particles and droplets in the emulsion move faster and collide more. This reduces the interfacial tension and enhances drop coalescence. In other words; the higher the temperature, the lower the emulsion stability. Higher temperature will also result in a decrease of the viscosity of the emulsion. This will also promote demulsification. Because an increase of temperature does not affect the viscosity of water in the same degree as oil, a smaller viscosity decrease will be expected as the water cut increases. A temperature increase is not emulsion breaking on its own, but it does promote destabilization mechanisms.

3.2.2   Energy dissipation

Energy dissipation is the process of which energy in a homogenous thermodynamic system is irreversibly transformed from one form to another. The potential energy of a system is always less in its final form than in its initial. When water and oil flow together through pipes, this dissipation is the energy source that creates W/O or O/W emulsions.

When making an emulsion by mixing the components in a blender, the flow becomes turbulent, and the energy dissipation is given by the turbulent dissipation rate, ε, where

$$\varepsilon = \frac{Power, blender}{Mass, emulsion}$$

ε has the unit *W/kg*. (Petrowiki, 2018)

3.2.3   Aging

Aging of the emulsion affects its rheological properties. Both viscosity and the shear-thinning effect will decrease if the emulsion is allowed to age. According to Pal (1996), the viscosity reduction caused by aging will be more prominent at lower shear rates.

According to Pal, aging will lead to a coarsening of the droplets. Aging gives demulsification mechanisms like coalescence or Ostwald ripening more time to work. The result is a larger mean droplet size of the dispersed phase, and a higher level of polydispersity. This results in a decrease of rheological parameters for W/O emulsions.

3.2.4   Shear stress

Kokal (1999) found that emulsion stability increases with increased shear. If all other factors are held constant, higher shear will result in a tighter, and therefore more stable emulsion. The increase in shear rate will create smaller droplets of the dispersed phase, making the emulsion harder to break.

3.2.5   Demulsification mechanisms

3.2.5.1   *Sedimentation and Creaming*

In most practical cases, oil has got a lower density than water. Due to the density differences between the dispersed and continuous phase, the emulsion will get an uneven distribution of oil and water. The bottom of the emulsion will be more "watery", while the top will tend to be more "oily". When the dispersed phase falls to the bottom, this process is called sedimentation. If the dispersed phase settles on top, it is called creaming.

It can be shown that the velocity of the dispersed droplets can be expressed as

$$\frac{dx}{dt} = \frac{2r_d^2(\rho_2 - \rho_1)g}{9\eta} \tag{2}$$

Where r is the droplet radius, ρ_1 is the density of the continuous phase, ρ_2 is the density of the dispersed phase and η is the viscosity of the fluid. The derivation of eq. 2 can be found in appendix A. From this equation one can see that a larger droplet radius will give a larger droplet velocity, resulting in a more rapid creaming or sedimentation. An increase in viscosity will make the process happen more slowly, as will a reduction in density difference between the dispersed and continuous phase.

Sedimentation or creaming are not demulsification mechanisms in themselves, they do not alone cause an emulsion to break. However, the process does promote flocculation by increasing the probability of droplet collision, which again can lead to the destabilization of the emulsion. (Schramm, 2014, s. 46)

3.2.5.2   Flocculation

In colloid chemistry, flocculation, also referred to as aggregation or coagulation, is a destabilizing mechanism where the dispersed particles "floc", or cluster together, forming primary particles. These primary particles remain in suspension, they do not necessarily precipitate and fall to the bottom or rise to the surface.

Flocculation rate is dependent on the viscosity of the fluid. A higher viscosity results in a lower flocculation rate, according to Hemmingsen et al. (2005). High viscosity will hinder flocculation, which increases emulsion stability.

The driving mechanism behind flocculation is particle attraction. Although the particles floc together, they do not lose their identity, and the total surface area of the dispersed phase remains somewhat constant. Because of this, flocculation cannot, like sedimentation, cause an emulsion to break on its own. But, flocculation may lead to coalescence, another demulsification mechanism. (Schramm, 2014), (Pal, 1996)

3.2.5.3   Coalescence

Coalescence is the process where drops of the dispersed phase fuse together, forming larger drops. If this process is allowed to continue long enough, the drops will eventually be so large that an emulsion will break and separate in to two phases. Emulsifiers create a film around each droplet, preventing them from coalescing (Schramm, 2014). Unlike flocculation, where the dispersed particles keep their identity, the particles that coalesce lose their identity and becomes part of a new, larger particle. This leads to a reduction in the total surface area of the dispersed phase. As the droplet size increases, so does the coalescence rate. Coarser emulsions are therefore less stable than fine emulsions. A higher viscosity will result in a lower coalescence rate, according to Hemmingsen et al. (2005).

An illustration of the different mechanisms can be seen in Figure 5.
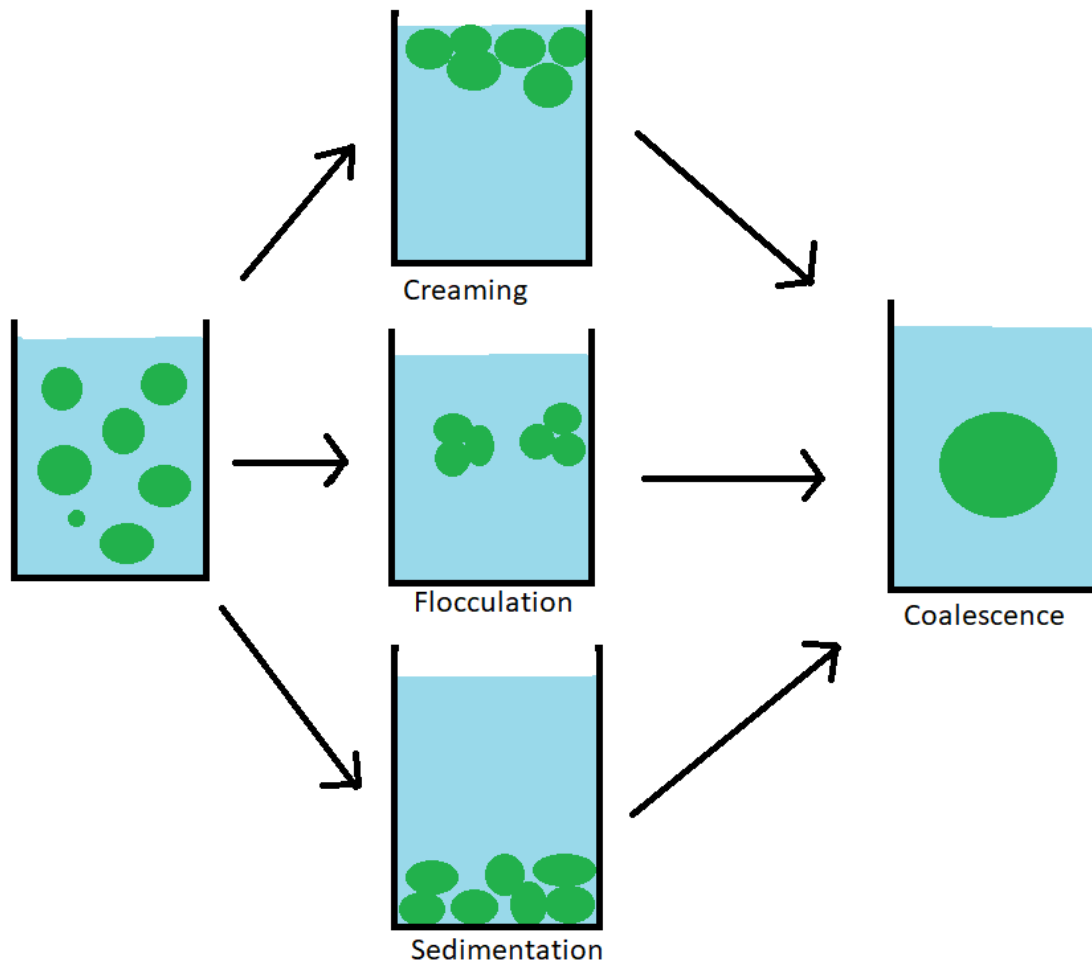
Figure 5: An illustration of the different mechanisms causing demulsification

3.2.5.4 Ostwald ripening

Ostwald ripening, or competitive growth, is a phenomenon where large particles grow even larger at the expense of smaller ones. This is illustrated in Figure 6. An emulsion consist of dispersed particles, and these particles consists of both surface molecules and internal molecules. The surface molecules are less thermodynamically stable than the internal ones. This also means that larger particles are more thermodynamically stable than small ones. This is because the fraction of internal molecules to surface molecules are larger for a large particle compared to a small one.

The smallest particles are the most unstable ones. As said by the laws of thermodynamics, the unstable particle will try to reduce its free energy in order to increase its stability. In order to do that, the particle will try to "get rid of" the unstable molecules, reducing its size in the process. The small particle becomes even smaller, and you will get more free particles dispersed in the solution. When time passes, enough of these molecules will have detached from the particle for the solution to be supersaturated. This means that the solution contains more of the free molecules than is sustainable. This supersaturation will cause the free molecules to redeposit or settle on the surface of larger, more

stable particles, making them grow. This whole process causes large particles to become even larger, and small particles to become smaller and eventually disappear (Voorhees, 1985), (Kontogeorgis & Kiil, 2016).
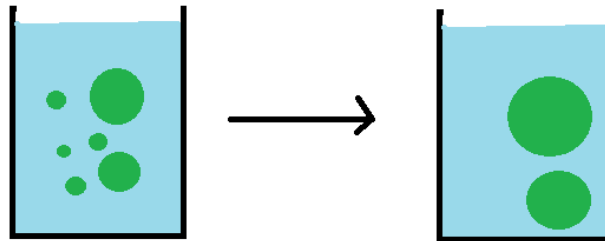
Figure 6: Illustration of the process of Ostwald ripening

3.2.5.5   *Phase inversion*

If an emulsion is very unstable, exposure to additional stress can cause a phase inversion. A phase inversion is when the dispersed and the continuous phase "switch place". A W/O emulsion will turn in to an O/W emulsion and vice versa. An illustration can be seen in Figure 7. The change is permanent, so when the stress that caused the inversion is removed, the phases remain inversed. An example of this is cream, an O/W emulsion that turns into the W/O emulsion butter if it is whipped too long. (Schramm, 2014)
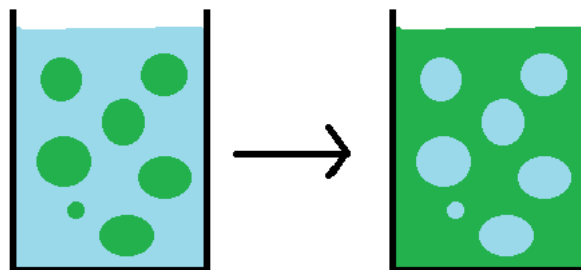
Figure 7: Phase inversion, from oil-in-water to water-in-oil.

11

3.3 FLOW PROPERTIES

3.3.1 Viscosity

Rheology is defined as the study of the flow of materials, and how materials deform when a force is exerted. (Schramm, 2014) Viscosity is a measure of a fluids resistance to flow, or its resistance to deform when shear or tensile stress is applied. In a simpler way, viscosity can be seen as a measure of a fluids thickness. "Honey is thicker than water" is the everyday way of saying that honey has a higher viscosity than water. When a material is exposed to enough stress, it will deform. For a viscous material this deformation is irreversible, which means that the material does not return to its original state when the stress is removed.

The definition behind the term viscosity can be explained by a Couette flow, which is a drag-induced flow between two parallel plates (Cimbala & Cengel, 2014). An incompressible Newtonian fluid with density ρ is contained between two parallel plates that are a distance x apart, as shown in Figure 8. The plates are considered infinitely long and wide. The lower plate is stationary. The upper plate is moved and obtains a velocity V when a force F is applied. The contact area between the plate and the fluid is A. The fluid can be seen as a group of many thin layers parallel to the plates, with a distance dy between them. The fluid layer closest to the moving plate will move with the same velocity as the plate, while the fluid layer closest to the stationary plate will not flow at all. This motionless state is called the no-slip condition. The shear stress, τ, acting on the top layer is $\frac{F}{A}$. The layers in between the bottom and top layers will have increasing velocities with decreasing distance to the moving plate. Between adjacent layers there will occur a velocity difference, du. In a laminar steady flow, this velocity difference will vary linearly between 0 and V. The corresponding velocity gradient will then be $\frac{du}{dy} = \frac{V}{x}$. This velocity gradient is a measure of the fluids rate of deformation, and is called shear rate, Υ. By experiments, it is found that the force exerted upon the upper plate, the shear stress, τ, is proportional to the rate of deformation. In other words,

$$\tau \propto \frac{du}{dy} \qquad (3)$$

The constant of proportionality between the shear stress and the velocity gradient is the viscosity of the fluid, μ:

$$\mu = \frac{\tau}{\left(\frac{du}{dy}\right)} = \frac{\tau}{\Upsilon} \qquad (4)$$

This is the dynamic, or absolute viscosity of the fluid. The unit is *Pa·s*, but it is common to use centipoise, where 1 *cp* is equal to 1 *mPa·s*.
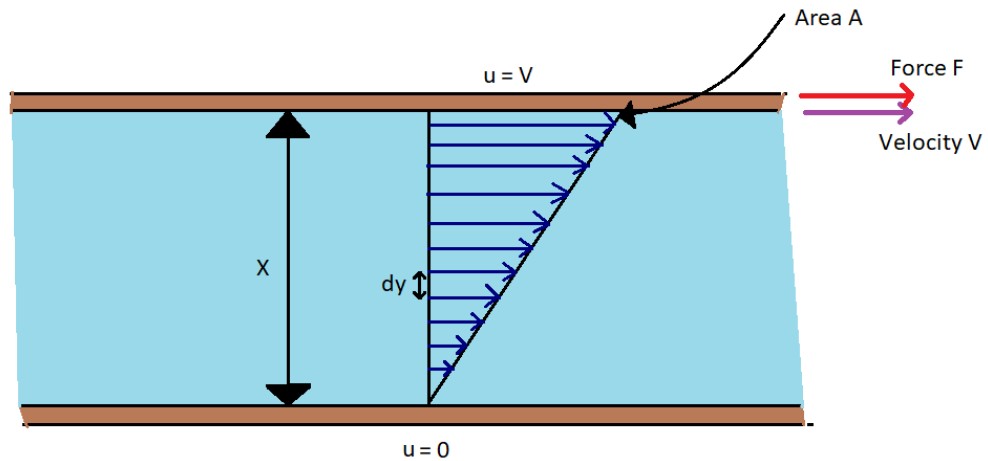
Figure 8: Viscous flow between two parallel plates

For liquids, viscosity is caused by the cohesive forces between the molecules. These forces will vary greatly depending on the temperature. As the temperature increases, the molecules in the liquid possesses more energy. The molecules will then be able to oppose the intermolecular cohesive forces more effectively, and can move more freely. Because of this, the viscosity of liquids decreases with increasing temperature. (Cimbala & Cengel, 2014)

3.3.2 Viscoelasticity

As mentioned previously, a material with viscous properties will experience an irreversible deformation when stress is applied. If a material is considered an elastic solid, applying stress will result in a deformation that is reversible up to a certain point. When the source of stress is removed, it returns to its original state. Materials do not necessarily have either elastic or viscous properties. A material that shows both elastic and viscous characteristics when deforming is called a viscoelastic material. A fluid with viscoelastic properties will return, either partially or fully, to its original state once the applied stress is removed. Mayonnaise and toothpaste are examples of fluids that possess viscoelastic properties. If no stress is applied, the toothpaste behaves as a solid and will remain inside the tube. If you apply enough pressure on the tube, the toothpaste will flow out of the tube as a high viscous fluid. Once the pressure ceases, the toothpaste will stop flowing. Viscoelastic behavior can be seen in emulsions that possesses a yield stress.

3.3.3 Newtonian and non-Newtonian fluids

Fluids like water, gasoline and alcohol are what we call **Newtonian fluids**. What characterizes a Newtonian fluid is that its shear stress and shear rate exhibit a linear relationship. The viscosity is only dependent on temperature and pressure. At a constant pressure and temperature, the viscosity remains constant and is described by the ratio between the shear stress and shear rate of the fluid (Cimbala & Cengel, 2014). Rearranging the equation for the dynamic viscosity obtained previously, one gets the following equation for the shear stress acting on a Newtonian fluid:

$$\tau = \mu \cdot \Upsilon \qquad\qquad (5)$$

Where τ is the shear stress, μ is the fluids viscosity and Υ is the shear rate.

Non-Newtonian fluids are fluids that exhibit a non-linear relationship between shear stress and rate of deformation. Its viscosity, or apparent viscosity, varies with the applied shear rate, and the viscosity alone is not adequate to describe the fluid behavior.

Emulsions can be referred to as "pseudo non-Newtonian". In some definitions, the term "non-Newtonian fluid properties" can only refer to fluids that are homogenous on a molecular level. If this definition is used, emulsions, that consist of two phases, is not a non-Newtonian fluid. Since most emulsions have rheological behavior that coincides with non-Newtonian fluids, the term "pseudo non-Newtonian" can be used. (McAuliffe, 1973) For the purpose of this thesis, since the experiments conducted does not go down to molecular level, the emulsions will be considered non-Newtonian, and referred to as such.

A Non-Newtonian fluid can be split into different categories, depending on how the viscosity changes with the duration and the magnitude of an applied shear stress. (Cimbala & Cengel, 2014)

Dilatant, or shear thickening fluids, are fluids that experience an increase in viscosity as the shear rate increases. Quicksand or the mixture of corn starch and water are examples of dilatant fluids.

Pseudoplastic fluids are fluids that exhibit a shear thinning behavior. This means that the fluid's viscosity decreases as increased shear rate is applied. Ketchup is an everyday example of a pseudoplastic fluid. If you do not shake the bottle sufficiently, the ketchup remains in the bottle. It is only when you shake it harder, that is you increase the applied shear, that the ketchup will start flowing. Drilling muds have often got pseudoplastic qualities, as the pseudoplastic behavior allows for both high drilling rates with low viscosity mud and effective transportation of cuttings with high viscosity mud.

Thixotropic and **rheopectic** fluids are fluids that exhibit time dependent shear thinning and shear thickening behavior, respectively. When exposed to a constant shear rate, the viscosity of these fluids changes with time. An example of a rheopectic fluid is cream, that gets thicker the longer you stir it. Paint is an example of a thixotropic fluid. (Schramm, 2014)

Figure 9 shows the behavior of thixotropic and rheopectic fluids.
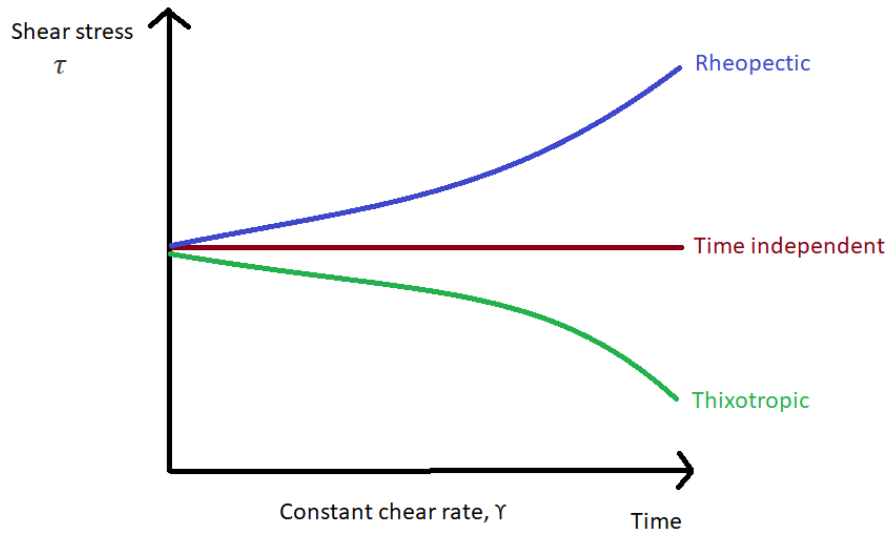
Figure 9: Illustration of the time dependency of rheopectic and thixotropic fluids.

3.3.3.1 Power law

The most common way of describing the behavior of pseudoplastic and dilatant fluids is by using the **power law** model:

$$\tau = K \cdot \Upsilon^n \tag{6}$$

where τ is the shear stress, K is the consistency index, γ is the shear rate and n is the power law index. For shear thinning fluids, $0 < n < 1$. For shear thickening fluids, $n > 1$. (Schramm, 2014). The determination of the parameters K and n for power law fluids can be found in appendix A.

The power law model is a rheological model that describes the relationship between the viscosity or shear stress, and the shear rate for non-Newtonian fluids without yield strength.

The volumetric flow of a power law-fluid can be described with the following equation

$$Q = \left(\frac{\Delta P R}{2LK}\right)^{\frac{1}{n}} \cdot \frac{\pi R^3}{\left(\frac{1}{n}+3\right)} \tag{7}$$

where Q is the volumetric flow rate, R is the radius of the pipe and ΔP is the hydraulic potential, $\Delta P = \rho g h$. The full derivation of eq. 7 can be found in appendix A.

For power law fluids, a viscosity change will be observed immediately after a stress is applied. This can be seen from the shear stress response figure, Figure 10. The flow of power law fluids starts in the origin.

3.3.3.2 Bingham plastic and Herschel-Bulkley

Bingham plastic and **Herschel-Bulkley** fluids are fluids that possesses a yield point or a yield stress. The yield point is the minimum shear-stress value at which the material will behave like a fluid. If the

16

applied stress is too little to disrupt the internal structural forces, the material will behave like a solid. (Chen, 2017) The yield point can be seen on Figure 10 as τ_0. For a Bingham Plastic, the relationship between shear stress and shear rate is described by the following equation:

$$\tau = \tau_0 + \mu_p \Upsilon \tag{8}$$

where τ is the shear stress, Υ is the shear rate, τ_0 is the yield point and μ_p is the plastic viscosity. (Beris, Tsamopoulos, Armstrong, & Brown, 1985). After the yield point is reached, a Bingham Plastic will behave like a Newtonian fluid.

A Herschel-Bulkley fluid will, after the yield strength is reached, behave in a non-Newtonian manner. It can be both shear thinning and shear thickening, depending on the power law index. If $n < 1$ it is shear thinning, if $n > 1$ it is shear thickening, and if $n = 1$ it behaves like a Bingham plastic. The relationship between shear stress and shear rate is described by the following equation:

$$\tau = \tau_0 + K \Upsilon^n \tag{9}$$

where τ is the shear stress, Υ is the shear rate, τ_0 is the yield stress, K is the consistency index and n is the power law index. (Hemphill, Campos, & Pilehvari, 1993) The determination of the parameters K and n for a Herschel-Bulkley fluid can be found in appendix A.

When describing rheological behavior of drilling fluids, Herschel-Bulkley is the preferred model as it usually results in the most accurate results. (Hemphill, Campos, & Pilehvari, 1993)

The volumetric flow of a Herschel-Bulkley fluid can be described with the following equation:

$$Q = v_0 \pi \left(r_0 + \frac{2n+2}{2n+1} r_0 (r_w - r_0) + \frac{n+1}{3n+1} (r_w - r_0)^2 \right) \tag{10}$$

where $\qquad r_0 = \tau_0 \frac{2L}{\Delta p} \qquad$ and $\qquad v_0 = -\left(\frac{\Delta p}{2KL} \right)^{\frac{1}{n}} \frac{n}{n+1} (r_w - r_0)^{\frac{n+1}{n}}$

The derivation of this equation can be found in appendix A.
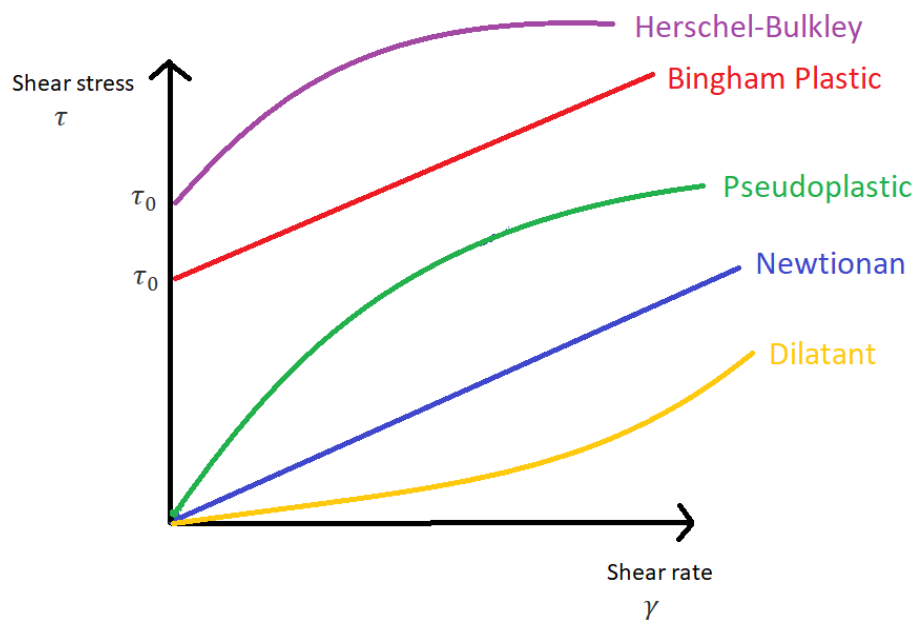
Figure 10: Shear stress responses for different fluids

3.3.4   Fluid flow in pipes

When emulsions are formed during oil production, the fluids flow through circular pipes. It is therefore of interest to see what kind of mechanisms and forces take place when fluids flow through circular pipes.

As mentioned when explaining a Couette flow, a fluid can be seen a group of many thin parallel layers. In fluid dynamics, one separates between laminar and turbulent flow. When a fluid flows laminarly through a circular pipe, all the layers flow parallel to the pipe wall. The streamlines are smooth, and the flow is orderly. The velocity profile for a fully developed laminar pipe flow can be seen in Figure 11. From this figure one can see that the average velocity of a fully developed laminar pipe flow, v_{avg} is half the maximum velocity, v_{max}. (Cimbala & Cengel, 2014) The average velocity is commonly used when calculating laminar pipe flow, since the actual velocity is difficult to obtain.
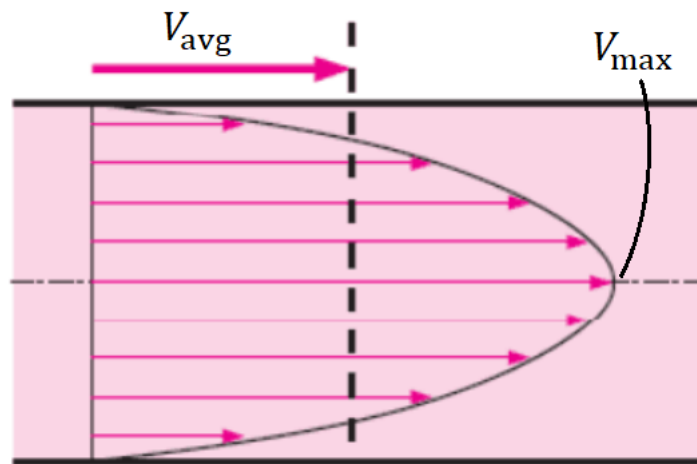
Figure 11: Velocity profile for a fully developed laminar flow. Adapted from (Cimbala & Cengel, 2014)

When the velocity of a fluid flow passes a certain velocity, it changes from laminar to turbulent flow. The velocity at which this occurs is called the critical velocity. A turbulent flow is characterized by chaotic flow lines and disruption between the layers. Its average velocity is more difficult to define, as it varies continuously. Compared to the velocity profile of laminar flow, which is parabolic, a turbulent flow velocity profile is much flatter.

Whether the flow regime is laminar, turbulent or a transition between the two depends on many factors, including flow velocity, temperature, geometry, type of fluid and the surface roughness of the pipe. A way of predicting the flow regime in a specific situation is by using the Reynolds number. The Reynolds number is defined as the ratio between inertial and viscous forces, and for an internal flow in a circular pipe the Reynolds number is

$$Re = \frac{V_{avg}D}{v} = \frac{\rho V_{avg}D}{\mu} \tag{11}$$

where V_{avg} is the average flow velocity, D is the characteristic length of the geometry, in this case the diameter of the pipe, and $v = \frac{\rho}{\mu}$ is the kinematic viscosity of the fluid. For a non-Newtonian fluid, this viscosity will depend on the applied shear rate, and the Reynolds number will vary with the current flow conditions. Calculating the Reynolds number for a non-Newtonian fluid is very comprehensive. It is often considered sufficient to apply simplifications if the flow is considered laminar. (Madlener, Frey, & Ciezki, 2009) For the experiments conducted in this thesis, the method for approximating the Reynolds number shown in eq. 11 is used. To ensure the accuracy of the results, the Reynolds number was calculated based on a range of viscosities. Viscosities corresponding to shear rates up to 1200 s^{-1} were used, to make sure that the flow regime stayed laminar during the whole experiment.

Although the flow regime of a circular pipe also depends on several other things, the following values can be used in most cases to determine flow regime:

Re ≤ 2300	Laminar flow
2300 ≤ Re ≤ 4000	Transitional flow
Re ≥ 4000	Turbulent flow

Fluid flow is a very complex and comprehensive subject. So far, the theoretical solution for fully developed laminar flow in a circular pipe is one of very few theoretical solutions existing for fluid flow. For fluid problems that do not fall under this category, one must use experimental results and empirical relations to analyze the flow. This give room for errors, and the accuracy of "non-ideal" fluid flow calculation is expected to be worse than for a fully developed laminar flow. (Cimbala & Cengel, 2014)

High viscosity fluids, such as emulsions, flowing through small pipes are one of the few practical examples where the flow is laminar. (Cimbala & Cengel, 2014) If the flow were to turn turbulent, the flow would become chaotic and disorderly. This would result in much higher shear rates experienced by the emulsion, which again results in larger viscosity changes. Given the complexity of turbulent flow, the focus of the experiments conducted in this thesis have been on laminar flow.

3.3.5 Entry length

When discussing the velocity profiles of laminar flow, the flow is assumed to be fully developed. When a fluid enters a circular pipe, there is a certain length where the flow is not yet fully developed, and viscous effects and velocity changes are significant. This region is called the boundary layer. Due to the no-slip condition and viscous forces, a fluid entering a circular pipe will have a velocity gradient that gradually develops along the pipe. Further down the pipe the velocity becomes fully developed.

The distance from the pipe inlet to the point where the flow becomes fully developed is called the hydrodynamic entrance length, L_h.
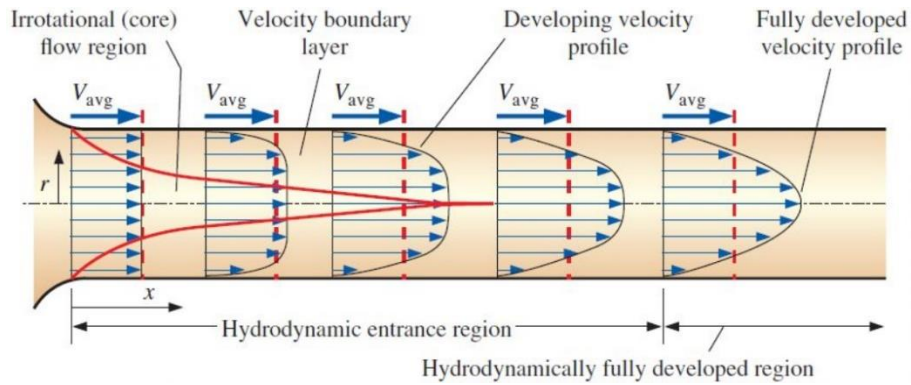
Figure 12:The development of a velocity boundary layer in a pipe. (Cimbala & Cengel, 2014, s. 351)

For laminar flow, the dimensionless hydrodynamic entrance length is given by

$$\frac{L_{h,laminar}}{D} \cong 0{,}05Re$$

For turbulent flow, the entry length is given by

$$\frac{L_{h,turbulent}}{D} = 1{,}359Re^{\frac{1}{4}}$$

Since turbulent flow is much less dependent on the entry length, it is often approximated as

$$\frac{L_{h,turbulent}}{D} \approx 10$$

4 EXPERIMENTS

4.1 PREPARING THE EMULSIONS

For the purpose of this thesis, a standard 15w-40 engine oil was used. The engine oil contains natural emulsifiers, so an additional emulsifier was not needed. It is also assumed that the emulsion made from engine oil will have rheological properties similar to an emulsion made with a crude oil found in a reservoir. This made the engine oil a reasonable alternative to crude oil, as the purpose of the experiment was to investigate the physical rheological behavior of the emulsion. As W/O emulsions are the most encountered type of emulsion in the oil industry, this is the type of emulsion used in the experiments.

All emulsions were prepared using a synthetic brine with 3% NaCl. The brine was made by mixing 3 grams of NaCl per 100 mL distilled water.

Before mixing the two fluids, their density was measured using a pycnometer.

The pycnometer works by using the relationship between mass, volume and density. The volume of the pycnometer is known, and by weighing the pycnometer both with and without the fluid, the weight of the fluid is obtained. Then the density can easily be found by applying that $\rho = \frac{m}{V}$. The results obtained are shown in Table 1.

Table 1: The measured densities of engine oil and saltwater, obtained using a pycnometer

Engine oil [g/cm^3]	Saltwater 3wt%NaCl [g/cm^3]
0.8989	1.02274

An oil density of 0.8989 g/cm^3 corresponds to an API gravity of 25,9. This corresponds to a medium heavy crude oil. (petroleum.co.uk, 2018)

Seven different W/O emulsions were made, with water content ranging from 10-70 wt%. To separate the different emulsions, they are named according to their amount of water and oil, with the water content stated first. An emulsion with a water content of 30% and an oil content of 70% will be referred to as W30-O70. The emulsions were made in batches of 400 mL, and the amount of water and oil needed to meet the required weight percentages was found using the relationship

$$m = \rho \cdot V \qquad\qquad (12)$$

The amounts used are shown in Table 2. A complete derivation of how the wt% was found can be found in appendix A.

Table 2: The amount of saltwater and engine oil used to make 400 mL of emulsion with water content from 10-70%

wt% of Water	Water [g]	Oil [g]
10	36.4	372.6
20	61.3	211.6
30	92.0	185.1
40	122.7	158.7
50	153.4	132.2
60	184.0	105.8
70	214.7	79.3

The emulsions were made by mixing the saltwater and engine oil together in a 400W blender with a rpm of 18,000 for 90 seconds. The ambient temperature was 21 °C. All emulsions were mixed for the same amount of time, to ensure that they all created a stable emulsion. When making the W70-O30 emulsion, it was originally mixed for the same amount of time as the previous emulsions; 1.5 minutes. This resulted in a very unstable emulsion that separated shortly after mixing. This can be seen in Figure 13. In order to create a more stable emulsion, mixing time was increased to 20 min. This resulted in an emulsion that did not separate after mixing, and was fit for further testing.

Longer mixing time could affect the stability and rheological properties of the emulsion. In order to have a basis for comparison for the W70-O30 emulsion, additional W50-O50 and W60-O40 emulsions were made with a mixing time of 20 minutes. This ensured that the effect of mixing time and energy dissipation could be studied.

To ensure that the emulsions were W/O and not O/W emulsions, a simple drop test was conducted right after mixing. The test was done by putting a small drop of the emulsion in a water-filled container. A drop from a W/O emulsion would still hold its shape due to the hydrophobic forces, while an O/W emulsion would dissolve in the water. Figure 14 shows the drop test. In the picture to the left, a few drops of the emulsion are poured in water. On the picture to the right, the same emulsion is poured in oil. One can clearly see that the drops in the picture to the left hold their shape, while they blend together with the continuous phase in the picture to the right. All the emulsions were confirmed as W/O emulsions.

Figure 13: Emulsions after mixing. To the left: W30-O70 emulsion shortly after mixing. To the right: W70-O30 emulsion shortly after mixing. One can clearly see that the emulsion has separated in to two distinct layers.
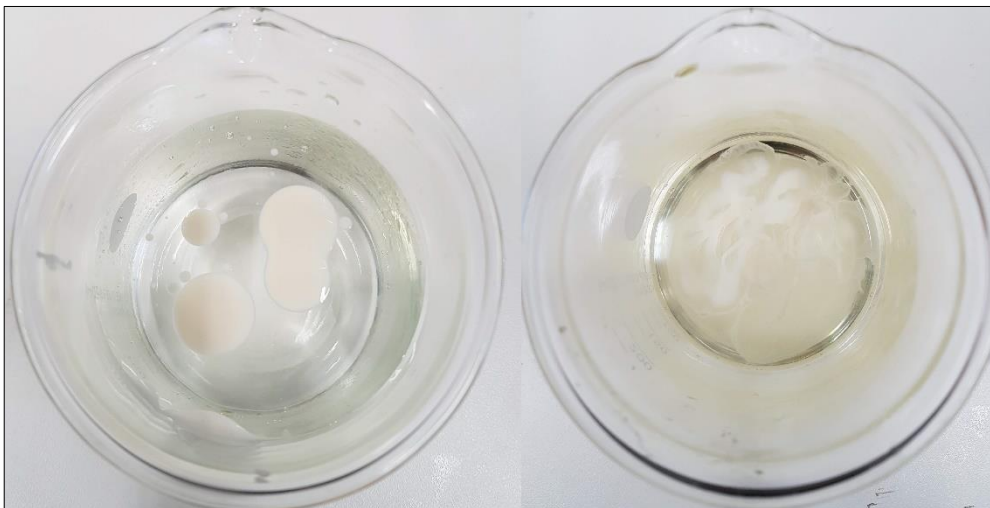
Figure 14: Pictures of the drop test. To the left, clearly defined drops of emulsion in water. To the right, same emulsion dissolving in soy oil.

The density of the emulsions was found using a mud balance. A pycnometer was intended to be used, but the samples were too viscous, and a mud balance, or a mud scale, was chosen instead for the sake of convenience. A mud balance consists of a graduated beam with a cup in one end and an adjustable weight in the other. A small bubble on the beam indicates when it is leveled. The liquid is poured in to the cup, filling it completely. The weight is adjusted so that the beam is leveled, and the density can be read off the point where the weight sits. The densities were measured when the samples were fresh. The results are shown in Table 3. The corresponding dissipation rate for the different emulsions are shown in Table 4.

Table 3: Densities of the different emulsions, measured using a mud balance

Water content [%]	Density, fresh sample [g/cm^3]
10	0.844
20	0.869
30	0.875
40	0.908
50	0.920
60	0.929
70* mixed for 20 min	0,971

Table 4: The dissipation rate for the different emulsions

Emulsion [%]	Dissipation rate [W/kg]
10	1184.8
20	1150.7
30	1142.9
40	1101.3
50	1087.0
60	1076.4
70* mixed for 20 min	1029.9

4.2 DETERMINATION OF FLUID MODEL

To find out what kind of rheological model best matches the different emulsions, their rheological qualities need to be determined. This was done using an Anton Paar Modular Compact Rheometer 302, shown in Figure 16. The test conducted was a flow curve test, which measures the viscosity and the shear stress of the emulsions at different share rates and temperatures. For these purposes the rotary bob and associated cup were used, as illustrated in Figure 15. A sample of the emulsion was poured in to the cup, and both the cup and rotary bob was attached to the rheometer. Then the desired shear rates and temperatures were set, and the test was run. The cup remained stationary while the bob rotated.

The emulsions were tested at share rates ranging from 0.1-1200 s^{-1}. During oil production and processing, fluids can experience share rates at around 1000 s^{-1}, and the range of share rates were

therefore chosen to reach such a level. The samples were also tested at different temperatures. The temperatures that were tested were 4, 20, 40 and 60 °C, which are temperatures that oil is likely to obtain during the recovery process or in-citu. Although the temperature in a real operating process can exceed 60 °C, this was set as maximum for safety reasons. The engine oil and synthetic brine used to make the emulsions were also tested under the same conditions.
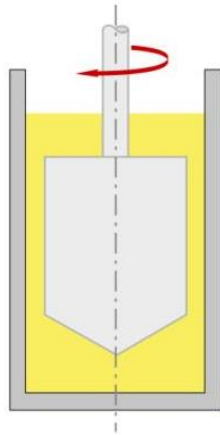

Figure 15: Rotary bob and cup.   Figure 16: The Anton Paar MCR 302 (Consult, 2017)

The flow curve test was run several times, to see the effect of aging. The samples were tested when they were fresh, after 5 hours, after 24 hours, after 1 week, and finally after 2 weeks had passed. If any oil had come out of solution during aging, the samples were gently stirred before the tests were run.

The flow curve test conducted only tests how the fluid behaves once it is already flowing. If the emulsion possesses any yield strength, this would not be possible to see from this test.

To check if any stress must be applied to initiate fluid flow, a test using the "Steady State Stress Sweep Method" was conducted using the Anton Paar Modular Compact Rheometer 302. (Chen, 2017) In this test, a stress is applied incrementally in logarithmic steps, from a very low shear rate value up to a value where the fluid starts to flow. Before the yield point is reached, the viscosity remains constant with increasing shear rate. After the yield point is reached, the viscosity decreases many orders of magnitude over a small range of shear rates. The "Steady State Stress Sweep Method" was found fitting as the fluids tested are medium viscosity materials. The method is not suited for low viscosity fluids, as it is hard to get accurate results if the yield stress is too low. It is also unsuited for very high viscosity fluids because one might have wall slippage between the bob or cup and the fluid. When conducting the test, 15 points per decade were chosen to get sufficiently accurate results. The test was run at 4, 20, 40 and 60 °C.

The amount of oil to come of solution was also investigated. This was to see how the amount of water affects the maturation of the emulsion. Samples of W20-O80 and W60-O40 emulsion were kept in ovens with different temperatures. This was to see how temperature effects the amount of oil to come

out of solution. The emulsions were kept at 23, 40 and 60 °C, and the amount of oil to come out of solution was inspected visually and measured using a measuring band. A sample of W60-O40 emulsion mixed for 20 minutes was also kept at the same temperatures. This was to compare the two W60-O40 emulsions and see if mixing time had any effect on amount of oil to come out of solution.

4.3   DROPLET SIZE/DISTRIBUTION ANALYSIS

The droplet size and distribution of the water dispersed in the oil was also investigated. The emulsions were studied using an optical microscope. After testing the different lenses, the 40x magnifying lens was chosen as the most suited one. The microscope was connected to a camera and the program Stream Basic, which allows one to record and take pictures of the substance being investigated. When using the 40x magnifying lens, not a lot of light gets through. In order to get a bright enough image of the emulsion, the exposure time on the camera had to be set high enough. After trying several different exposure times, 195 ms was chosen as an appropriate time. Figure 17 shows the difference between short and long exposure time.
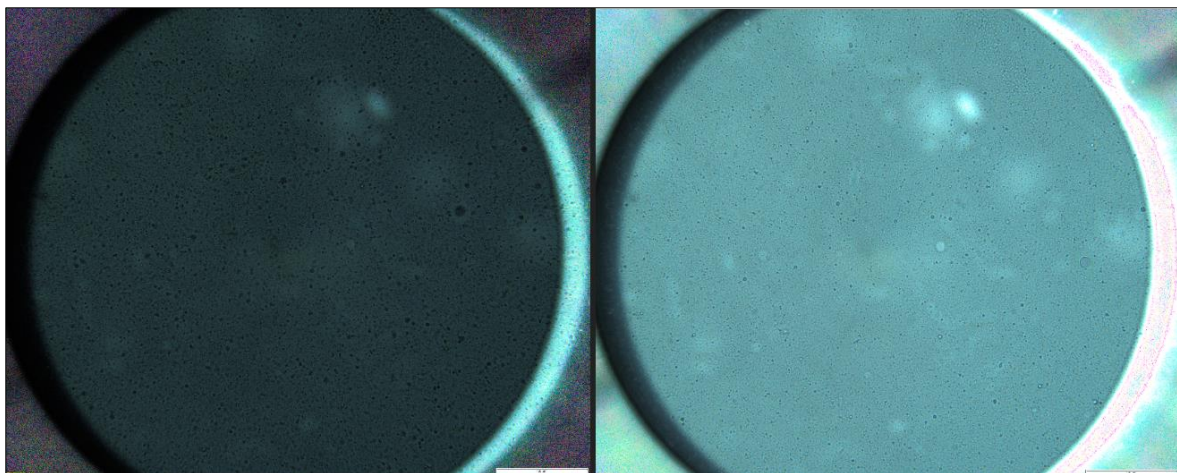
Figure 17: Difference in exposure time. To the left: Low exposure time. To the right: Increased exposure time.

Before analyzing, a single drop of emulsion was diluted with 1.5 mL of engine oil. This was done in order to get an image that is easier to process. The amount of oil needed to dilute the emulsion sufficiently was found by trial and error.

Figure 18 shows the difference between too little dilution and the right amount of dilution. A single drop of the diluted emulsion was then placed between two glass plates, and investigated through the microscope.
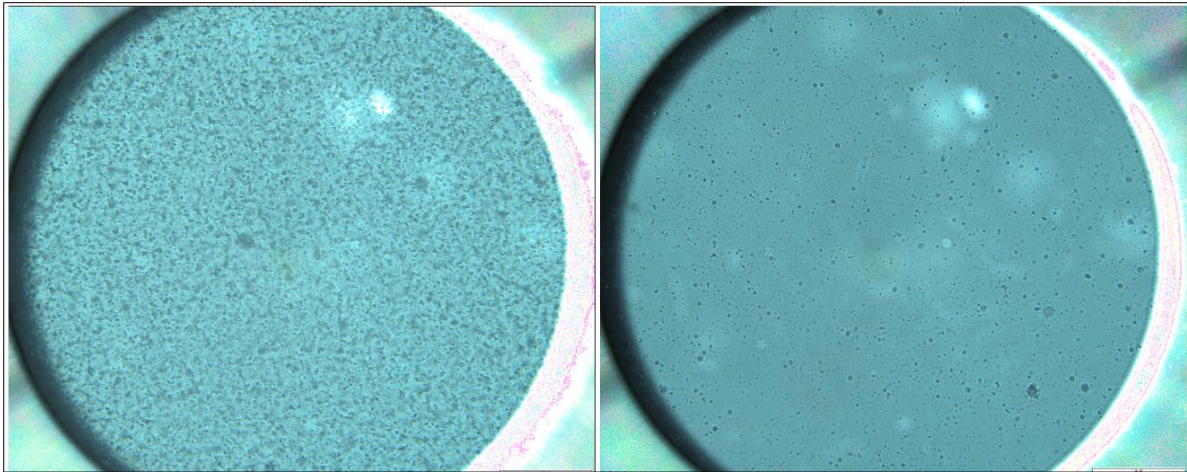
Figure 18:Dilluting the emulsion. To the right, too little dilution. To the right, appropriate amount of dilution.

The resulting images were then processed using ImageJ, a scientific image processing program. (ImageJ, 2018) An evenly illuminated section of the image was chosen, as seen in Figure 19, and the section was processed so that the dispersed water droplets could be analyzed. Contrasts on the image were enhanced, and the image was made black and white. If any droplets had not been detected by ImageJ, these had to be manually drawn in. This process can be seen in Figure 20. A detailed procedure of how the images were processed in ImageJ can be found in appendix B.
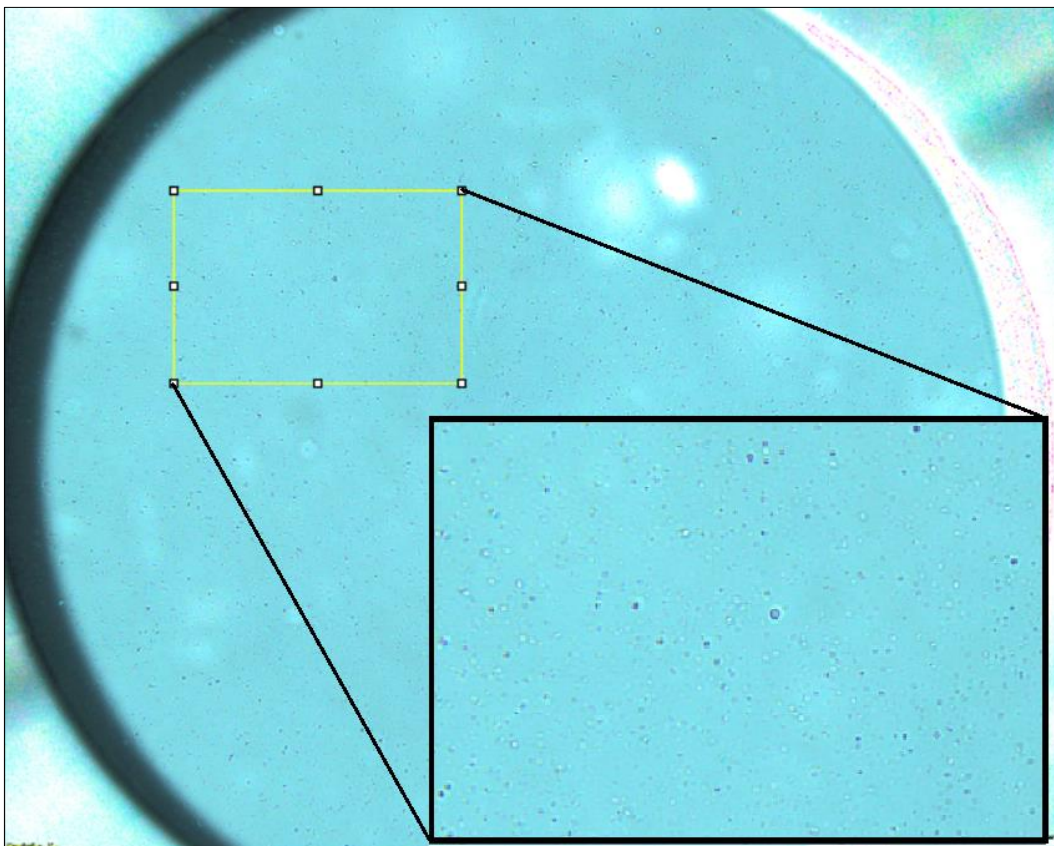
Figure 19: Image processing. Choosing an even illuminated part of the picture for further processing.

ImageJ analyzes the processed image, and returns the area, Feret diameter and minimum Feret diameter of the droplets. The Feret diameter can be defined as "The distance between two parallel tangents on opposite sides of the image of a randomly oriented particle." (Merkus, 2009) An illustration of the Feret diameter can be seen in Figure 21.
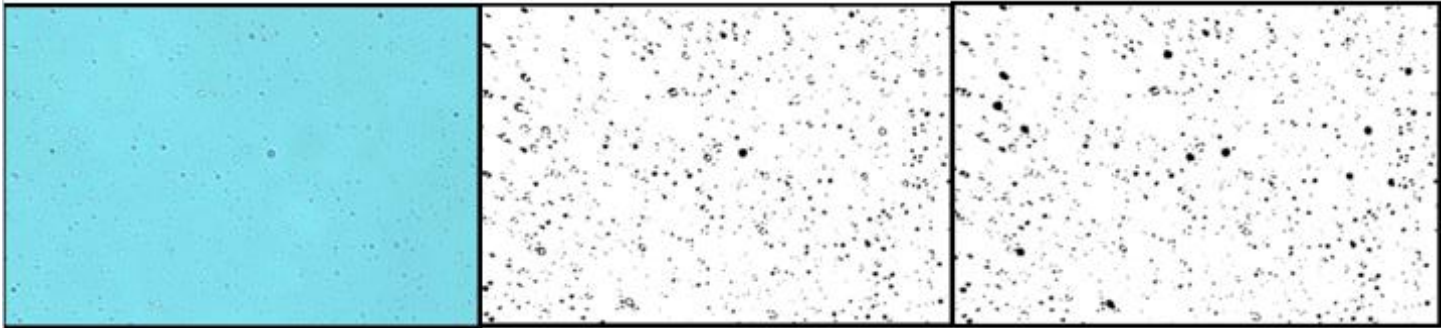
Figure 20: Analyzing the droplets. Left: The untouched image. Middle: After applying filters and enhancing contrasts, the image is made black and white. Right: Any obvious droplets not detected by ImageJ is manually drawn in. The original photo is used to compare.

A MatLab script, made by Harald A. Asheim was then used to give a graphical representation of the droplets. The droplets were assumed to have the shape of a rotational ellipsoid, where the volume is calculated the following way:

$$V = \frac{4}{3}\pi \cdot r_{Feret,min} \cdot r_{Feret,max}^2 \qquad (13)$$

and the droplet surface area is found using the following equation:

$$S_f = \pi \cdot \left(\frac{d_{max}^{2pf} + 2d_{max}^{pf} \cdot d_{min}^{pf}}{3}\right)^{\frac{1}{p_f}} \qquad (14)$$

The parameter p_f is assumed to have the value 1,6075, as this is the optimal value for nearly spherical ellipsoids. (Michon, 2015)
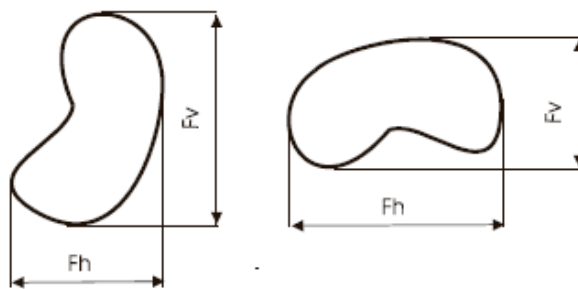
Figure 21: Feret diameter

The script produces two graphs, as can be seen in Figure 22. The top graph shows the cumulative distribution of the droplet volume. It depicts the measured distribution along with an optimized

distribution and a log-normal distribution based to the optimized parameters. If the measured distribution deviated severely from the optimized distribution, the results were not considered. The script also gives the mean value, and the measured standard deviation. The standard deviation was calculated by numerical integration. A large standard deviation indicates a wide distribution in droplet size, and is synonymous with a polydisperse emulsion.

The bottom graph shows the distribution density of the droplet volume. On this curve one can see the most encountered droplet volume, which occurs where the curve has its maximum. The value of the distribution density gives an indication of how well distributed the droplet volumes are. If the distribution density is high at certain volume, it means that a large number of the droplets have that specific volume.
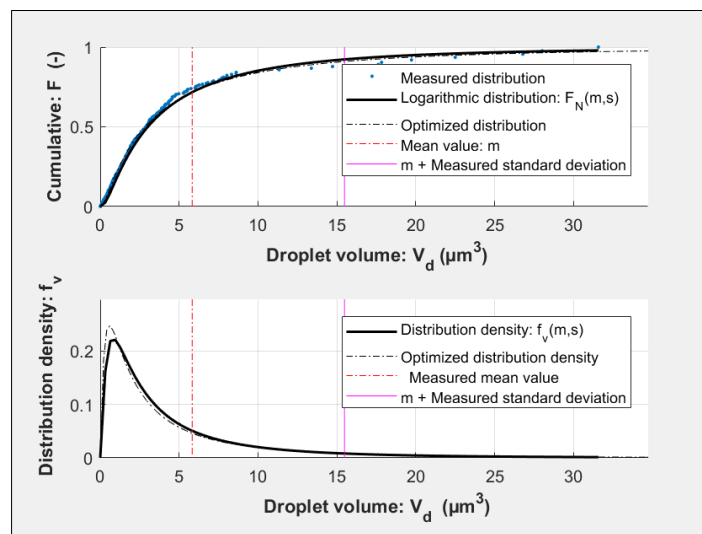
*Figure 22: The resulting graphs from running the MatLab script*

4.4   INTERFACIAL TENSION

In order to explain why the emulsions behave differently at different temperatures, it is of interest to see how the interfacial tension between the engine oil and the synthetic brine changes with varying temperature. To do this, the two liquids were tested using a drop shape analyzer, DSA. The DSA uses the pendant drop method to measure the interfacial tension. The IFT was tested at 4, 20, 40 and 60 °C. A picture of the process is shown in Figure 23.

A pendant drop of the engine oil is submerged in the denser saltwater. The pendant drop will deform due to gravity, and the degree of deformation depends on the interfacial forces. The DSA takes a shadow image of the pendant drop, and analyzes the shape. By using the Young-Laplace equation and comparing the shadow image with the calculated drop shape, the interfacial forces acting between the two fluids can be found.

31

The B factor, or the shape factor, measures the correlation between the calculated and the actual drop image. The B factor should be at least 0,4 to ensure accurate results.

Figure 23: Measuring the IFT between engine oil and synthetic brine at 60 °C

4.5 FLOW EXPERIMENT

Earlier studies and the tests conducted so far have indicated that the emulsions behave non-Newtonian, and have properties matching either the power law or the Herschel-Bulkley fluid model. Theoretical solutions for calculating the volumetric flow of power law and Herschel-Bulkley fluids have been derived.

In order to compare the calculated flow rates with the actual flow rates, a flow experiment was conducted. A miniature flow setup was built in the lab using buckets, tubes and valves.

The measurements of the setup were designed using the emulsion parameters found from testing, combined with the Herschel-Bulkley flow rate equation. The setup was designed so that the emulsion would flow laminarly, and that it would flow for a reasonable amount of time. To do this, the Reynolds number was needed. All emulsions were assumed to show shear thinning behavior, and the Reynolds number was calculated for shear rates up to 1200 s^{-1}, to ensure that the flow would not turn turbulent during the course of the experiment. The entry length was also calculated, to make sure it did not affect the results. The largest entry length experienced was found to be 1,2% of the total tube

length, and therefore negligible. A schematic of the final measurements can be seen in Figure 24. The actual setup is shown in Figure 25.

It was decided that only the W20-O80 and W60-O40 emulsions would be tested in the flow setup. A significant amount of emulsion was needed to conduct the experiment, and based on the results obtained from the flow curve test, it was considered sufficient to only run the test on these two emulsions. 5 liters of each emulsion was made in batches of 400 mL, and poured into the top bucket with the valve closed. The emulsion was given time to fill the tube completely before the valve was opened.

The volumetric flow of the emulsions was found by continuously measuring the mass of emulsion flowing through the tube. An empty bucket was placed under the valve, and the bucket was placed on a scale, as shown in Figure 26. A logging program created using LabView, a systems engineering software, continuously recorded the weight as the emulsion filled the bucket.

The recorded weight was then plotted against time, and the mass rate was found taking the slope of the linear part of the plot. Each emulsion was run through the flow rig two times.

The emulsions were tested fresh and after 2 weeks had past.
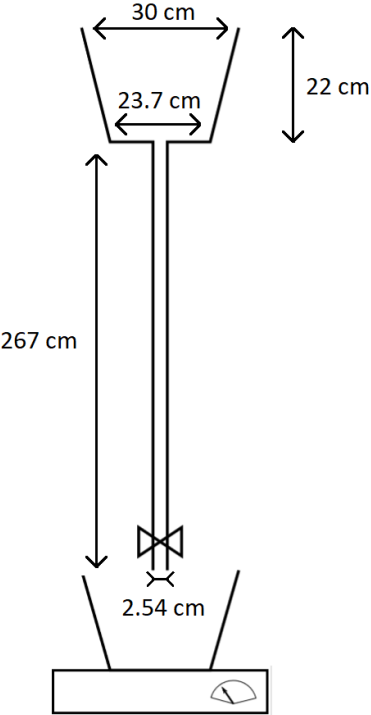
Figure 24:A schematic of the flow setup.

Figure 25: The actual flow setup

Figure 26: Weight connected to LabView

After the flow test was run, the actual flow rates were compared to the theoretical flow rates obtained from the power law and the Herschel-Bulkley approximations. In addition, the measured flow rates were compared to flow rates obtained using the Hagen-Poiseuille equation. The Hagen-Poiseuille equation is an equation that assumes an incompressible Newtonian fluid that flows laminarly through a circular pipe. The Hagen-Poiseuille equation for volumetric flow can be written as follows:

$$Q = \frac{\frac{\rho g h}{L} \cdot \pi D^4}{128 \mu}$$

(15)

where $\rho g h$ is the hydrostatic pressure, D is the diameter of the pipe, L is the length of the pipe and μ is the dynamic viscosity. Since the fluids tested possess non-Newtonian fluid properties, a single value for the viscosity is hard to obtain. An average viscosity was therefore used based on the results from the Anton Paar viscometer test. The viscosities used where 2,0 Pa·s for the W60-O40, and 0,4 Pa·s for the W20-O80 emulsion.

The Hagen-Poiseuille equation was added to compare it to the other approximations, and see what difference using the appropriate model makes. The two non-Newtonian models should provide more accurate results.

5 RESULTS AND DISCUSSION

All the emulsions showed a non-linear relationship between shear rate and shear stress, and a viscosity dependency that coincides with a non-Newtonian fluid. At low shear rates, all emulsion samples showed shear thinning behavior. At higher shear rates, some emulsions showed more Newtonian behavior, depending on the conditions. Increased shear rate seems to promote emulsion breaking. This contradicts the results found by Kokal (1999), where high shear rates were associated with stable emulsions.

From the results obtained from the yield test and the flow curve test, it can be concluded that the emulsions behave according to the Herschel-Bulkley fluid model. Many of the emulsions had a yield point so low that the power law model could be used as a simplified model.

Figure 27 shows the viscosity of the engine oil and synthetic brine compared to the W20-O80 emulsion at 20 °C. As can be seen from the graph, the emulsion possesses a viscosity that is closer to the continuous phase. Both the engine oil and the brine show a viscosity that is independent of shear conditions, and behaves Newtonian.
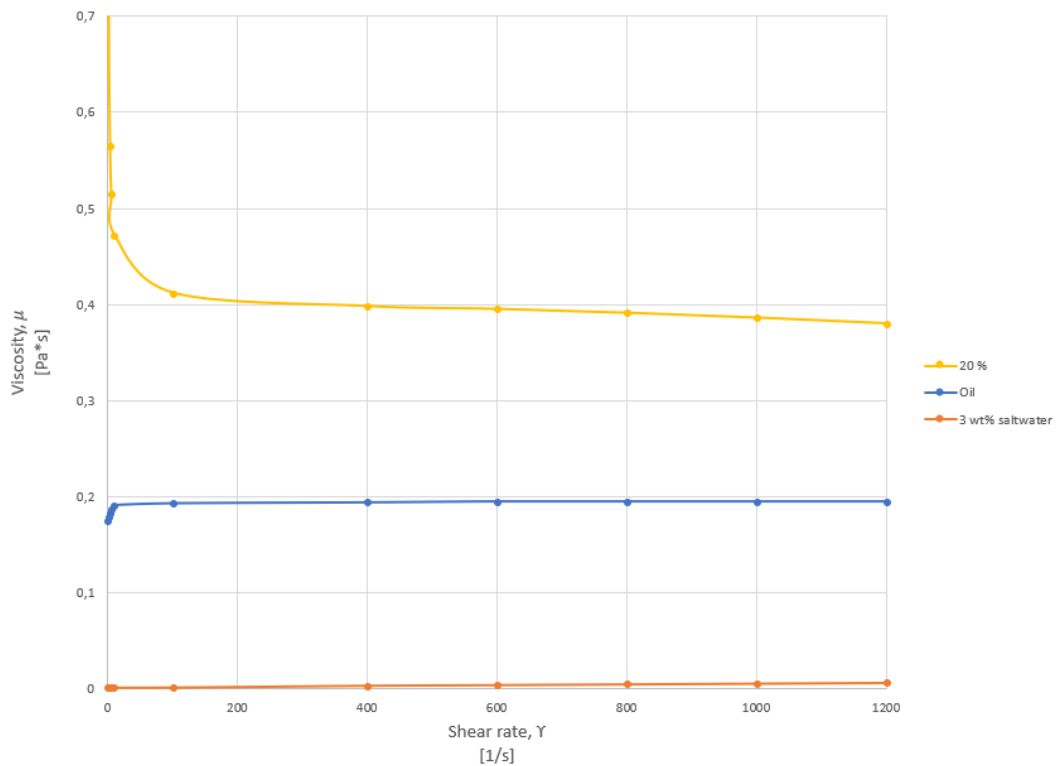
Figure 27: Viscosity of the engine oil and 3 wt% saltwater at 20 °C. W20-O80 emulsion for comparison.

5.1 YIELD STRESS

Table 5 shows the measured yield stress from the yield test using the Steady State Stress Sweep Method. As one can see from the table, all emulsions possess some yield strength. Figure 28 shows the yield test for the W40-O60 emulsion at 20 °C. It shows a constant viscosity of almost 16 $Pa \cdot s$ with increasing shear rate up until about 0.006 s^{-1}, then it drops. This is a clear indication of yield strength.

Table 5: Measured Yield Points

Yield point [Pa]				
Temp.[°C] \ wt% W	4	20	40	60
20%	0.109	0.02	0.014	0.011
30%	0.18	0.04	0.04	0.03
40%	0.3	0.084	0.07	0.06
50%	0.32	0.22	0.94	0.18
50% 20 min	0.1	0.07	0.05	0.05
60%	0.33	0.434	1.38	0.32
60% 20 min	0.11	0.09	0.06	0.05
70% 20 min	0.6	3.3	1.97	1.62

Although all emulsions had a yield point, many of them occurred at very low shear rates and had a very low shear stress value. Most of the emulsions showed a decreasing yield strength with increasing temperature.

If the samples mixed for 20 minutes are ignored, the yield strength seems to increase with increasing water content.

The emulsions mixed for 20 minutes shows a lower yield strength than the emulsions mixed for only 1.5 minutes.
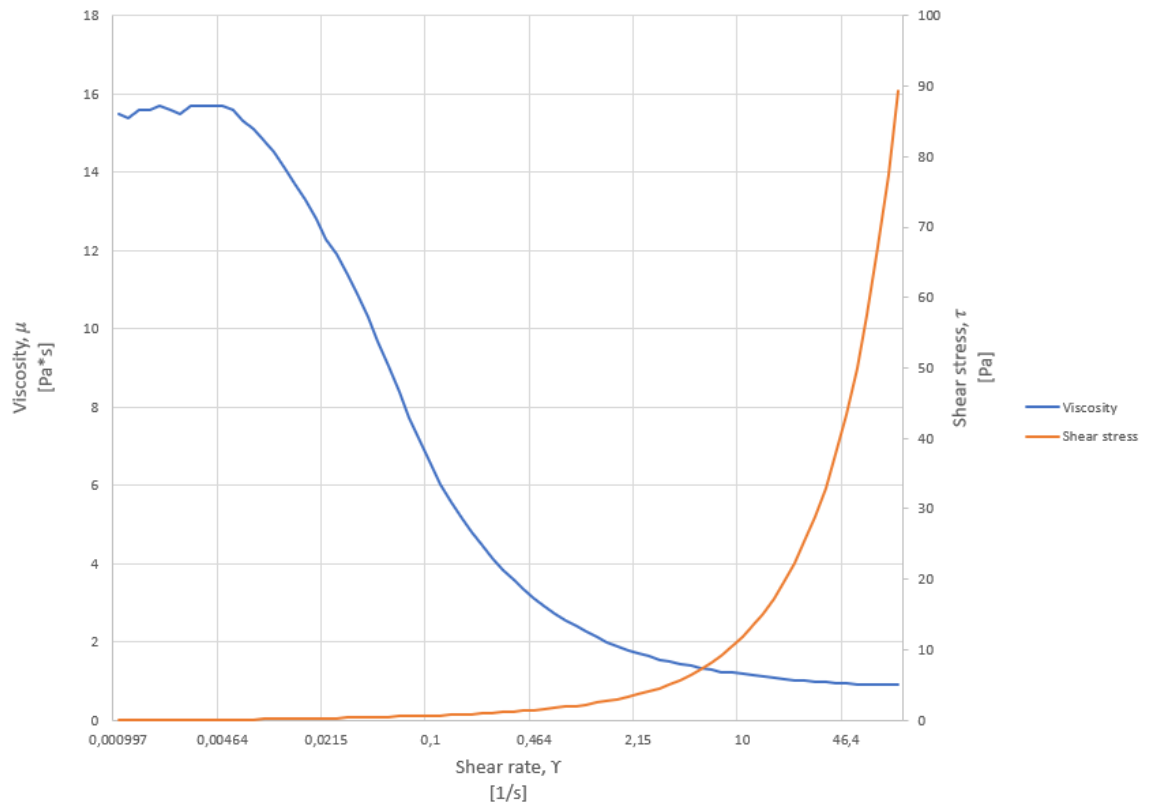
Figure 28: Yield test for W40-O60 emulsion at 20 °C.

5.2 INTERFACIAL TENSION

Figure 29 shows the IFT between the engine oil and synthetic brine at the different temperatures. One can see that the IFT is generally decreasing with increasing temperature. This is to be expected. The IFT shows a slight increase from 20 °C to 40 °C. This contradicts the previous assumptions. A possible reason for this could be that the oil droplet that was used to measure the IFT at 40 °C had been created an hour before the measurement was made. Aging of the droplet could affect the results. It can also be seen from Figure 29 that the IFT at 4 °C is significantly higher than at the other temperatures. This is reflected in the other rheological test, where the emulsions at 4 °C shows significantly higher viscosities and breaks at lower shear rates.
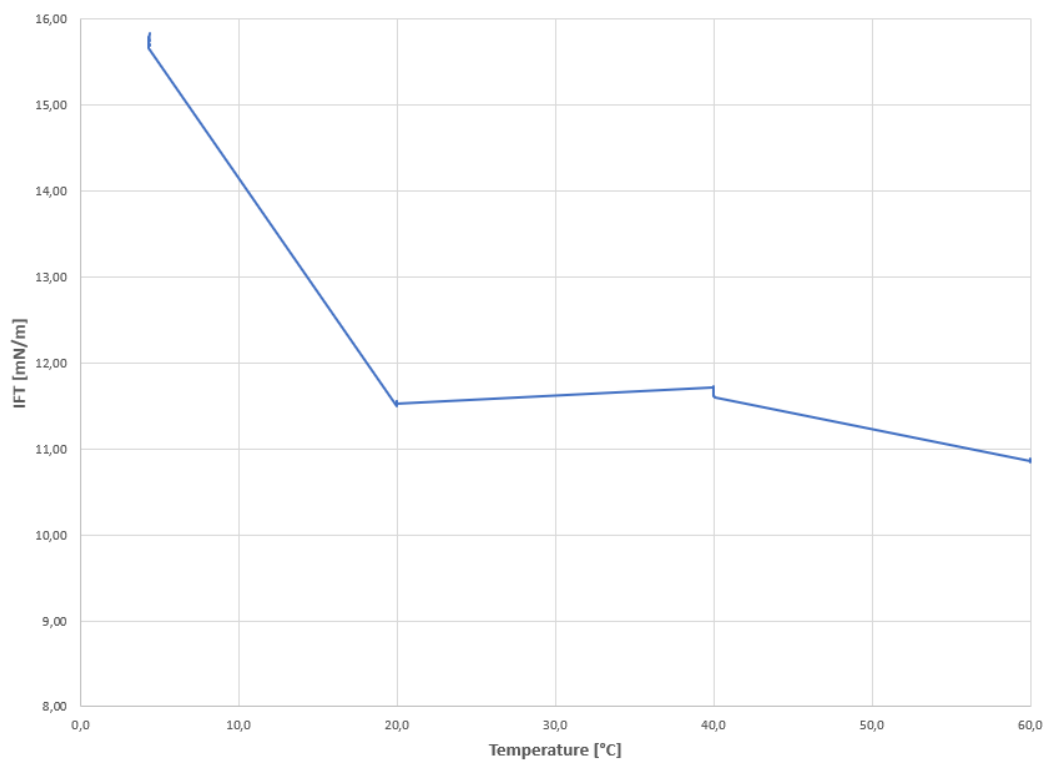
Figure 29: IFT vs temperature for engine oil and synthetic brine

5.3   WATER CONTENT

In Figure 30, the emulsions are plotted when tested at 4 °C. The emulsions show increased shear stress with increased water fraction. The W60-O40 emulsion breaks at around 1000 s^{-1}. Higher water content seems to promote emulsion breaking. This is in line with the findings of Kokal (1999). Higher water content results in a looser emulsion that will break at lower shear rate.

Figure 31 shows apparent viscosity plotted against shear rate at 60 °C. One can clearly see that a higher water content results in higher viscosities. It can also be seen from the plot that the higher water content, the more shear thinning behavior the emulsion exhibits. The emulsion with the lowest water content shows nearly Newtonian behavior over the entire range of shear rates.

Hemmingsen et al. (2005) found that higher viscosities result in more stable emulsions. In this case, higher viscosity corresponds to a higher water content. High water content was just found to cause a less stable emulsion, so this contradicts the results obtained. A possible conclusion is that water content plays a bigger role in emulsion stability than viscosity does.
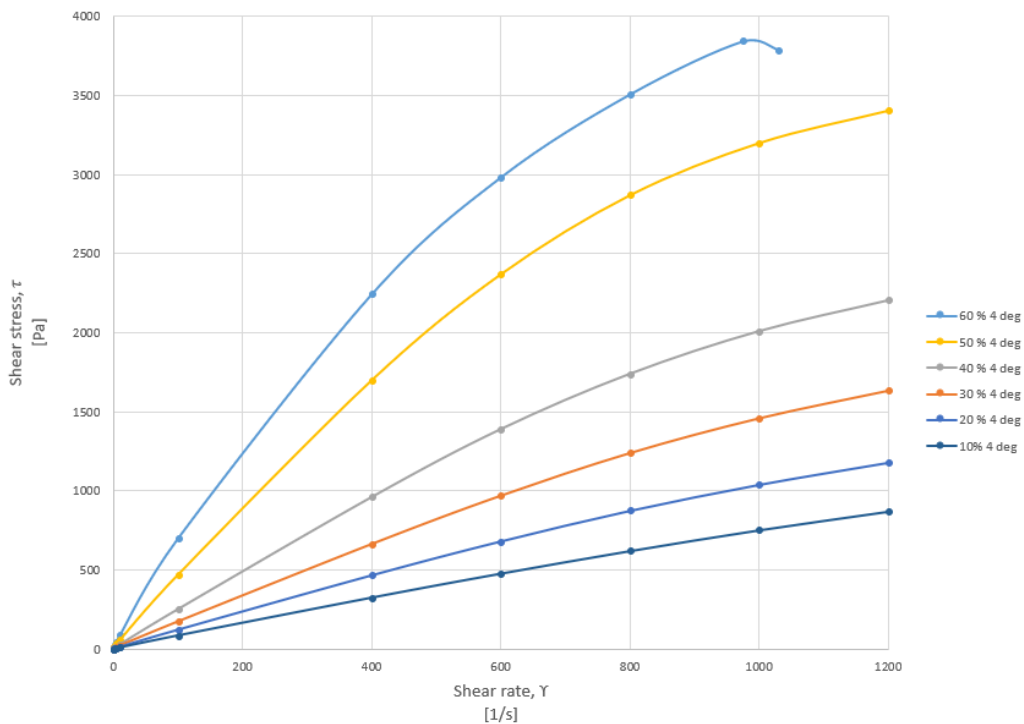
Figure 30: Shear stress vs shear rate for emulsions with different water content at 4 °C
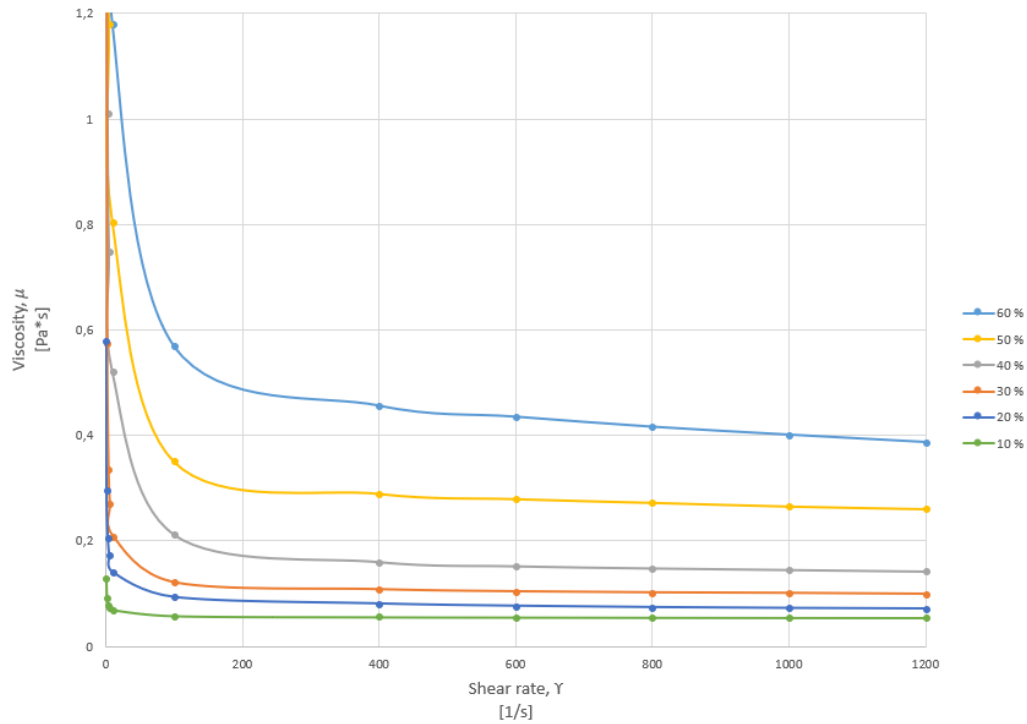
Figure 31: Apparent viscosity vs shear rate at different water content. Test run at 60 °C.

As predicted by Schramm (1992), an increase in water fraction will result in a wider distribution of the droplet size. This was investigated by comparing the droplet distributions obtained by the microscope analysis. Figure 32 shows the cumulative droplet volume distribution of the W80-O20 and the W60-O40 emulsion, respectively. The standard deviation of the droplet volume, in the figures market with a purple line, shows how much the droplet size distribution deviates. The W60-O40 emulsion shows a much higher deviation in droplet size. This can also be seen from comparing the distribution densities of the emulsions. If comparing the most normal droplet volume for the two emulsions, the W60-O40 has got a distribution density of a little less than 0.06, while the W20-O80 emulsion has got a distribution density of 0.1. This means that the W60-O40 emulsion is more polydisperse than the W20-O80 emulsion.
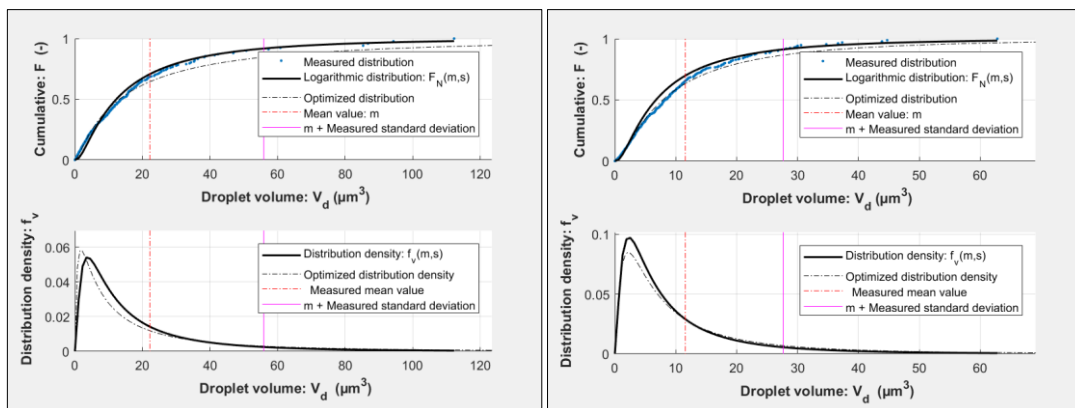
Figure 32: Droplet volume distribution. Left: W80-O20 emulsion. Right: W60-O40 emulsion.

42

Figure 33 shows the cumulative droplet volume distribution and distribution density of the W30-O70, W40-O60 and W50-O50 emulsions. Average droplet volume is market with a red line. The figure shows an increasing average droplet size with increasing water content. This coincides with the results obtained by Schramm (1992) and Pal (1996). Higher water fraction results in a larger average droplet size. From these graphs you can also see that the distribution density for the most normal droplet volume decreases as the water fraction increases.

Figure 34 compares the cumulative volume distribution for different emulsion. From this graph it is easy to see that a larger water fraction results in larger droplet volumes.
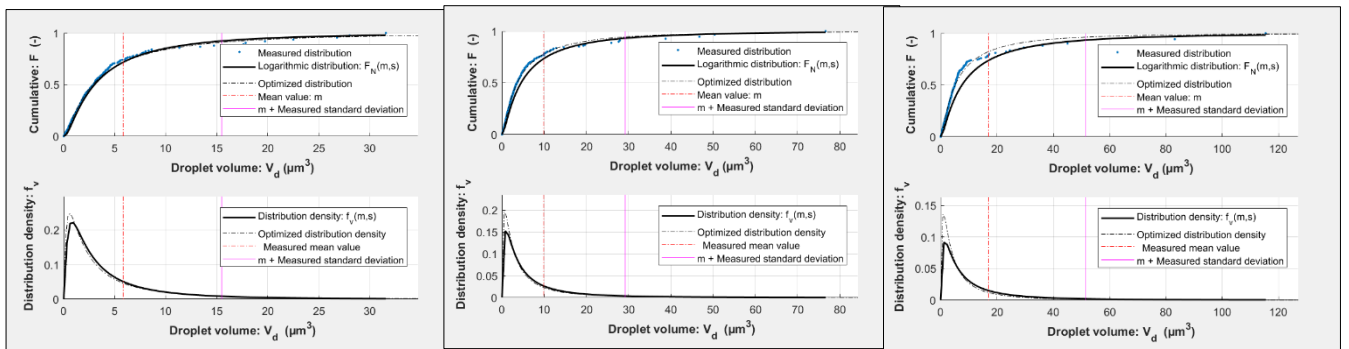
Figure 33: Cumulative droplet volume distribution and distribution densityof the W30-O70, W40-O60 and W50-O50 emulsion
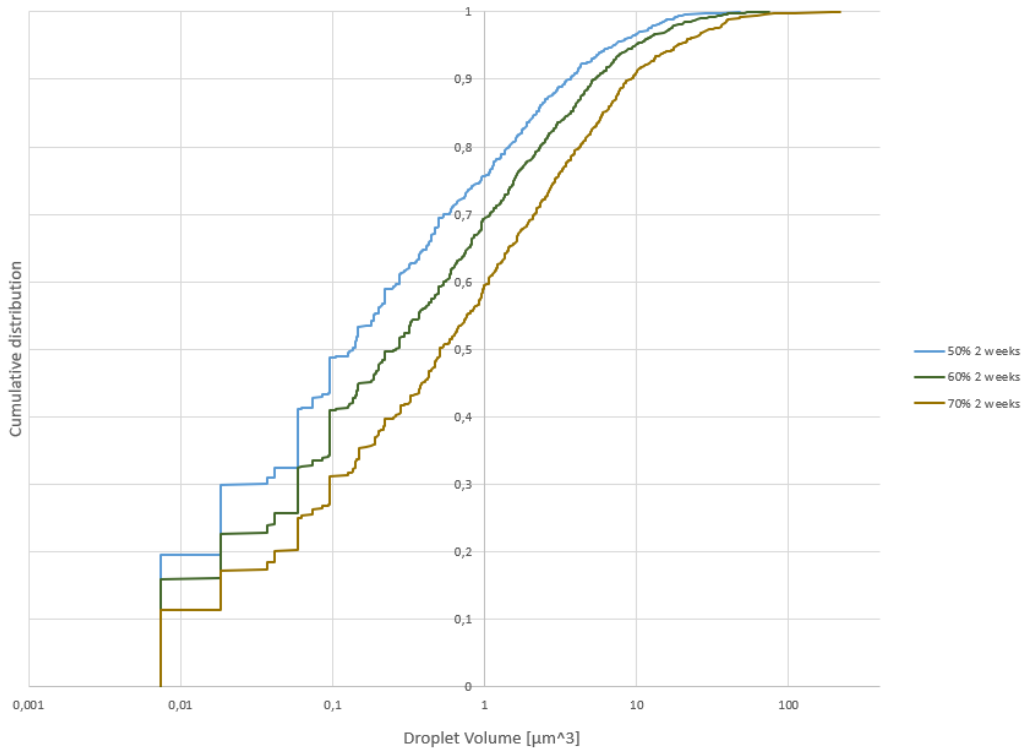
Figure 34: Cumulative distribution of the droplet volume for the emulsions mixed for 20 minutes.

5.4 TEMPERATURE

Figure 35 shows that there is a connection between low temperatures and emulsion breaking. It shows shear stress plotted against shear rate for the W60-O40 emulsion at different temperatures. At 4 °C the emulsion breaks at around 1000 s^{-1}, while no breaking occurs over the range of shear rates at the other temperatures. It can be interpreted from these results that at lower temperatures the emulsion becomes less stable, and breaking will occur at lower shear rates. In other words, decreased temperature seems to promote emulsion breaking. The IFT was significantly higher at 4 °C, so there can be drawn a connection between high IFT and decreased emulsion stability. This contradicts the previous hypothesis based on the findings of Kokal (1999). They found that the emulsion became stronger as the temperature decreased, which is the opposite of the findings in this experiment.

From Figure 35 it is also clear to see that the emulsion becomes more dependent on the shear conditions as the temperature decreases. At 4 °C, the emulsion shows a clear non-linear relationship between shear stress and rate. The non-linearity becomes less prominent as the temperature increases. The emulsion at 4 °C stands out compared to the other temperatures, and has much higher shear stress values than the emulsions at 20, 40 and 60 °C. Again, this could be connected to the high IFT occurring at 4 °C.
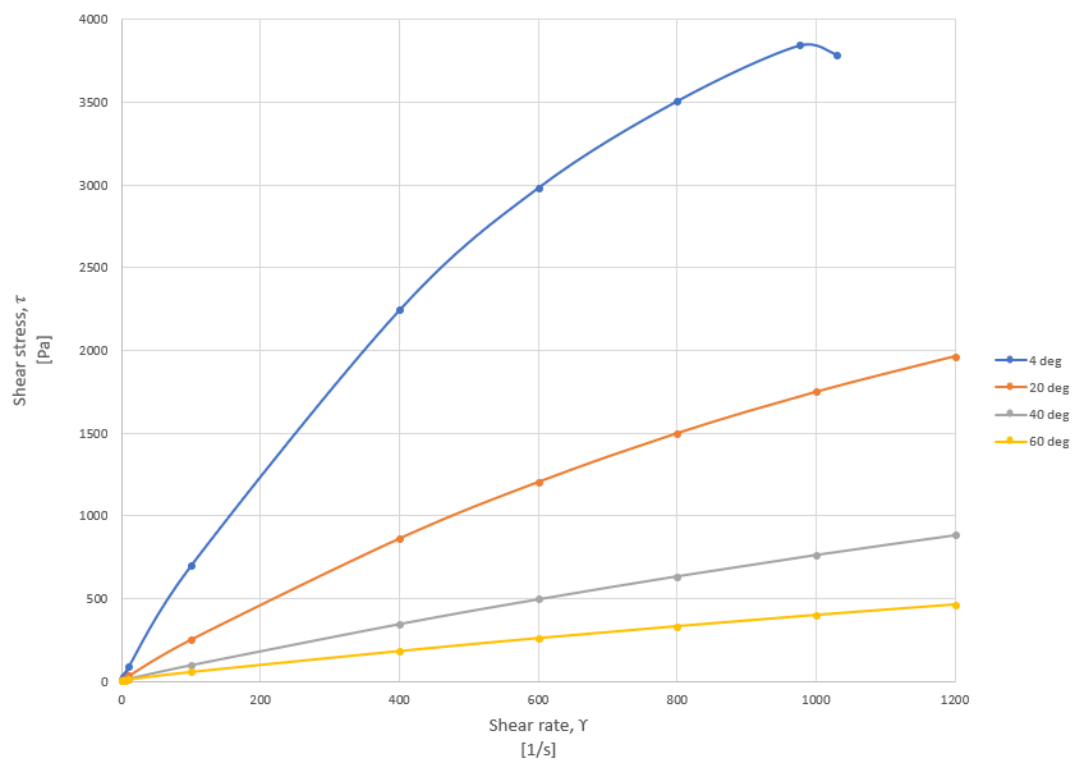
Figure 35: Fresh W60-O40 emulsion at different temperatures.

The emulsion viscosity was also tested over the same range of shear rates, and at the same temperature. The viscosity of the W60-O40 emulsion at different temperatures can be seen in Figure 36. The plot shows that an increase in temperature is associated with a decrease in viscosity. An increase in temperature results in a decrease in IFT, which again will result in a viscosity reduction. The emulsion shows shear thinning behavior at low shear rates at all temperatures, but only the test run at 4 °C shows a clear shear thinning behavior during the whole range of shear rates. This indicates that the emulsion becomes more shear thinning as the temperature decreases.

At 60 °C, the emulsion behaves almost Newtonian, and the viscosity decrease at higher shear rates is almost negligible.
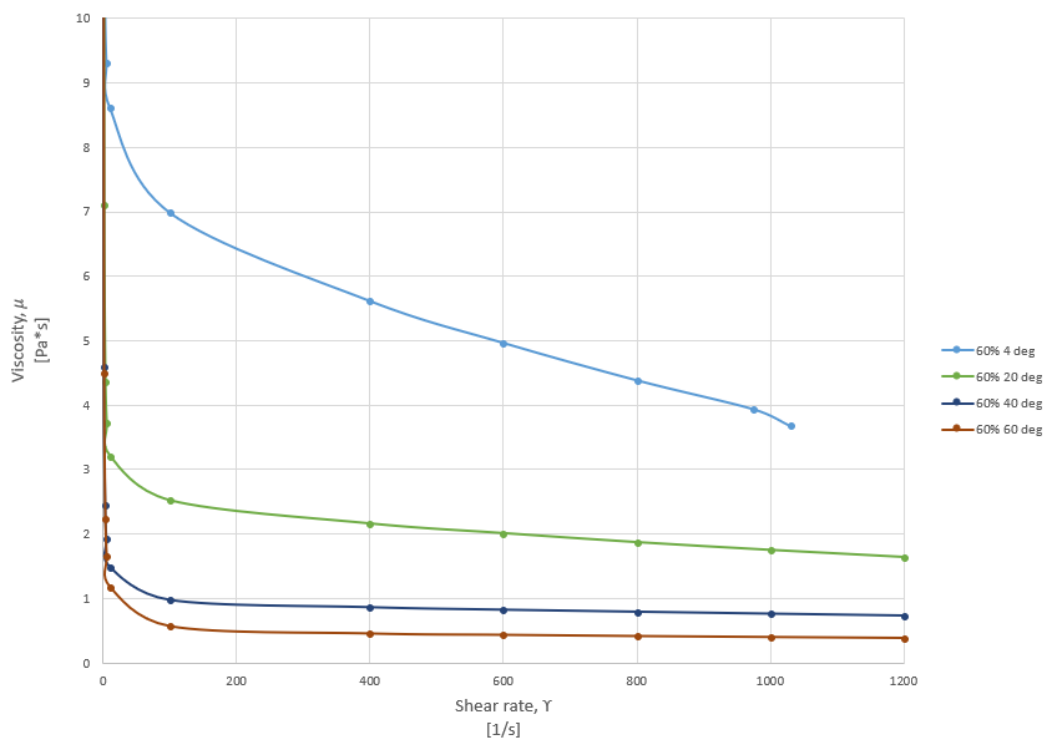
Figure 36: Comparing apparent viscosity vs shear rate for W60-O40 emulsion at different temperatures

5.5 AGING

Figure 37 and Figure 38 show the effect of aging on the W30-O70 emulsion. Here the fresh test results are compared to the 2-week-old ones. At 60 °C, the difference between the two samples is minimal, but for the other temperatures there is a slight difference between the fresh and the 2-week-old emulsion. Both the shear stress and the viscosity is higher for the fresh emulsion.

In Figure 39, the viscosity of emulsions with different water content are compared, to see if the water fraction has any effect on aging. From the plot one can see that the W60-O40 emulsion shows a larger decrease in viscosity after 2 weeks compared to the W20-O80 emulsion.

Aging seems to cause a slight decrease in viscosity and shear thinning behavior, especially at the lower temperatures. This is in line with the finding of Pal (1996). The aging effect seems to be more prominent with increasing water content.

No apparent correlation could be found between droplet size and aging. A graph showing this was decided not to be included in the thesis, but can be found in appendix   .
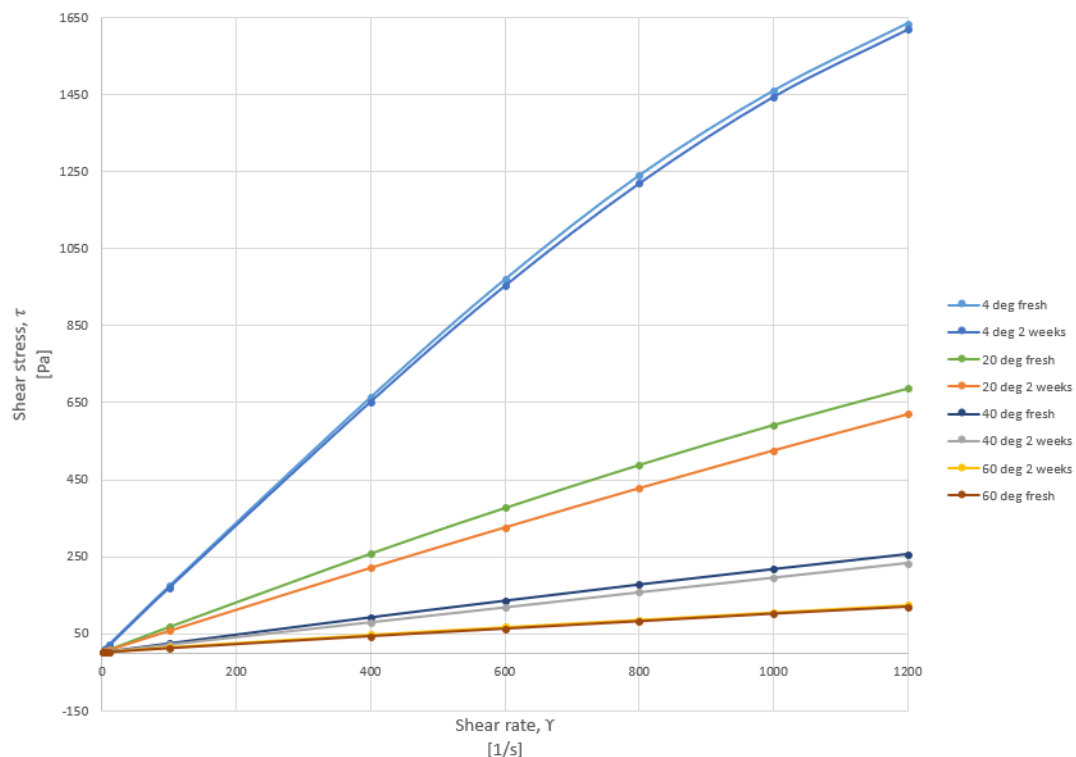
Figure 37: W30-O70 emulsion at different temperatures, tested fresh and after two weeks
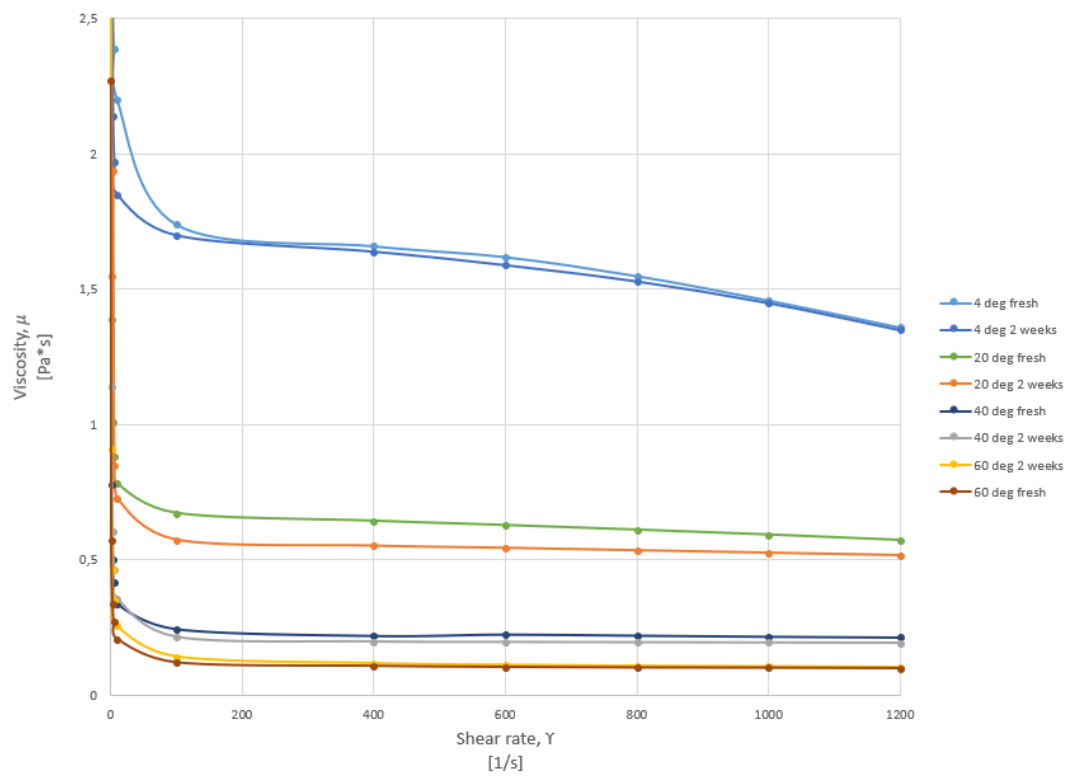
Figure 38: Viscosity of W30-O70 emulsion at different temperatures, tested fresh and after 2 weeks
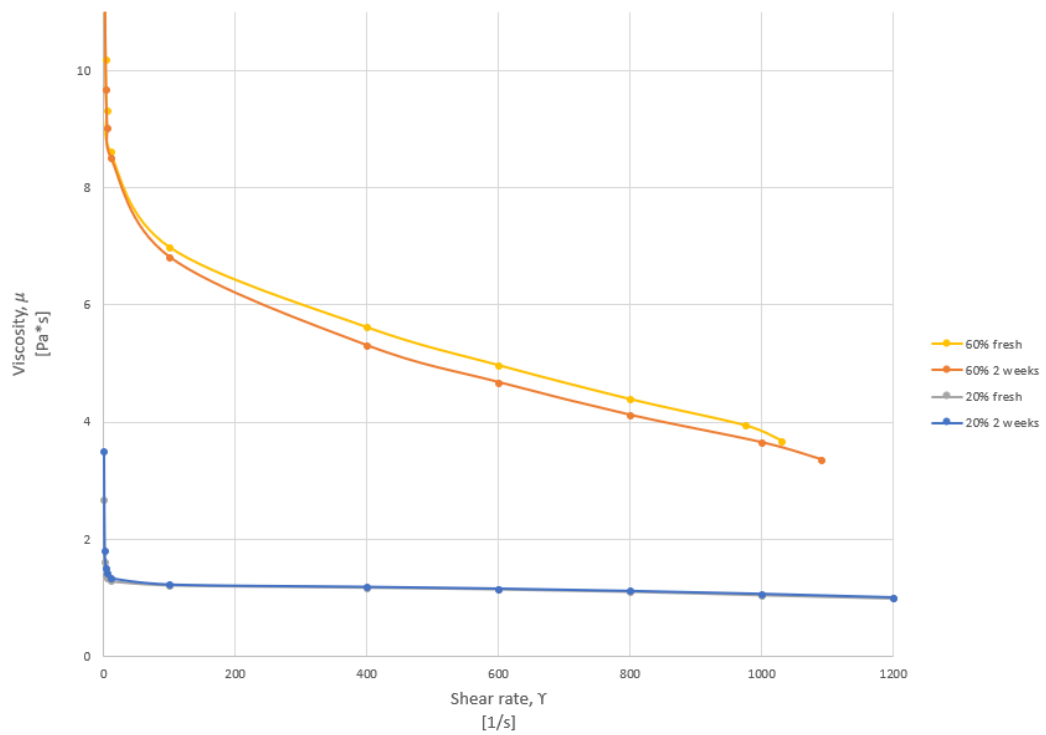
Figure 39: Viscosity of W60-O40 and W20-O80 emulsions at 4 °C, fresh and after 2 weeks

Figure 40 and Figure 41 show the amount of oil that came out of solution for the W60-O40 and the W30-O70 emulsion. It is clear to see that a higher oil content causes more oil to go out of solution. This is to be expected.

Hemmingsen et al. (2005) predicted that high viscosity gives a more stable emulsion. The W60-O40 emulsion has got higher viscosities, and less oil is separated out of this emulsion. This is in line with the prediction of Hemmingsen et al. (2005)
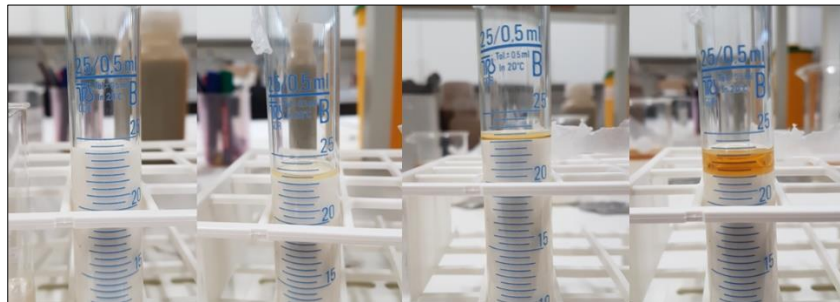
Figure 40: Amount of oil coming out of solution for the W60-O40 emulsion after 0, 3, 6 and 16 days, respectively

Figure 41: Amount of oil coming out of solution for the W30-O70 emulsion after 0, 3, 6 and 16 days, respectively

Table 6, Table 7 and Table 8 shows the amount of oil that had separated out of the W20-O80 emulsion, the W60-O40 emulsion mixed for 1.5 minutes, and the W60-O40 emulsion mixed for 20 minutes at different temperatures. The W20-O80 emulsion is pictured Figure 42.

Table 6: Amount of oil to come out of solution for W20-O80 emulsion

W20-O80, fresh 24.04			
Date	23°C	40°C	60°C
25.04	2 mm	9 mm	7 mm
30.04	16 mm	27 mm	57 mm
04.05	23 mm	29 mm	65 mm
27.05	37 mm	43 mm	77 mm

Table 7: Amount of oil to come out of solution for W60-O40 emulsion

W60-O40, fresh 24.04			
Date	23°C	40°C	60°C
25.04	0 mm	0 mm	0 mm
30.04	0 mm	0 mm	0.5 mm
04.05	0 mm	0 mm	1 mm
27.05	0 mm	0 mm	2 mm

W60-O40 mixed 20 min, fresh 01.05			
Date	23°C	40°C	60°C
04.05	0 mm	0 mm	0 mm
07.05	0 mm	0 mm	0 mm
27.05	0 mm	0 mm	0.8 mm
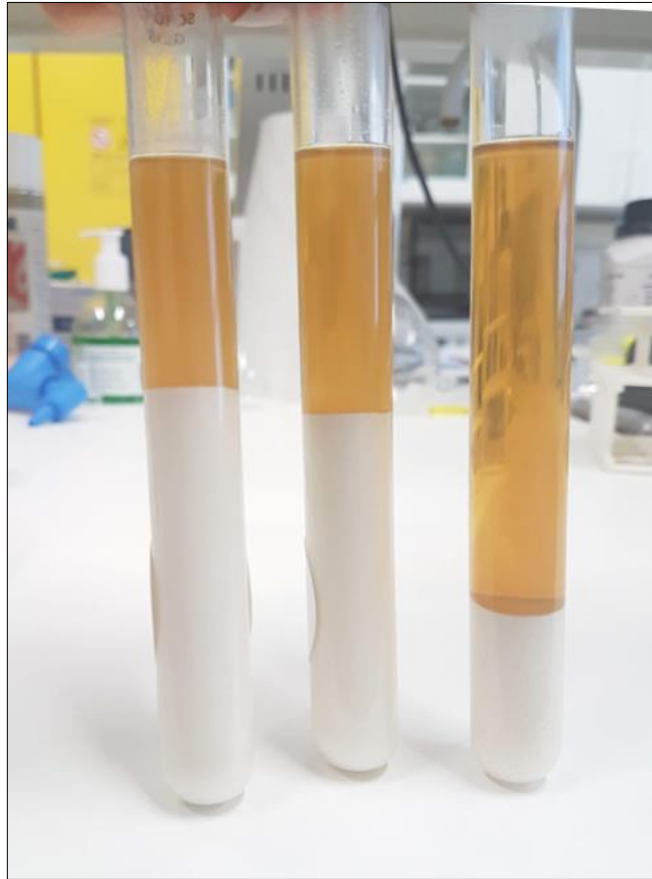
Figure 42: Amount of oil to come out of solution for the W20-O80 after 33 days at 23 °C, 40 °C and 60 °C, respectively

From the tables and Figure 42 one can see that there is a clear connection between temperature and amount to come out of solution. An increase in temperature results in a higher secretion of oil.

The W60-O40 emulsions mixed for 1.5 and 20 minutes did not segregate any oil at 23 or 40 °C. At 60 °C, the segregation is slightly higher for the sample mixed for 1.5 minutes. From these data, longer mixing time seem to cause less oil to come out of solution.

5.6 MIXING TIME

Longer mixing time results in a finer emulsion with a smaller average droplet size. This can be seen from Figure 43, that shows the cumulative droplet volume distribution of the W60-O40 emulsion after 2 weeks, mixed for 1.5 and 20 minutes, respectively. The emulsion mixed for 20 minutes has got a lower mean droplet volume. From the plots it can also be seen that the most normal droplet volume size for the emulsion mixed for 1.5 minutes is around 8 μm^3, while it is around 3 or 4 μm^3 for the emulsion mixed for 20 minutes. The distribution density is higher for the emulsion mixed for 20 minutes. This shows that longer mixing time results in a finer, more monodispersed emulsion.
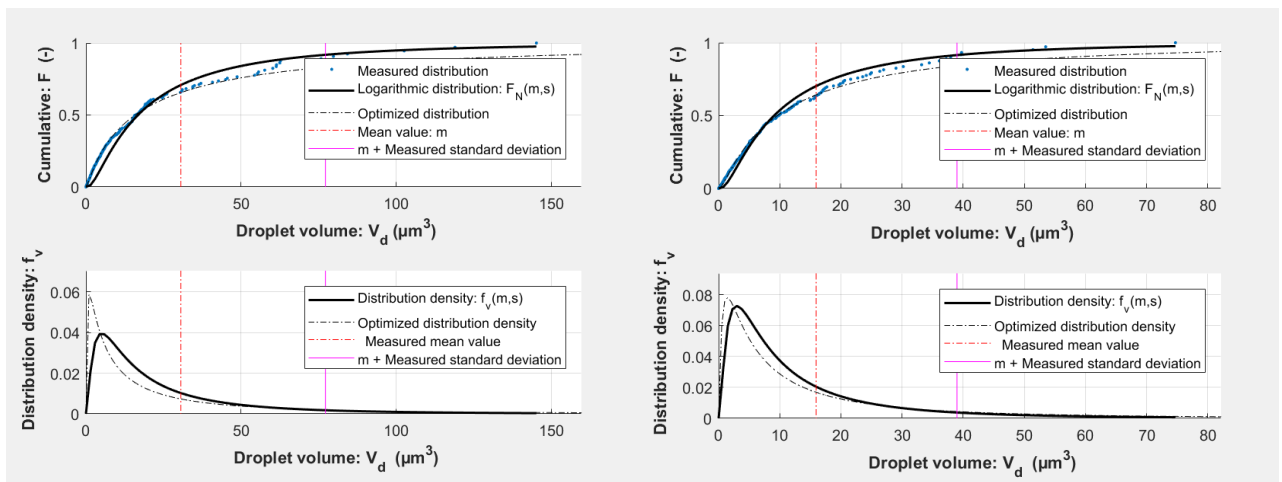
Figure 43: Droplet volume distribution. Left: W60-O40 emulsion mixed for 1.5 minutes. Right: W60-O40 emulsion mixed for 20 minutes.

Both shear stress and viscosity are lower for the emulsions mixed for 20 minutes. This can be seen in Figure 44 and Figure 45, that shows the viscosities and shear stress at different temperatures for the W50-O50 and W60-O40 emulsions mixed for 1.5 and 20 minutes.

This contradicts the findings of Pal (1996). A decrease in droplet volume should according to him result in a smaller distance between the dispersed droplets. This again should result in larger hydrodynamic forces between the droplets, which will result in an increase of the viscosity.

From this graph it can also be concluded that the differences between the short and long mixed emulsions increases as the temperature decreases. Mixing time seems to be more significant at lower temperatures.
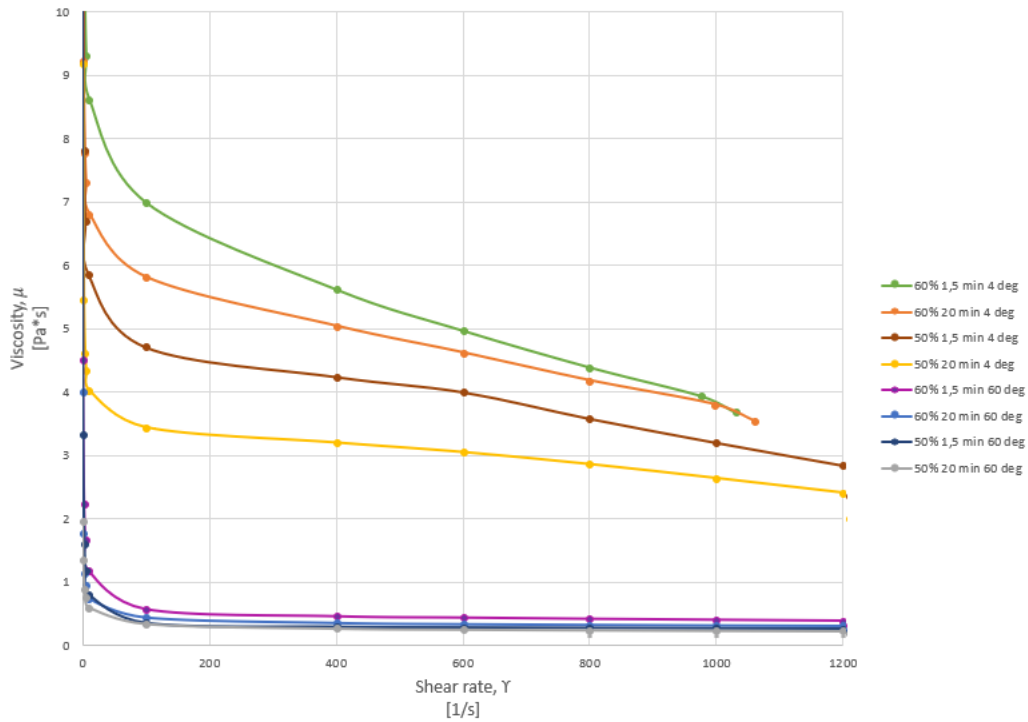
Figure 44: Viscosities of W50-O50 and W60-O40 emulsions with different mixing time, at 4 and 60 °C.

Pal (1996) also predicted that fine emulsions exhibit stronger shear thinning effects. From the results, there cannot be observed any significant difference in shear thinning between short and long mixing time. If anything, the emulsions mixed for 1.5 minutes are slightly more shear thinning.

Figure 46 shows the cumulative distribution of the droplet surface area for the W60-O40 emulsion. From this it seems that longer mixing time results in a larger surface area. This coincides with the previous findings, that longer mixing time gives a finer emulsion. It has to be mentioned that the cumulative surface area plot for the W50-O50 emulsion did not give as clear results, and more data is needed to be able to draw a definite conclusion.
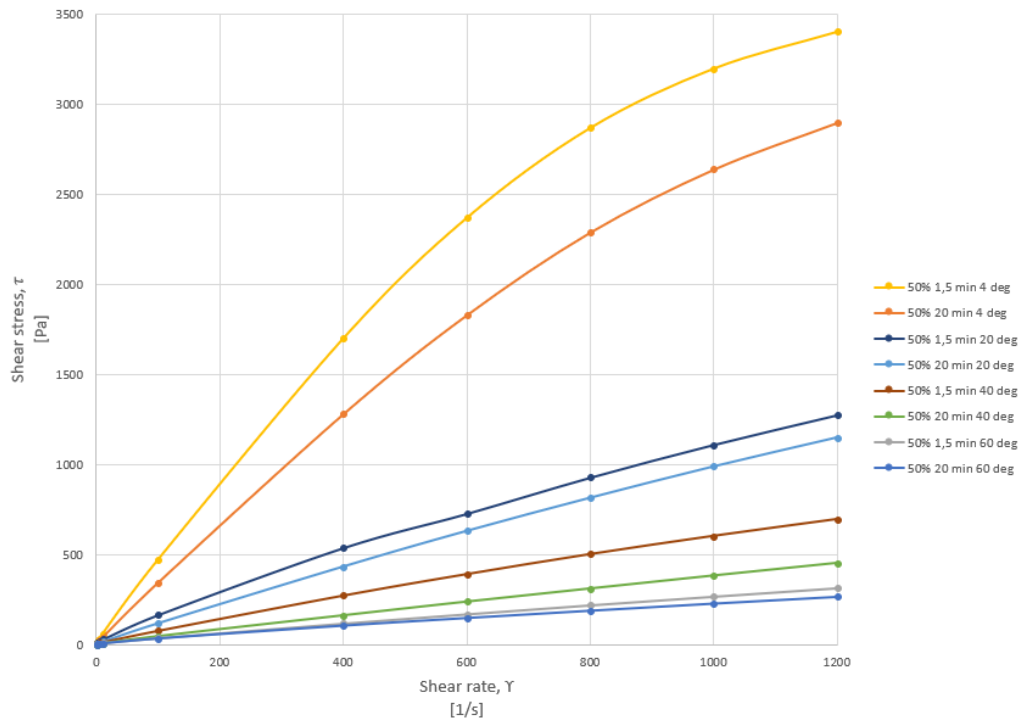
Figure 45: Shear stress vs shear rate at different temperatures for the W50-O50 emulsion, mixed for 1.5 and 20 minutes
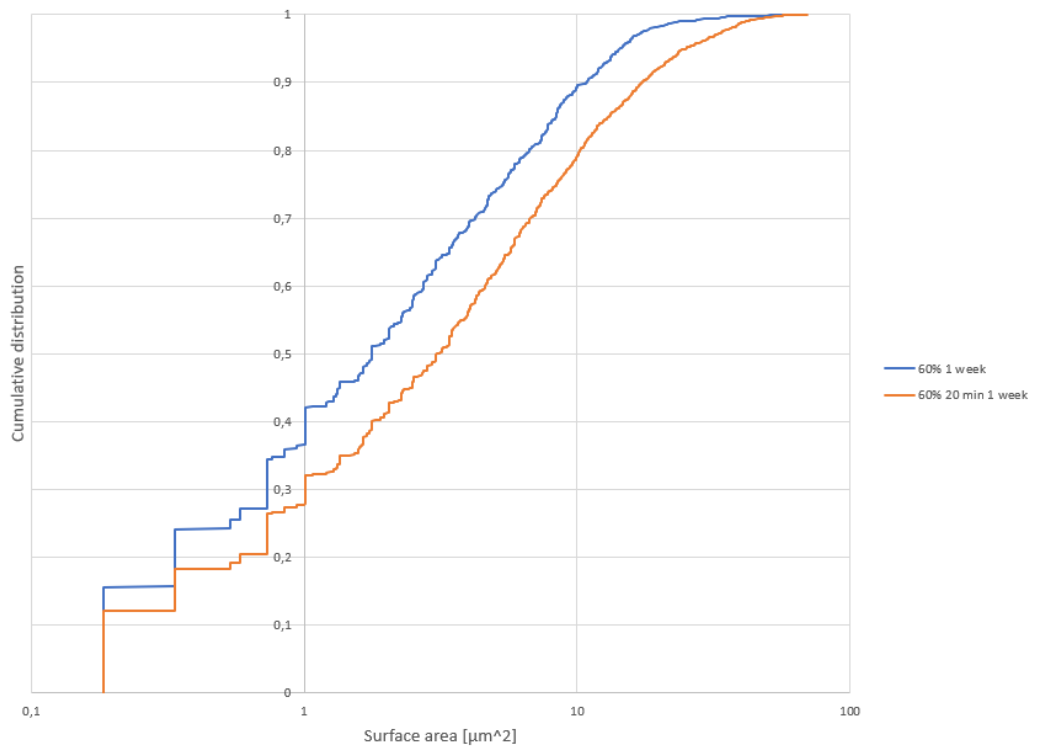
Figure 46: Larger surface area for longer mixing time

5.7   FLOW EXPERIMENT

Figure 47 shows the mass flow rate of the fresh W60-O40 emulsion. As one can see from the graph, the flow becomes linear immediately after the valve is opened. The flow remains linear up to a certain point for all cases. It can also be noted that for the second run, there seems to be slightly less total emulsion weight. This was the case for all emulsions except from one. Some of the emulsion may remain in the top bucket. During the first run, the emulsion is exposed to stress. This could lead to changes in the intermolecular structure of the emulsion, which could cause more of the emulsion to remain in the bucket, and the rate to decrease. In Figure 48, the flow rate of the W20-O80 and W60-O40 emulsions are compared. One can clearly see that the W20-O80 flow rate is much higher.
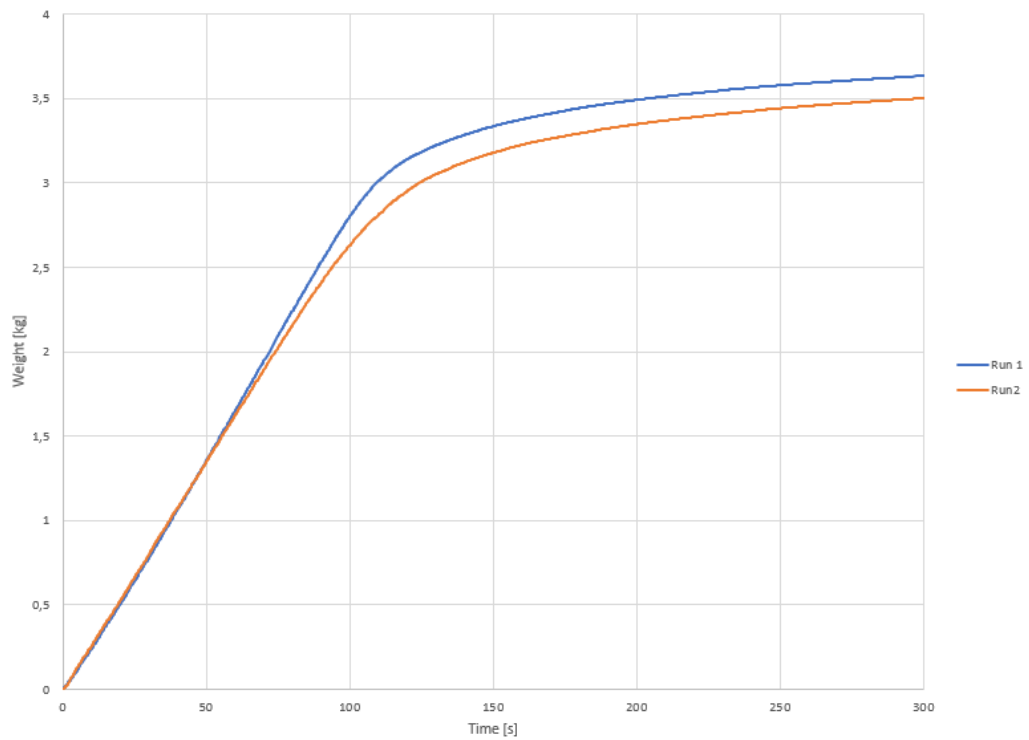
Figure 47: The measured mass flow of the fresh W60-O40 emulsion, run 1 and 2.
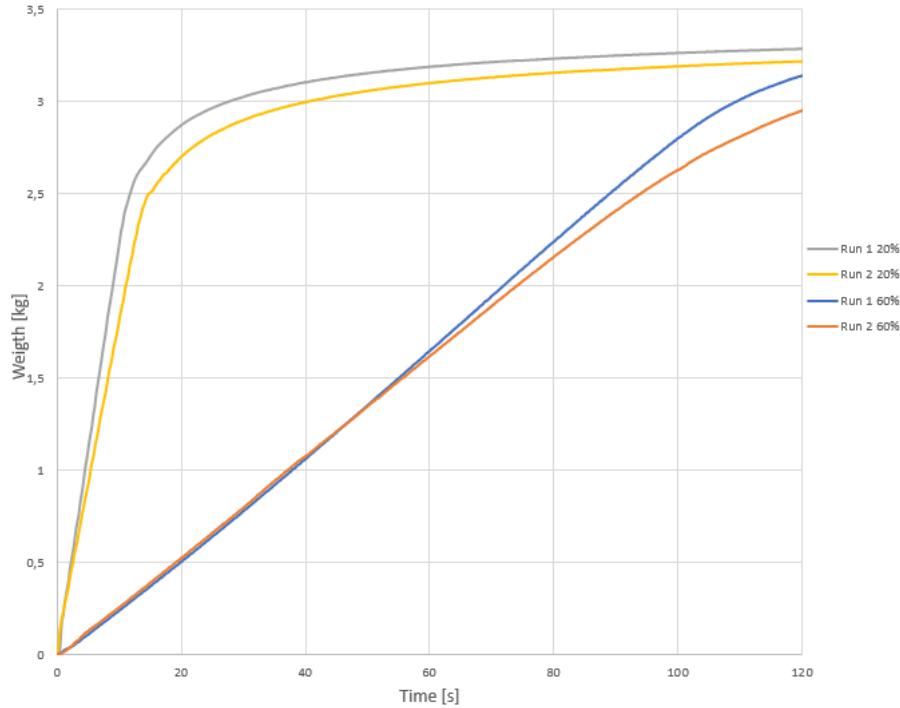
Figure 48: Comparison of the measured mass flows of the W20-O80 and W60-O40 emulsions measured fresh. The graph shows both runs.

Table 9 and Table 10 shows the measured mass and corresponding volumetric flow rates for the two runs of W20-O80 and W60-O40 emulsions tested fresh and after 2 weeks. Figure 49 shows the effect of aging on the flow rate. Both the W20-O80 and W60-O40 emulsion shows a decrease in flow rate when the emulsion has aged for two weeks. This contradicts the earlier findings, that showed that aging resulted in a decrease in viscosity. A decrease in viscosity should result in a higher flow rate. A possible reason for why the aged samples show a decreased flow rate could be due to loss of emulsion when moving it from the flow setup and to the container where it was stored in between testing. The properties of the emulsions made it difficult to transfer it from one container to another, and some emulsion was lost in the process.
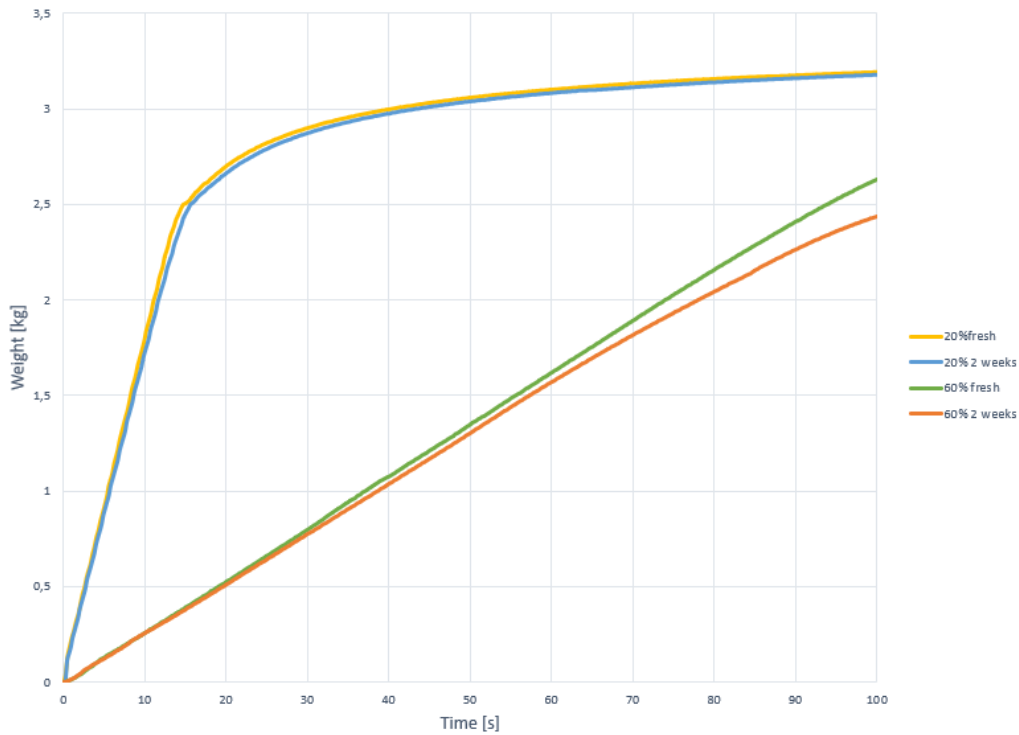
Figure 49: Flow rate for fresh and aged emulsion

Table 11 shows the calculated volumetric flows using the power law, Herschel-Bulkley and Hagen-Poiseuille flow models. Figure 50, Figure 51 and Figure 52 are graphical representations of the measured and calculated flow rates. Table 12 shows the % deviation of calculated flow rate from the measured flow rate.

Table 9: Measured mass flow and corresponding volumetric flow for the fresh emulsions

Run	Emulsion	Mass flow [kg/s]	Volumetric flow [l/s]
1	20%W	0.2237	0.2574
2	20%W	0.1750	0.2014
1	60%W	0.0286	0.0308
2	60%W	0.0269	0.0290

Table 10: Measured mass flow and corresponding volumetric flow for the 2-week-old emulsions

Run	Emulsion	Mass flow [kg/s]	Volumetric flow [l/s]
1	20%W	0.2203	0.2535
2	20%W	0.1658	0.1908
1	60%W	0.0243	0.0262
2	60%W	0.0256	0.0275

55

Table 11: The calculated volumetric flows using power law, Herschel-Bulkley and Hagen-Poiseuille flow models

Emulsion	Yield point [Pa]	Volumetric flow, power law [l/s]	Volumetric flow, Herschel-Bulkley [l/s]	Volumetric flow, Hagen-Poiseuille [l/s]
20 %	0.044	0.1940	0.1983	0.2226
60 %	0.434	0.0206	0.0215	0.0476

Table 12: % deviation from the measured flow when applying the different models. Green marks the most accurate result, red marks the least.

	Power Law		Herschel Bulkley		Hagen-Poiseuille	
Run	1	2	1	2	1	2
20% fresh	24.63	3.69	22.96	1.55	13.51	-10.51
20% 2 weeks	23.46	-1.66	21.77	-3.91	12.18	-16.64
60% fresh	33.15	28.85	30.13	25.64	-54.46	-64.41
60% 2 weeks	21.26	25.18	17.71	21.80	-81.93	-72.89

From Table 12 and the figures one can see that the Herschel-Bulkley model overall gives the best approximation for the volumetric flow of the emulsions. The power law model gave the most accurate result for the two-week-old W20-O80 emulsion with a deviation of only 1.66%, but the Herschel-Bulkley model also provided quite accurate results here, with a deviation of 3.91%. The most accurate results were found for the fresh W20-O80 emulsion using the Herschel-Bulkley model, with a deviation of only 1.55%. The accuracy drastically improved from the first to the second run. This can be seen in Figure 50. The accuracy of the flow models in significantly poorer for the W60-O40 emulsion compared to the W20-O80 emulsion. The actual and the approximated flow rates for the W60-O40 emulsion can be seen in Figure 51. The decrease in accuracy is to be expected, as the W60-O40 emulsion has got a higher viscosity, and therefore has a much lower volumetric flow rate. The volumetric flow rate of the W20-O80 emulsion is one order of magnitude larger than the W60-O40 emulsion. This makes the W60-O40 emulsion more sensitive to errors, and small changes in the volumetric flow results in a large % deviation. Figure 52 shows both the W20-O80 and the W60-O40 emulsion in the same plot, for comparison.

The Hagen-Poiseuille equation gives much better results for the W20-O80 than for the W60-O40 emulsion. Previous results indicate that the W20-O80 emulsion behaves more Newtonian than the W60-O40 emulsion, so this is to be expected. Unexpectedly, the Hagen-Poiseuille approximation is better than the Power law and Herschel-Bulkley models for the W20-O80 emulsion at the first run, but at the second run Power Law and Herschel-Bulkley are more accurate. The Hagen-Poiseuille equations gives very inaccurate results for the W60-O40 emulsion, which is to be expected.
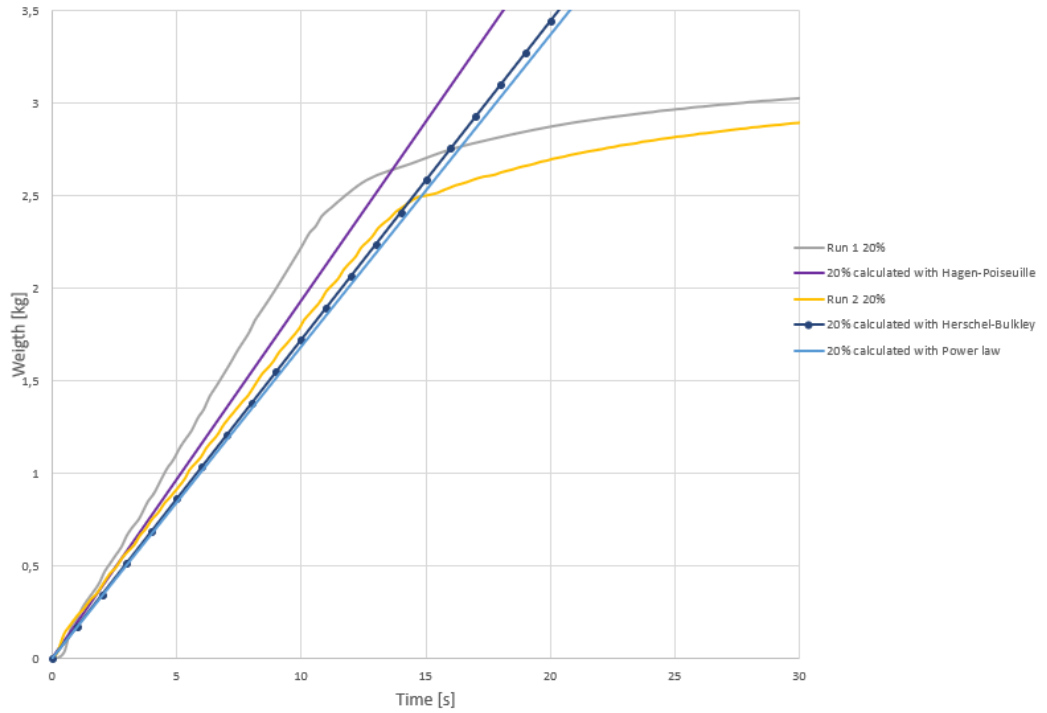
Figure 50: Comparing the two measured runs for W20-O80 emulsion with approximations using power law, Herschel-Bulkley and Hagen-Poiseuille model. Measured and aproximated solutions show little deviation.
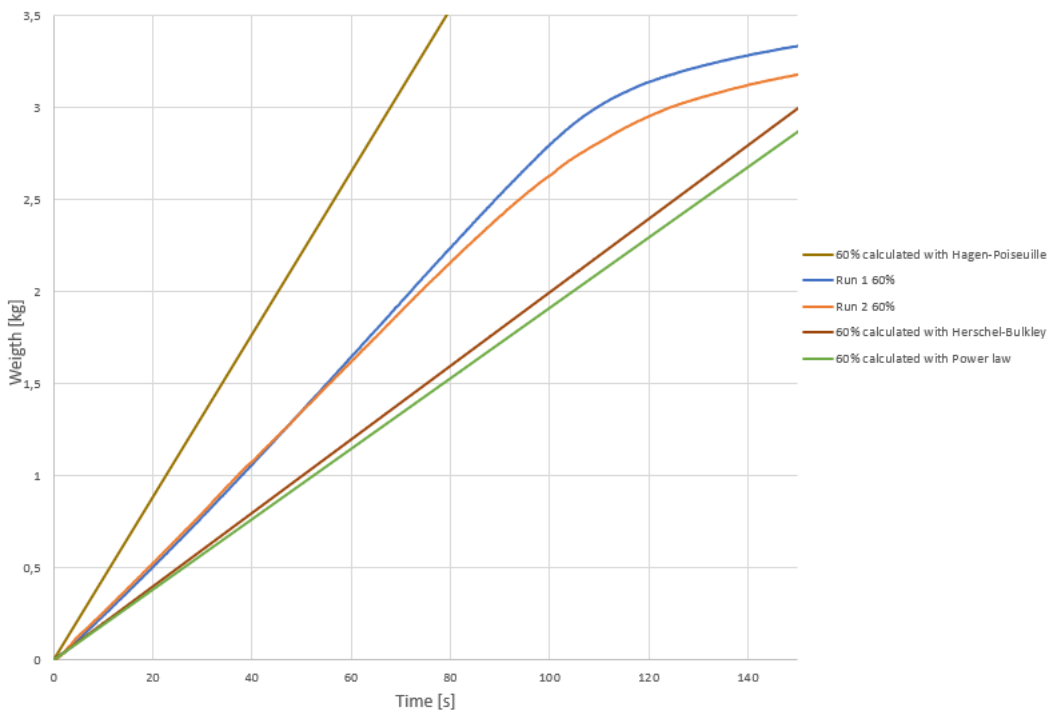
Figure 51: Comparing the two measured runs for W60-O40 emulsion with approximations using power law, Herschel-Bulkley and Hagen-Poiseuille model. Measured and approximated solutions show higher degree of deviation.

57
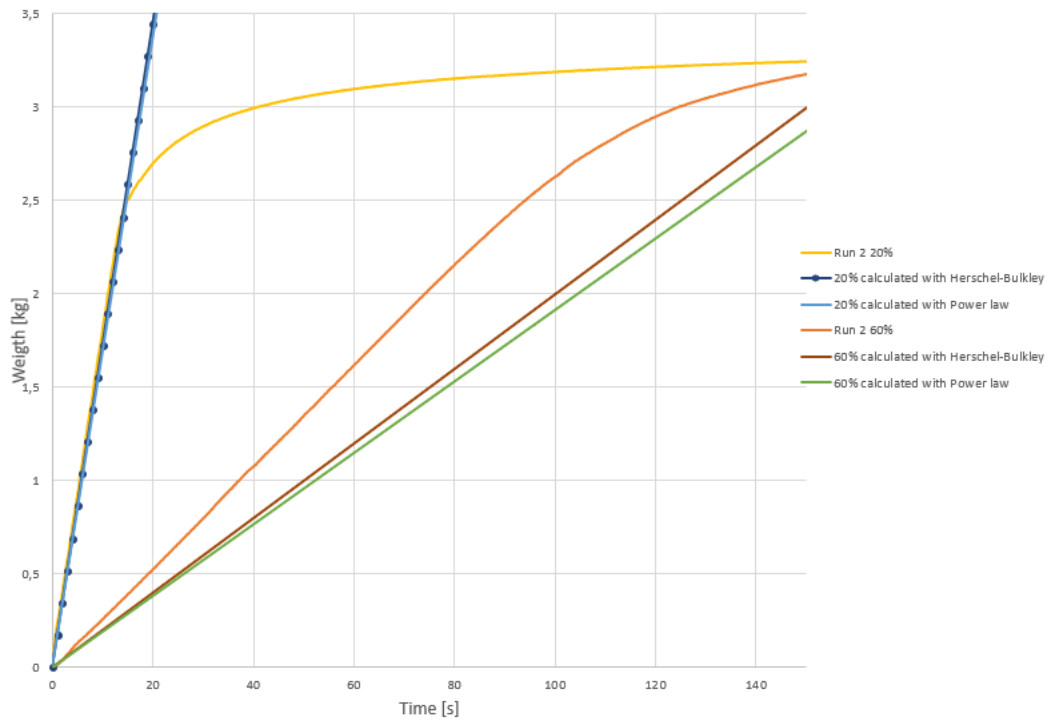
Figure 52: Graphical representation of the measured flow rate compared to the flow rates estimated using the power law and Herschel-Bulkley model.

5.8 RECOMMENDATIONS FOR FURTHER WORK

o Use heavy crude oils of different compositions to make the emulsions. Do the same rheological tests in the Anton Paar Modular Compact Rheometer 302, and test at different shear rates and temperatures. Compare the results with previously obtained data.

o Investigate further the size and distribution of the dispersed droplets. See how the distribution changes with aging.

o Expand the range of shear rates when testing in the Anton Paar Modular Compact Rheometer 302. Increase the frequency of measurements at low shear rates, and include higher shear rates than $1200\ s^{-1}$.

o Try adding different substances, e.g. asphaltenes, to see how this affects the stability of the emulsion.

o Make oil-in-water emulsions, to be able to conduct next point.

o Inject emulsion into core samples to see if one can achieve a reduction of core permeability. Vary the temperature and water fraction to see what conditions most effectively reduces the permeability.

o Explore if the yield point changes with maturation

o Keep emulsions stored at the respective temperatures between testing for a more accurate representation of the temperature effect.

o Investigate droplet size and dispersion for emulsions at different temperatures.

o Investigate if the emulsions show thixotropic or rheopectic behavior.

6   CONCLUSIONS

The following conclusions can be drawn, based on the results and discussion:

o All emulsions possessed a yield stress, but most yield points occurred at very low shear stresses. The value of the yield stresses ranged from 0.011 to 1.97 Pa. Most of the emulsions showed a decreasing yield stress with increasing temperature, while an increase of water content caused the yield stress to increase. Longer mixing time resulted in a lower yield.

o All the emulsions showed a clear shear thinning tendency. The relationship between shear rate and shear stress, combined with the fact that the emulsion had a yield point, indicated that the Herschel-Bulkley model was a good description of the emulsions behavior.

o From the flow test, it can be concluded that the Herschel-Bulkley model overall gives the best approximation for the volumetric flow of the emulsions. For the fresh W20-O80 emulsion the calculated results deviated from the measured results by 1.55%. The power law model gave slightly less accurate results. The deviation for the fresh W20-O80 emulsion using the power law model was 3.69%. The accuracy of the flow models declined with increasing water content. The Herschel-Bulkley model gave a deviation of 25.64% for the fresh W60-O40 emulsion, while using the power law model resulted in a deviation of 28.85%. The Hagen-Poiseuille equation have quite accurate results for the W20-O80 emulsion, with a deviation of 10.51%. For the W60-O40 emulsion, the Hagen-Poiseuille equation resulted in a deviation of 64.41%.

o Aging seems to have an increasing effect on viscosity and shear thinning behavior, especially at low temperatures. The aging effect seems to be more prominent with increasing water content

o Longer mixing time results in a finer emulsion with a smaller average droplet size. Both shear stress and viscosity decrease as mixing time is increased. The effect of mixing time seems to be more significant at lower temperatures. No apparent difference in shear thinning behavior can be observed between short and long mixing time.

o A decrease of temperature resulted in a looser emulsion that destabilized at lower shear rates. Decreasing the temperature also resulted in higher viscosities. An increase of temperature made the emulsions behave more Newtonian, and reduced the shear thinning behavior.

o An increase of shear rate resulted in earlier breaking of the emulsions. Increased shear promoted emulsion instability.

o A high water content resulted in higher viscosities and a more shear thinning behavior. Increasing the amount of water also resulted in a looser emulsion. An increase in water fraction increases the polydispersity and results in a wider distribution of droplet size and an increase of the average droplet volume. This causes the emulsion to destabilize and break at lower shear rates.

o Based on these results, one is able to make a reasonably good prediction about the flow rate of W/O emulsions flowing laminarly through a circular pipe.

7 REFERENCES

Acherson, D. J. (1990). Elementary fluid dynamics. *Oxford University Press*.

Ahmad, M. U., & Xu, X. (2015). *Polar lipids: biology, chemistry and technology*. Elsevier. doi:https://doi.org/10.1016/B978-1-63067-044-3.50012-1

Anton Paar. (2018, Juni 5). Hentet fra How to measure viscosity: https://wiki.anton-paar.com/en/how-to-measure-viscosity/

Anton Paar. (2018, June 7). Hentet fra Viscosity of Crude Oil: https://wiki.anton-paar.com/en/crude-oil/

Beris, A. N., Tsamopoulos, J. A., Armstrong, R. C., & Brown, R. A. (1985). Creeping motion of a shere through a Bingham plastic. *Journal of Fluid Mechanics*, ss. 219-244.

Brown, W. H., Foote, C. S., Iverson, B. L., & Anslyn, E. (2011). *Organic Chemistry*. Cengage Learning.

Buenrostro-Gonzalez, E., Groenzin, H., Lira-Galeana, C., & Mullins, O. C. (2001). The overriding chemical principles that define asphaltenes. *Energy & Fuels*, ss. 972-978.

Chen, T. (2017). Rheological techniques for yield Stress analysis . *TA Instruments Applications Note*.

Chen, T. (u.d.). Rheological techniques for yield stress analysis. *TA Instruments Applications Note* .

Cimbala, J. M., & Cengel, Y. A. (2014). *Fluid Mechanics: Fundamentals and Applications*. McGraw Hill Higher Education.

Consult, I. C. (2017, Desember 13).

Eötvös, R. (1886). Ueber den Zusammenhang der Oberflächenspannung der Flüssigkeiten mit ihrem Molecularvolumen. *Annalen der Physik*(263), ss. 448-459.

Hemmingsen, P. V., Silset, A., Hannisdal, A., & Sjöblom, J. (2005). "Emulsions of heavy crude oils. I: Influence of viscosity, temperature, and dilution. *Journal of dispersion science and technology*.

Hemphill, T. C. (1993). Yield-power law model more accurately predicts mud rheology. *Oil and Gas Journal*.

Hemphill, T., Campos, W., & Pilehvari, A. (1993). Yield-power law model more accurately predicts mud rheology. *Oil and Gas Journal*.

Ibero Chemie Consult. (2017, December 13). Hentet fra Products: http://www.ibero-chemie.de/en/products/

ImageJ. (2018, Juni 2). Hentet fra ImageJ: https://imagej.net

Johansen, E. J., Skjärvö, I. M., Lund, T., Sjöblom, J., Söderlund, H., & Boström, G. (1988). Water-in-crude oil emulsions from the norwegian continental shelf part I. Formation, characterization and stability correlations. *Colloids and surfaces*, ss. 353-370.

Johnsen, E. E., & Rønningsen, H. P. (2003). Viscosity of 'live' water-in-curde-oil emulsions: experimental work and validation of correlations. *Journal of Petroleum Science and Engineering*, ss. 23-36.

Kantzas, A., Bryan, J., & Taheri, S. (2016). *Fundamentals of Fluid Flow in Porous Media*.

Keleşoğlu, S., Pettersen, B. H., & Sjöblom, J. (2012). Flow properties of water-in-North Sea heavy crude oil emulsions. *Journal of Petroleum Science and Engineering*, ss. 14-23.

Kokal, S., & Al-Juraid, J. (1999, January). Quantification of various factors affecting emulsion stability: watercut, temperature, shear, asphaltene content, demulsifier dosage and mixing different crudes. *SPE Annual Technical Conference and Exhibition*.

Kontogeorgis, G. M., & Kiil, S. (2016). *Introduction to applied colloid and surface chemistry.* John Wiley & Sons.

Kosswig, K. (1994). Surfactants. *Ullmann's encyclopedia of industrial chemistry*.

Langevin, D., Poteau, S., Hénaut, I., & Argilier, J. F. (2004). Crude oil emulsion properties and their application to heavy oil transportation. *Oil & gas science and technology*.

Lervik, I. (2017). *Rheological properties and models for Water-in-Oil emulsions* .

Madlener, K., Frey, B., & Ciezki, H. K. (2009). Generalized Reynolds number for non-Newtonian fluids. *Progress in Propulsion Physics*(1), ss. 237-250.

McAuliffe, C. D. (1973). Oil-in-water emulsions and their flow properties in porous media. *Journal of petroleum technology*, ss. 727-733.

Merkus, H. G. (2009). *Particle size measurements: fundamentals, practice, quality* (17. utg.). Springer Science & Business Media.

Michon, G. P. (2015). *Numericana.* Hentet fra Spheroids & Scalene Ellipsoids: http://www.numericana.com/answer/ellipsoid.htm#thomsen

Pal, R. (1996). Effect of droplet size on the rheology of emulsions. *AlChE Journal*, ss. 3181- 3190.

petroleum.co.uk. (2018, Juni 4). Hentet fra API Gravity: http://www.petroleum.co.uk/api

Petrowiki. (2018, Mai 26). Hentet fra Petrowiki: http://petrowiki.org/Energy_dissipation_rate

Rimmer, D. P., Gregoli, A. A., Hamshar, J. A., & Yildirim, E. (1992). Pipeline emulsion transportation for heavy oils. *Advances in Chemistry*.

Rosen, M. J., & Kunjappu, J. T. (2012). *Surfactants and interfacial phenomena.* John Wiley & Sons.

Schramm, L. L. (1992). *Emulsions: Fundamentals and applications in the Petroleum Industry.* Advances in Chemistry Series, 321.

Schramm, L. L. (2014). *Emulsions, foams, suspensions, and aerosols: microscience and application.* John Wiley & Sons.

Tadros, T., Izquierdo, P., Esquena, J., & Solans, C. (2004). Formation and stebility of nano-emulsions. *Advances in colloid and interface science*.

Taylor, P. (1998). Ostwald ripening in emulsions. *Advances in colloid and interface science*, ss. 107-163.

Voorhees, P. W. (1985). The theory of Ostwald ripening. *Journal of Statistical Physics*, ss. 231-252.

Wikiversity. (2018, Juni 2). Hentet fra Microfluid Mechanisms/Flow Phenomena in Microflows: https://en.wikiversity.org/wiki/Microfluid_Mechanics/Flow_Phenomena_in_Microflows

APPENDICES

A. DERIVATIONS

Droplet velocity for sedimentation/creaming

Stokes law states that "The force of viscosity on a small sphere moving through a viscous fluid is given by:"

$$f_d = 6\pi\eta r_d v$$

where f_d is the frictional force acting between the droplet and the continuous phase, η is the dynamic viscosity, r_d is the radius of the droplet and v is the droplet velocity. (Cimbala & Cengel, 2014, s. 618). When the droplets sediment or cream, their motion is driven by gravitational forces. It can be described using the following formula:

$$f_g = mg = V(\rho_2 - \rho_1)g = \frac{4}{3}\pi r_d^3(\rho_2 - \rho_1)g$$

where V is the droplet volume, ρ_2 is the density of the dispersed phase/droplet, ρ_1 is the density of the continuous phase and g is the gravitational constant.

When the frictional force equals the gravitational force, the droplet reaches its settling velocity, also known as terminal velocity. Setting $f_d = f_g$, and solving for $v = \frac{dx}{dt}$, you get the following equation for the droplet velocity:

$$\frac{dx}{dt} = \frac{2r_d^2(\rho_2 - \rho_1)g}{9\eta}$$

K and n parameters:

$$\tau = K\Upsilon^n$$

K and n are temperature dependent. Their values are found the following way:

First, a log-log plot of shear stress vs shear rate is constructed.

$$\log(\tau) = n \cdot \log(\Upsilon) + \log(K)$$

$$\tau^* = \log(\tau)$$

$$\Upsilon^* = \log(\Upsilon)$$

$$\tau^* = n \cdot \Upsilon^* + b$$

Where n is the slope of the line, and $b = \log(K)$ is the intercept on the (log)y-axis

For Herschel-Bulkley fluids:

$$\tau = \tau_0 + K\Upsilon^n$$

$$\tau - \tau_0 = K\Upsilon^n$$

$$\log(\tau - \tau_0) = n \cdot \log(\Upsilon) + \log(K)$$

So, in a log-log plot of $(\tau - \tau_0)$ vs Υ, n is the slope of the line and log(K) is the intercept on the (log)y-axis.

<u>Weight percentages:</u>

$$V_{tot} = V_w + V_o$$

$$V_o = V_{tot} - V_w$$

$$\frac{\rho_w V_w}{\rho_w V_w + \rho_o V_o} = x$$

$$x = wt\%$$

$$\frac{\rho_w V_w}{\rho_w V_w + \rho_o (V_{tot} - V_w)} = x$$

$$\rho_w V_w = x * \rho_w V_w + x * \rho_o V_{tot} - x * \rho_o V_w$$

$$V_w(\rho_w - x * \rho_w + x * \rho_o) = x * \rho_o V_{tot}$$

$$V_w = \frac{x * \rho_o V_{tot}}{(1 - x) * \rho_w + x * \rho_o}$$

$$V_o = V_{tot} - V_w$$

Volumetric flow of power law fluids:

Area: $A = \pi r^2$

Circumference: $S = 2\pi r$

Pressure: $P = \frac{F}{A} \quad \rightarrow \quad F = P \cdot A$

Volumetric flow: $Q = u \cdot A$

Force balance gives:

$$\Delta P \cdot A = \tau \cdot S \cdot L$$

$$\Delta P \cdot \pi \cdot r^2 = \tau 2\pi r L$$

$$\Delta P \cdot r = \tau 2L$$

$$\frac{\Delta P}{L} = \frac{2\tau}{r} \quad \rightarrow \quad \tau = \frac{\Delta P \cdot r}{2L}$$

$\frac{\Delta P}{2L}$ assumed constant and independent of r, this gives:

$$\tau = C \cdot r$$

With boundary conditions:

@ r=0, τ=0

@ pipe wall, r=R=D/2, $\tau = \tau_e$

$$\tau_e = C \cdot \frac{D}{2} \quad \rightarrow \quad C = \frac{2\tau_e}{D}$$

$$\tau = \frac{2\tau_e}{D} r$$

Since $\frac{D}{2} = R, \tau = \tau_e \frac{r}{R}$

$$\tau_e = C \cdot \frac{D}{2} = \frac{\Delta P}{2L} \cdot \frac{D}{2} = \frac{\Delta P \cdot R}{2L}$$

Power law model: $\tau = K \cdot \gamma^n$

$$\gamma = -\frac{du}{dr}$$

$$\tau = -K \left(\frac{du}{dr}\right)^n$$

Combining gives:

$$\tau_e \frac{r}{R} = -K \left(\frac{du}{dr}\right)^n$$

$$\frac{\Delta P \cdot R}{2L} \cdot \frac{r}{R} = -K \left(\frac{du}{dr}\right)^n$$

$$\frac{\Delta P \cdot r}{2L} = -K\left(\frac{du}{dr}\right)^n$$

$$\frac{du}{dr} = -\left(\frac{\Delta P \cdot r}{2LK}\right)^{\frac{1}{n}}$$

$$du = -\left(\frac{\Delta P \cdot r}{2LK}\right)^{\frac{1}{n}} dr$$

$$\int du = -\int \left(\frac{\Delta P \cdot r}{2LK}\right)^{\frac{1}{n}} dr = -\left(\frac{\Delta P}{2LK}\right)^{\frac{1}{n}} \cdot \int r^{\frac{1}{n}} dr$$

$$u = -\left(\frac{\Delta P}{2LK}\right)^{\frac{1}{n}} \cdot \left(\frac{n}{n+1}\right) r^{\frac{1}{n}+1} + C$$

Boundary conditions:

u=0 @ r=R

$$0 = -\left(\frac{\Delta P}{2LK}\right)^{\frac{1}{n}} \cdot \left(\frac{n}{n+1}\right) R^{\frac{1}{n}+1} + C$$

$$C = \left(\frac{\Delta P}{2LK}\right)^{\frac{1}{n}} \cdot \left(\frac{n}{n+1}\right) R^{\frac{1}{n}+1}$$

$$u = -\left(\frac{\Delta P}{2LK}\right)^{\frac{1}{n}} \cdot \left(\frac{n}{n+1}\right) r^{\frac{1}{n}+1} + \left(\frac{\Delta P}{2LK}\right)^{\frac{1}{n}} \cdot \left(\frac{n}{n+1}\right) R^{\frac{1}{n}+1}$$

$$u = \left(\frac{\Delta P}{2LK}\right)^{\frac{1}{n}} \cdot \left(\frac{n}{n+1}\right) (R^{\frac{1}{n}+1} - r^{\frac{1}{n}+1})$$

$$Q = uA = \int u dA$$

$$A = 2\pi r$$

$$dA = \int 2\pi r dr$$

$$Q = \int_{r=0}^{R} u(r) 2\pi r dr$$

$$Q = \left(\frac{\Delta P}{2LK}\right)^{\frac{1}{n}} \cdot \left(\frac{n}{n+1}\right) \cdot 2\pi \int_{0}^{R} r(R^{\frac{1}{n}+1} - r^{\frac{1}{n}+1}) dr$$

$$\left(\frac{\Delta P}{2LK}\right)^{\frac{1}{n}} \cdot \left(\frac{n}{n+1}\right) \cdot 2\pi = B$$

$$Q = B \int_{0}^{R} r(R^{\frac{1}{n}+1} - r^{\frac{1}{n}+1}) dr = B \int_{0}^{R} (rR^{\frac{1}{n}+1} - r^{\frac{1}{n}+1} \cdot r^1) dr = B \int_{0}^{R} (rR^{\frac{1}{n}+1} - r^{\frac{1}{n}+2}) dr$$

$$= B\left[\frac{r^2}{2}R^{\frac{1}{n}+1} - \frac{r^{\frac{1}{n}+2+1}}{\frac{1}{n}+2+1}\right]_0^R = B\left[\frac{r^2}{2}R^{\frac{1}{n}+1} - \frac{r^{\frac{1}{n}+3}}{\frac{1}{n}+3}\right]_0^R = B\left[\frac{R^2}{2}R^{\frac{1}{n}+1} - \frac{R^{\frac{1}{n}+3}}{\frac{1}{n}+3} - 0 + 0\right]$$

$$= B\left[\frac{R^{\frac{1}{n}+3}}{2} - \frac{R^{\frac{1}{n}+3}}{\frac{1}{n}+3}\right] = B\left[\frac{R^{\frac{1}{n}+3}}{2} - \frac{nR^{\frac{1}{n}+3}}{1+3n}\right]$$

$$= B\left[\frac{(1+3n)R^{\frac{1}{n}+3} - 2nR^{\frac{1}{n}+3}}{2(1+3n)}\right]$$

$$= B\left[\frac{(1+n)R^{\frac{1}{n}+3}}{2(1+3n)}\right]$$

$$Q = \left(\frac{\Delta P}{2LK}\right)^{\frac{1}{n}} \cdot \left(\frac{2\pi n}{n+1}\right) \cdot \left[\frac{(1+n)R^{\frac{1}{n}+3}}{2(1+3n)}\right]$$

$$(1+n)R^{\frac{1}{n}+3} = (1+n)R^{\frac{1}{n}} + (1+n)R^3$$

This gives

$$Q = \left(\frac{\Delta P}{2LK}\right)^{\frac{1}{n}} \cdot \left(\frac{2\pi n}{n+1}\right) \cdot \left[\frac{(1+n)R^{\frac{1}{n}} + (1+n)R^3}{2(1+3n)}\right]$$

$$= \left(\frac{\Delta PR}{2LK}\right)^{\frac{1}{n}} \cdot \frac{2\pi nR^3}{2(1+3n)}$$

$$Q = \left(\frac{\Delta PR}{2LK}\right)^{\frac{1}{n}} \cdot \frac{\pi nR^3}{(1+3n)} = \left(\frac{\Delta PR}{2LK}\right)^{\frac{1}{n}} \cdot \frac{\pi R^3}{(\frac{1}{n}+3)}$$

70

Volumetric flow of Herschel-Bulkley fluids:

The following method is developed by Harald A. Asheim.

1 - General Force balance

Force balance along pipe gives shear stress: $\tau_w = \frac{\Delta p r_w}{2L}$

Potential pressure drop, Δp is the same given any radial distance, r, so this gives:

$$\tau(r) = \frac{\Delta p}{2L} r = \frac{r}{r_w} \tau_w \qquad (1)$$

2 - Herschel-Bulkley Rheology

Assume an initial yield stress, τ_o. When this is exceeded, the relationship between shear stress and shear rate will be described by the power law, as illustrated below.
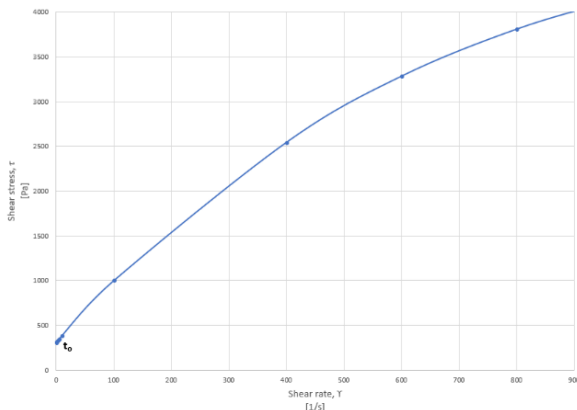
Figure 1: Rheology model

The relationship illustrated in figure 1 can be expressed as

$$\tau = \tau_0 + K \left(\frac{dv}{dr}\right)^n \qquad (2)$$

For the liquid to flow, the shear stress needs to exceed the initial yield stress: $\tau(r) \geq \tau_o$. This value is reached at radius

$$r_o = \tau_o \frac{2L}{\Delta p} \qquad (3)$$

Within this radius the fluid will flow like a firm plug, outside it as a liquid. Velocity and shear stress is illustrated below.
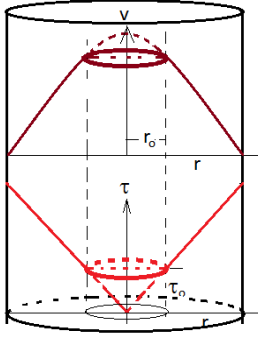
Figure 2: Velocity and shear stress for pipe flow

3 - Velocity profile

Combining (1), (2), (3) gives: $\tau(r) = \frac{\Delta p}{2L}r = \frac{\Delta p}{2L}r_0 + K\left(\frac{dv}{dr}\right)^n$

This gives the following velocity relation between the pipe wall and the plug, for $r_o < r_w$:

$$\frac{dv}{d\hat{r}} = C_1 \hat{r}^{\frac{1}{n}} \quad \ldots. \quad \text{where} \quad C_1 = \left(\frac{\Delta p}{2KL}\right)^{\frac{1}{n}} \text{ and } \hat{r} = r - r_o$$

Integreted, this gives: $v(\hat{r}) = C_1 \frac{n}{n+1}\hat{r}^{\frac{n+1}{n}} + v_o$ where the integrational constant, v_o indicates the velocity of the plug. At the pipe wall $\hat{r} = r_w - r_0$, and $v(\hat{r}) = 0$. This gives the following v_0:

$$v_0 = -\left(\frac{\Delta p}{2KL}\right)^{\frac{1}{n}} \frac{n}{n+1}(r_w - r_0)^{\frac{n+1}{n}} \ldots\ldots \text{ for: } 0 < r < r_o \tag{4}$$

The velocity of the plug inserted in the integrated velocity relation gives the velocity between plug and pipe wall, $r_o < r < r_w$:

$$v(\hat{r}) = v_o\left(1 - \left(\frac{\hat{r}}{\hat{r}_w}\right)^{\frac{n+1}{n}}\right) \quad \ldots\ldots\ldots \text{ where: } \hat{r}_w = r_w - r_o \tag{5}$$

4 - Flow rate

The volumetric flow rate can be found by integrating the velocity profile over the pipe, assuming a firm plug for $0 < r < r_0$, and a non-newtonian flow for $r_0 < r < r_w$

$$Q = \int_0^{r_w} v(r)2\pi r\,dr = v_o\pi r_o^2 + 2\pi\int_0^{\hat{r}_w} v(\hat{r})(\hat{r} + r_o)\,d\hat{r} \tag{6}$$

The velocity in (5), inserted in to (6), gives:

$$2\pi\int_0^{\hat{r}_w} v(\hat{r})(\hat{r} + r_o)\,d\hat{r} = 2\pi v_o\int_0^{\hat{r}_w}\left(1 - \left(\frac{\hat{r}}{\hat{r}_w}\right)^{\frac{n+1}{n}}\right)(\hat{r} + r_o)\,d\hat{r} = 2\pi v_o\int_0^{\hat{r}_w}\left(r_o + \hat{r} - \hat{r}_w^{-\frac{n+1}{n}}\hat{r}^{\frac{2n+1}{n}} - r_o\hat{r}_w^{-\frac{n+1}{n}}\hat{r}^{\frac{n+1}{n}}\right)d\hat{r}$$

Integrated, it becomes

$$= 2\pi v_o \left[r_o \hat{r} + \frac{1}{2}\hat{r}^2 - \hat{r}_w^{-\frac{n+1}{n}} \frac{n}{3n+1}\hat{r}^{\frac{2n+1}{n}+1} - r_o \hat{r}_w^{-\frac{n+1}{n}} \frac{n}{2n+1}\hat{r}^{\frac{n+1}{n}+1} \right]_0^{\hat{r}_w}$$

Inserted boundaries:

$$= 2\pi v_o \left(r_o \hat{r}_w + \frac{1}{2}\hat{r}_w^2 - \frac{n}{3n+1}\hat{r}_w^{-\frac{n+1}{n}}\hat{r}_w^{\frac{n+1}{n}+2} - \frac{n}{2n+1}r_o\hat{r}_w^{-\frac{n+1}{n}}\hat{r}_w^{\frac{n+1}{n}+1} \right) = 2\pi v_o \left(r_o\hat{r}_w + \frac{1}{2}\hat{r}_w^2 - \frac{n}{3n+1}\hat{r}_w^2 - \frac{n}{2n+1}r_o\hat{r}_w \right)$$

$$= \pi v_o \left(\frac{n+1}{3n+1}\hat{r}_w^2 + \frac{2n+2}{2n+1}r_o\hat{r}_w \right)$$

Inserted in (6) , this gives the following flow rate:

$$Q = v_o \pi r_w^2 \left(\left(\frac{r_o}{r_w} \right)^2 + \frac{2n+2}{2n+1}\frac{r_o}{r_w}\left(1 - \frac{r_o}{r_w} \right) + \frac{n+1}{3n+1}\left(1 - \frac{r_o}{r_w} \right)^2 \right) \tag{7}$$

Where

$$r_o = \tau_o \frac{2L}{\Delta p} \qquad \text{and} \qquad v_0 = -\left(\frac{\Delta p}{2KL} \right)^{\frac{1}{n}} \frac{n}{n+1}(r_w - r_0)^{\frac{n+1}{n}}$$

B. IMAGE J PROCESSING

1. Draw a straight line over the scale bar at the bottom right.

2. Analyze → Set scale → Known distance: 100 → Unit of length: µm → Check Global

3. Draw a rectangle around an evenly illuminated part of the picture

4. Image → Duplicate. Duplicate twice to compare original photo to the altered one

5. Process → FFT → Bandpass filter → Filter large structures down to: 30 pixels (Usually 30, try and see what is best)

6. Image → Adjust → Brightness/Contrast. Adjust so that the droplets become more prominent, when satisfied: apply.

7. Image → Type → 8-bit

8. Image → Adjust → Threshold. Adjust so that the color fits the drops. When satisfied: apply.

9. Process → Binary → Make Binary

10. Any droplets not detected are manually drawn in, using the original photo for comparison.

11. Process → Binary → Convert to mask

12. Process → Binary → Fill holes

13. Process → Binary → Watershed

14. Analyze → Set Measurements → check Area, Feret's diameter

15. Analyze → Analyze Particles → check Display Results, Exclude on edges

C. PLOTS
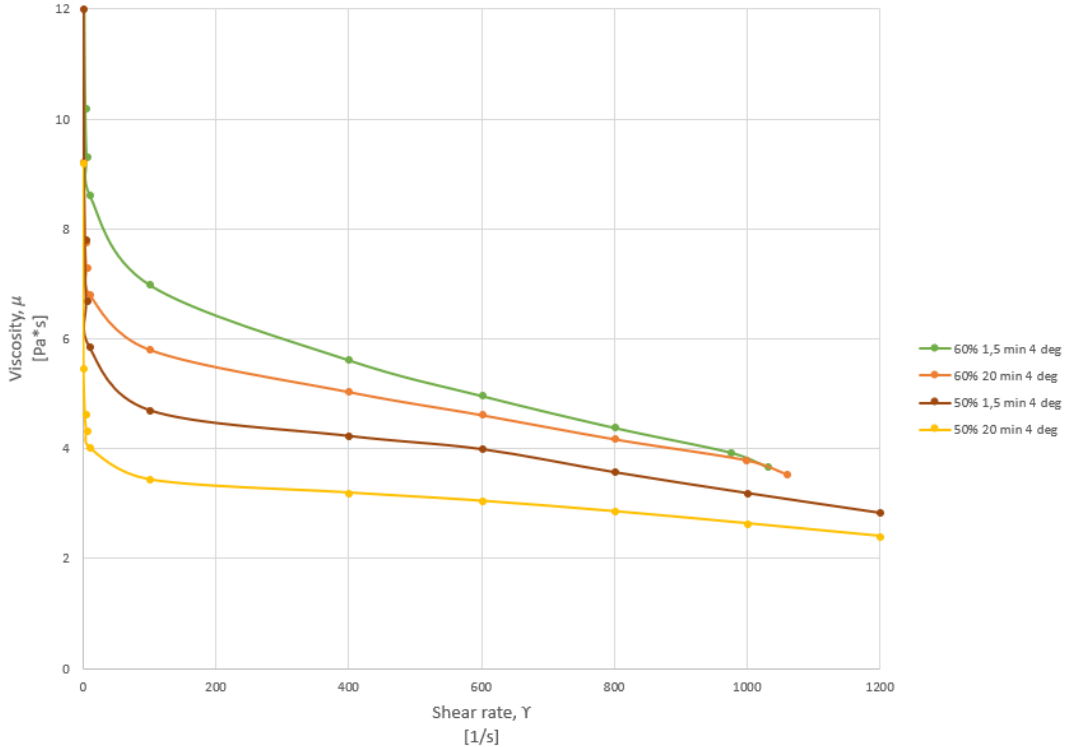
Viscosity for W50-O50 and W60-O40 emulsions mixed for 1.5 and 20 minutes, at 4 °C.
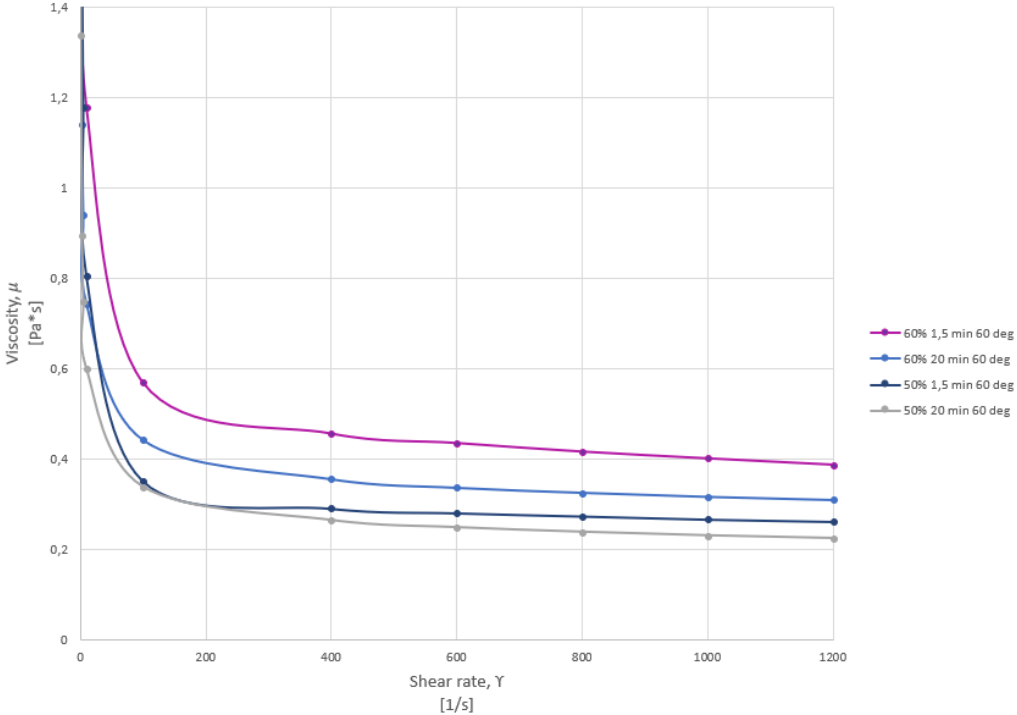
Viscosity for W50-O50 and W60-O40 emulsion mixerd for 1.5 and 20 minutes, at 60 °C
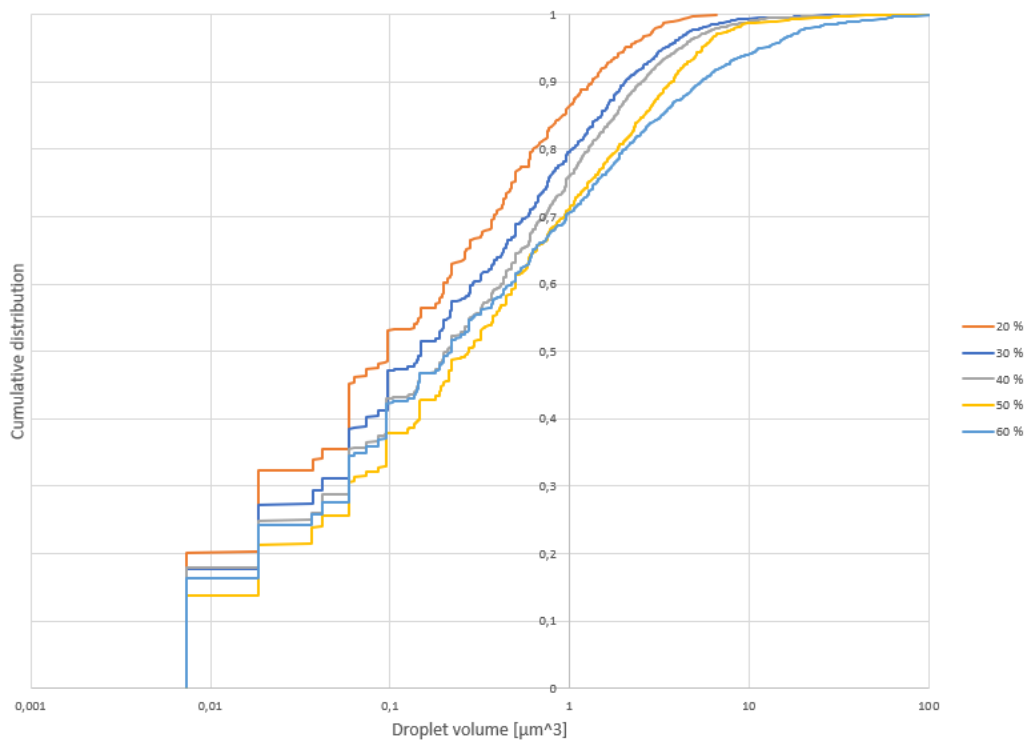
Cumulative droplet distributions with varying water content. If the W60-O40 emulsion is disregarded, the cumulative droplet volume is increasing with increasing water fraction
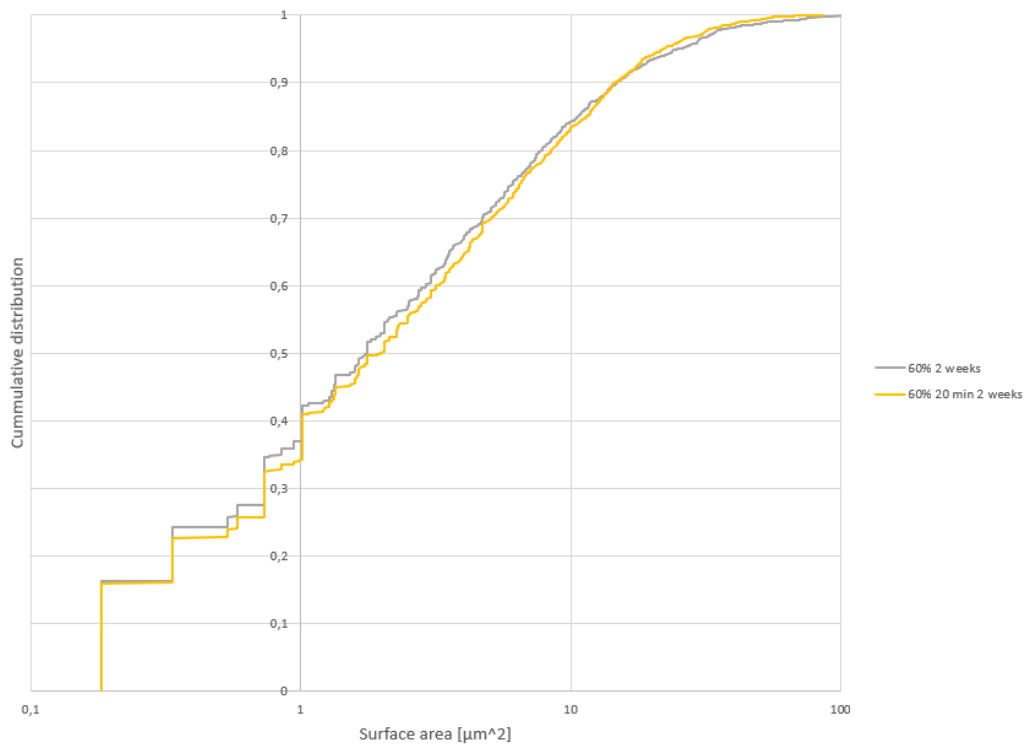
Cumulative distribution for the W60-O40 emulsions mixed for 1.5 and 20 minutes
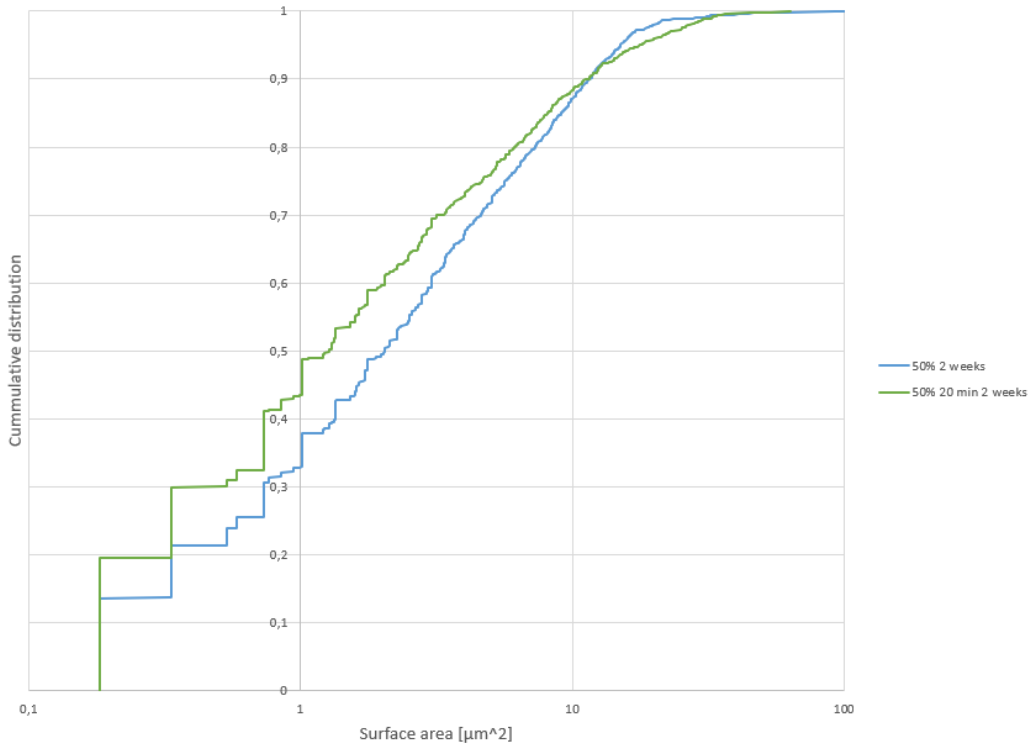
Cumulative distribution for the W50-O50 emulsions mixed for 1.5 and 20 minutes
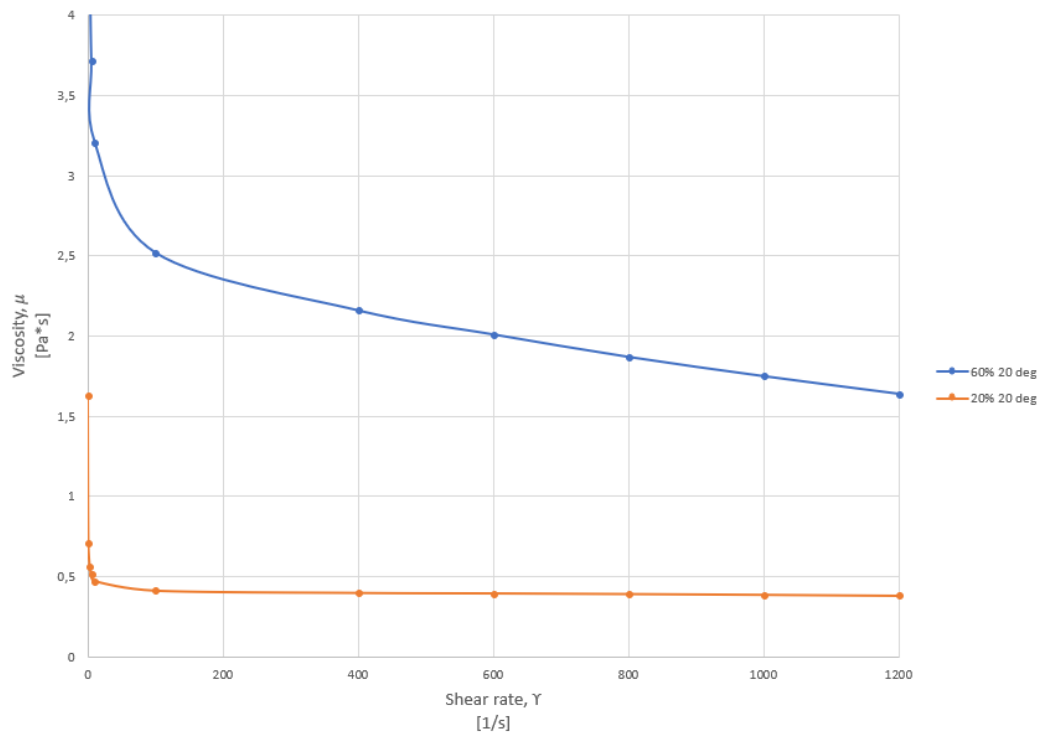
Viscosities of W20-O80 and W60-O40 emulsions at 20 °C
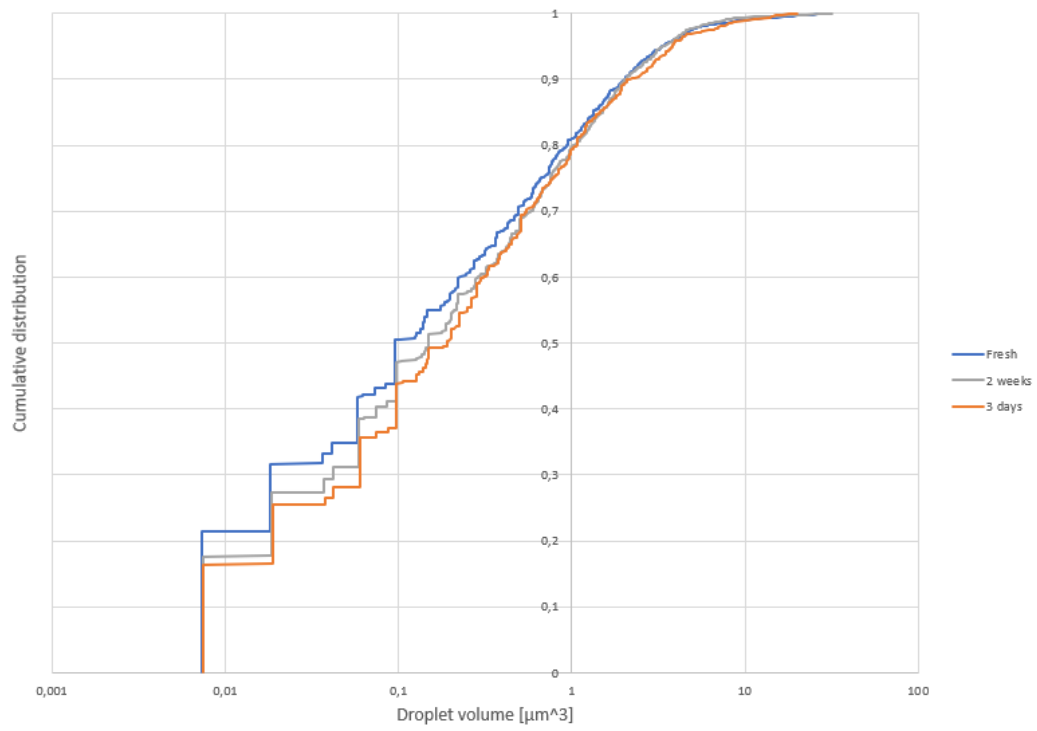
W30-O70 emulsion. No correlation found between aging and droplet volume.

D. MATLAB CODE- DROPLET VOLUME DISTRIBUTION

The following code is developed by Harald A. Asheim.

```
% LogNormal droplet distribution
clear
clf
load Twentyprosfresh.txt
data=Twentyprosfresh;
ant=size(data);
n=ant(1);        % mumber of measuring points
   A=data(1:n,2); % area calculated by ImageJ
   dmax=data(1:n,3); % Feret diameter
    dmin=data(1:n,4); %Minimum Feret diameter
% volum, assumed rotational ellipsoid
pf=1.6075;
for i=1:n
V(i)=4/3*pi*(dmin(i)/2)*(dmax(i)/2)^2;    % volum, rotational
ellipsoid
Sf(i)=pi*( (dmax(i)^(2*pf) +
2*dmax(i)^pf*dmin(i)^pf)/3)^(1/pf);  % surface, rotational
ellipsoid
end
%  Empirical distribution
   Vs=sort(V);  % sorts droplet volumes in rising order

   Vsum(1)=Vs(1);
   for i=2:n
   Vsum(i)=Vsum(i-1)+Vs(i);
   end
   Vtot=Vsum(n);
   Fe=Vsum/Vtot; % Fe(Vs) = empirical cumulative distribution
% surface area
    for i=1:n
   S(i)=(6*pi^(1/2)*Vs(i))^(2/3);   % surfaces, sorted
   end
   osp=40e-3; %surface tension
   Stot=sum(S);
   Srel=Stot/Vtot;
   Sfrel=sum(Sf)/Vtot;;
% Column diagram empirical probability density
nf=10;  % Number of discretization points
Vint=linspace(0,Vs(length(Vs))*1.001,nf); % interval division
for j=1:nf-1
   % find volume increase within every interval
   Vf(j)=0;
   for i=1:length(Vs)
       if Vs(i)>Vint(j)& Vs(i)<Vint(j+1)
   Vf(j)=Vf(j)+Vs(i);
       end
   end
```

```matlab
    Vip(j)=(Vint(j)+Vint(j+1))/2;          % center of
interval
    fV(j)=(Vf(j)/(Vint(j+1)-Vint(j)))/Vtot;  %  empirical
probabililty density
end

 % Mean value and varians of measured data
 Em=0;
for i=2:n
Em=Em+Vs(i)^2/Vtot;
end
var=0;
 for i=2:n
     var=var+Vs(i)^3/Vtot;
 end
 sm=var^0.5;

% Anticipated estimat of lokVsjons: mya, and scale parameter:
s2a
 my=log(Em)-0.5*log(1+var/Em^2);
 s2=log(1+var/Em^2);

 % deviation
 f=0;
 for i=1:n
Fi=0.5*erfc(-(log(Vs(i))-my)/(2*s2)^0.5);
f=f+(Fi-Fe(i))^2;     %
 end
 f=f/n; %average deviation
 errm=100*f^0.5;
% calculation of LogN-distribution before optimalization
x=linspace(0.001,Vs(n));
for i=1:length(x)
fv(i)=(1/(2*s2*pi)^0.5)/x(i)*exp(-(log(x(i))-my)^2/(2*s2));
Fv(i)=0.5*erfc(-(log(x(i))-my)/(2*s2)^0.5);
end

   %

 %
 %--------------- optimize -------------------------------
-
global Feg xg
Feg=Fe;           % empirical cumulativ distribution
xg=Vs;            % x-axes
pa0= [my s2 ];   % initial parameter estimate
[pa,fval]=fminunc(@optfun,pa0);

   % Optimized estimate of lokasjons: mya, and scale
parameter: s2a
 myopt=pa(1);
```

```matlab
    s2opt=pa(2);
 % print
 disp([ '....LogNormal distribution, adaption to measured
droplet volumes.'])
 disp(['.................  From entry data --------- '])
disp(['Standard deviation of measured data :
',num2str(sm,'%5.3e\n')])
disp(['Total droplet volume          :
',num2str(Vtot,'%5.3e\n'),' µm^3'])
disp(['Surface area/droplet volume     :
',num2str(Srel,'%5.3e\n')])
disp(['Surface area/droplet volume rotational ellipsoide    :
',num2str(Sfrel,'%5.3e\n')])
 % Surface
 C=(6*sqrt(pi))^(2/3);
  Sf(1)=0;
 for i=2:length(x)
 Sf(i)=Sf(i-1)+ C*fv(i)/x(i)^(1/3)*(x(i)-x(i-1));
% Surface
 end
 %
Sfmax=Sf(length(x));
Sf2=C*exp((1/18*(-6*my+s2)));              % analytical

disp(['.................  Direct adaption --------- '])
disp(['Mean value                   : ',num2str(Em,'%5.3e\n')])
disp(['Standard deviation             :
',num2str(sm,'%5.3e\n')])
disp(['Surface area/droplet volume
:',num2str(Sf2,'%5.3e\n'),'   (1/µm )'])
disp(['Adaptation error            :
',num2str(errm,'%5.3e\n'),'   %'])
% disp(['Optimized estimate of my-parameter
',num2str(my,'%5.3e\n')])
% disp(['Optimized estimate of s2-parameter
',num2str(s2,'%5.3e\n')])
%disp(['Location parameter optimized distribution
',num2str(myopt,'%5.3e\n')])
%disp(['Scale parameter for optimized distribution
',num2str(s2opt^0.5,'%5.3e\n')])


%  LogN-distribution based on optimized parameters
 z=linspace(0.0001,2*Vs(n), 300);
for i=1:length(z)
fao(i)=(1/(2*s2opt*pi)^0.5)/z(i)*exp(-(log(z(i))-
myopt)^2/(2*s2opt));
Fao(i)=0.5*erfc(-(log(z(i))-myopt)/(2*s2opt)^0.5);
end
   m=exp(myopt+s2opt/2);                    % mean value,
1. moment of distribution
```

```matlab
sd=((exp(s2opt)-1)*exp(2*myopt+s2opt))^0.5; % standard
deviation
 sdi2=0;
 for i=2:length(z)
     sdi2=sdi2+(z(i)-m)^2*fao(i)*(z(i)-z(i-1));
 end

 sdi=sdi2^0.5;   % standard deviation by numerical integration

 err=100*fval^0.5;
 dfsd=(1+(sd/m^2)^0.5);
disp(['.................  Optimized adaptation --------- '])
disp(['Mean value                    ',num2str(m,'%5.3e\n')])
disp(['Standard deviation
',num2str(sd,'%5.3e\n')])
disp(['Adaptation error
',num2str(err,'%5.3e\n'),'  %'])

  %
  xmax=1.1*Vs(n);
   subplot(2,1,1)
 hold on
 plot(Vs,Fe,'.')
 plot(x,Fv,'k','LineWidth',1.5)
  plot(z,Fao,'k-.')
  plot([Em Em],[0 1],'r-.')
    plot([Em+sm Em+sm],[0 1],'m-')
 hold off
 xlabel('\bf Droplet volume: V_d (µm^3)')
 ylabel('\bfCumulative: F  (-)')
 grid
 legend('Measured distribution','Distribution:
F_N(m,s)','Optimized distribution','Mean value: m','m +
Measured standard deviation')
axis([0 xmax 0 1 ])

 % density
 maxf=1.2*max(fao);
subplot(2,1,2)
hold on
%bar(Vip,fV)
 plot(x,fv,'k','LineWidth',1.5)
plot(z,fao,'k-.')
 plot([Em Em],[0 1],'r-.')
    plot([Em+sm Em+sm],[0 1],'m-')
% plot([E E],[0, max(f)],'b-.')
hold off
xlabel('\bf Drople volume: V_d  (µm^3)')
 ylabel('\bf Distribution density: f_v')
```

```matlab
 legend('Distribution density: f_v(m,s)','Optimized
distribution density','  Measured mean value','m + Measured
standard deviation')
grid
 axis([0 xmax 0 maxf ])
% legend(' Grouped measurements','Adapted logN')
```

E. RISK ASSESSMENT

ID	27015		Status	Date
Risk Area	Risikovurdering: Helse, miljø og sikkerhet (HMS)		Created	17.01.2018
Created by	Ingunn Lervik		Assessment started	17.01.2018
Responsible	Harald Arne Asheim		Actions decided	17.01.2018
			Closed	17.01.2018

Risk Assessment:
Master thesis, spring 2018

Valid from-to date:
1/17/2018 - 6/11/2018

Location:
Petroleumsteknisk senter

Goal / purpose
I want to conduct a risk assessment in order to reveal possible dangers that can occur during lab experiments.

Background
This risk assessment is conducted in connection with the work related to the master thesis.

Description and limitations
Subjects that might be affected by the risks evaluated in this risk assessment are me and my co-workers in the lab. The risk assessment is applicable for work in the PTS-lab only.

Prerequesites, assumptions and simplifications
Similar experiments have been conducted previously.

Attachments
[Ingen registreringer]

References
[Ingen registreringer]

Norges teknisk-naturvitenskapelige universitet (NTNU)	Print date:	Printed by:		Page:
Unntatt offentlighet jf. Offentlighetsloven § 14	17.01.2018	Ingunn Lervik		1/9

84

Summary, result and final evaluation

The summary presents an overview of hazards and incidents, in addtition to risk result for each consequence area.

Hazard:	Flammable waste				
Incident:	**Fire**				

Consequence area:	Helse		Risk before actions: 🟢	Risiko after actions: 🟢	
	Materielle verdier		Risk before actions: 🟡	Risiko after actions: 🟡	

Planned action		**Responsible**	**Registered**	**Deadline**	**Status**
Prevent fire		Ingunn Lervik	17.01.2018	11.06.2018	New

Hazard:	Inhalation of emulsion			
Incident:	**Illness**			

Consequence area:	Helse	Risk before actions: 🟢	Risiko after actions: ⚪

Final evaluation

There is little risk assosiated with this lab experiment.

Norges teknisk-naturvitenskapelige universitet (NTNU)	Print date:	Printed by:	Page:
Unntatt offentlighet jf. Offentlighetsloven § 14	17.01.2018	Ingunn Lervik	2/9

85

Organizational units and people involved

A risk assessment may apply to one or more organizational units, and involve several people. These are lsited below.

Organizational units which this risk assessment applies to

- Institutt for geovitenskap og petroleum

Participants
Ingunn Lervik

Readers
[Ingen registreringer]

Others involved/stakeholders
[Ingen registreringer]

The following accept criteria have been decided for the risk area Risikovurdering: Helse, miljø og sikkerhet (HMS):

Helse	Materielle verdier	Omdømme	Ytre miljø

Norges teknisk-naturvitenskapelige universitet (NTNU)	Print date:	Printed by:	Page:
Unntatt offentlighet jf. Offentlighetsloven § 14	17.01.2018	Ingunn Lervik	3/9

86

Overview of existing relevant measures which have been taken into account

The table below presents existing measures which have been take into account when assessing the likelihood and consequence of relevant incidents.

Hazard	Incident	Measures taken into account
Flammable waste	Fire	Protective equipment
	Fire	Fume hood and waste bucket
Inhalation of emulsion	Illness	Protective equipment

Existing relevant measures with descriptions:

Protective equipment
Goggles, safety boots and labcoat

Fume hood and waste bucket
A waste bucket is present to dispose of the oil. A fume hood is loacted above the bucket to prevent inhalation of the oil mist.

Lab tour
A guided tour through the lab to get familiar with the lab and its equipment.

HSE Introductory Course
Online HSE course

Norges teknisk-naturvitenskapelige universitet (NTNU)	Print date:	Printed by:		Page:
Unntatt offentlighet jf. Offentlighetsloven § 14	17.01.2018	Ingunn Lervik		4/9

87

Risk analysis with evaluation of likelihood and consequence

This part of the report presents detailed documentation of hazards, incidents and causes which have been evaluated. A summary of hazards and associated incidents is listed at the beginning.

The following hazards and incidents has been evaluated in this risk assessment:

- **Flammable waste**
  - Fire
- **Inhalation of emulsion**
  - Illness

Norges teknisk-naturvitenskapelige universitet (NTNU)	Print date:	Printed by:	Page:
Unntatt offentlighet jf. Offentlighetsloven § 14	17.01.2018	Ingunn Lervik	5/9

88

Detailed view of hazards and incidents:

Hazard: Flammable waste

Some of the fluids in use can be flammable

Incident: Fire

If flammable waste comes in contact with a flame, a fire could start.

Likelihood of the incident (common to all consequence areas): **Unlikely (1)**

> *Kommentar:*
> There is no source of fire present in the lab.

Consequence area: Helse

> *Assessed consequence:* **Medium (2)**

> > *Comment:* There are many escape routes.

Risk:
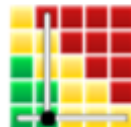
Consequence area: Materielle verdier

> *Assessed consequence:* **Large (3)**

> > *Comment:* If a fire occurs, some equipment will get destroyed.

Risk:

Norges teknisk-naturvitenskapelige universitet (NTNU)	Print date:	Printed by:	Page:
Unntatt offentlighet jf. Offentlighetsloven § 14	17.01.2018	Ingunn Lervik	6/9

89

Hazard: Inhalation of emulsion

One could inhale the emulsion

Incident: Illness

Consumption of emulsion could cause illness

Likelihood of the incident (common to all consequence areas): **Unlikely (1)**

Kommentar:

I know not to inhale the emulsions.

Consequence area: Helse   *Risk:*

Assessed consequence: **Small (1)**

Comment: Will probably not cause severe illness.

Norges teknisk-naturvitenskapelige universitet (NTNU)	Print date:	Printed by:	Page:
Unntatt offentlighet jf. Offentlighetsloven § 14	17.01.2018	Ingunn Lervik	7/9

90
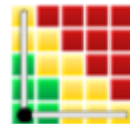
Overview of risk mitiating actions which have been decided:

Below is an overview of risk mitigating actions, which are intended to contribute towards minimizing the likelihood and/or consequence of incidents:

- Prevent fire

Overview of risk mitigating actions which have been decided, with description:

Prevent fire

Prevent fire in the lab by not bringing flames or flammable items in to the lab.

Action decided by:	Ingunn Lervik
Responsible for execution:	Ingunn Lervik
Deadline for execution:	6/11/2018

Norges teknisk-naturvitenskapelige universitet (NTNU)	**Print date:**	**Printed by:**		**Page:**
Unntatt offentlighet jf. Offentlighetsloven § 14	17.01.2018	Ingunn Lervik		8/9

91

Detailed view of assessed risk for each hazard/incident before and after mitigating actions

Hazard: Flammable waste

Incident: Fire

Likelihood assessment (common to all consequence areas)

Initial likelihood:	Unlikely (1)
Reason:	There is no source of fire present in the lab.
Likelihood after actions:	Unlikely (1)
Reason:	

Consequence assessments:

Consequence area: Helse   *Risk:*

Initial consequence:	Medium (2)
Reason:	There are many escape routes.

Consequence after actions:	Medium (2)
Reason:	

Consequence area: Materielle verdier   *Risk:*

Initial consequence:	Large (3)
Reason:	If a fire occurs, some equipment will get destroyed.

Consequence after actions:	Large (3)
Reason:	

Norges teknisk-naturvitenskapelige universitet (NTNU)	**Print date:**	**Printed by:**	**Page:**
Unntatt offentlighet jf. Offentlighetsloven § 14	17.01.2018	Ingunn Lervik	9/9

92